

**ENHANCEMENT OF PARKING SPOT DETECTION USING AN  
AFFORDABLE LASER RANGE SENSOR**

A Thesis  
Presented to  
The Academic Faculty

by

Nader Hammoud

In Partial Fulfillment  
of the Requirements for the Degree  
Master of Science in the  
School of Mechanical Engineering

Georgia Institute of Technology  
December 2015

**COPYRIGHT© 2015 BY NADER HAMMOUD**

**ENHANCEMENT OF PARKING SPOT DETECTION USING AN  
AFFORDABLE LASER RANGE SENSOR**

Approved by:

Dr. Bert Bras, Advisor  
School of Mechanical Engineering  
*Georgia Institute of Technology*

Dr. Seung-Kyum Choi  
School of Mechanical Engineering  
*Georgia Institute of Technology*

Dr. Roger Jiao  
School of Mechanical Engineering  
*Georgia Institute of Technology*

Date Approved: 11/24/2015



## **ACKNOWLEDGMENTS**

I wish to thank my advisor, Dr. Bert Bras, whose help and insights were paramount to completing this thesis. He has been a tremendous mentor throughout my graduate studies. I am forever grateful for his continued support in my academic endeavors, but also for his guidance during the start of my professional career.

I would also like to thank my committee members, Dr. Seung-Kyum Choi and Dr. Roger Jiao for their helpful comments and assistance in writing this thesis.

I also wish to extend my gratitude to my colleagues in the Sustainable Design and Manufacturing lab who have always offered their help and provided me with a great experience at the Georgia Institute of Technology.

Last but certainly not least, I would like to thank my family for their unconditional love and support. I would not be where I am today without their constant motivation, guidance and support.

# TABLE OF CONTENTS

AKNOWLEDGMENTS .....	iv
LIST OF TABLES .....	viii
LIST OF FIGURES .....	x
LIST OF EQUATIONS .....	xiv
SUMMARY .....	xv

## CHAPTER

1 INTRODUCTION .....	1
1.1 Effect of Time Wasted Looking For Parking on Traffic Congestion .....	1
1.2 The Need for Gathering Parking Spot Information .....	2
1.3 Thesis Organization .....	3
2 LITERATURE REVIEW .....	5
2.1 Available Parking Applications and Testing with Other Sensors.....	5
2.1.1 Parking Applications and Tools to Facilitate the Parking Experience.....	5
2.1.2 Ultrasonic Sensors.....	7
2.1.3 Vision Sensors.....	19
2.1.4 Anisotropic Magnetoresistive (AMR) Sensors .....	19
2.1.5 Using Models to Predict Parking Spot Occupancy .....	24
2.1.6 Wireless Sensor Networks .....	26
2.1.7 Overview of Sensor Technologies .....	28
2.2 The Need for Laser Sensors .....	28
2.2.1 Available Laser Sensor Technology .....	28
2.2.2 Combining Laser Sensor Technology and Other Sensors.....	40
2.2.3 Overview of Laser Sensor Technology.....	45
2.3 Summary of Available Sensor Technologies for Parking Detection .....	46
3 SYSTEM DESCRIPTION.....	49
3.1 Ideal System Requirements.....	49
3.1.1 Installing a laser range sensor .....	49
3.1.2 Integrating other data sources .....	50
3.1.3 Use case description.....	52

3.2	Infrared Laser Technology Overview .....	53
3.3	General System Description .....	54
3.3.1	System Requirements .....	55
3.3.2	Hardware Overview .....	55
3.3.3	Detection Algorithm.....	61
3.4	System Description Summary.....	67
4	EXPERIMENTS CONDUCTED .....	68
4.1	Experimental Set Up and Hypothesis .....	68
4.2	Additional Experiments .....	71
4.2.1	2D Image Generation .....	71
4.2.2	3D Image Generation .....	72
4.3	Summary of Experimental Setups .....	75
5	EXPERIMENTAL RESULTS.....	76
5.1	Accuracy of Laser Range Sensor .....	76
5.1.1	First Statistical Approach.....	77
5.1.2	Discussion of First Statistical Approach .....	79
5.1.3	Second Statistical Approach.....	81
5.1.4	Discussion of Second Statistical Approach.....	81
5.1.5	Third Statistical Approach .....	83
5.1.6	Discussion of Third Statistical Approach.....	84
5.2	Experiments under Inclement Weather.....	86
5.3	Experiments with Pivoting Laser Range Sensor.....	88
5.4	Generating a 2D Image .....	93
5.5	Generating a 3D Image .....	94
5.5.1	Results of 3D imaging by Frames .....	94
5.5.2	Results of 3D imaging by Points.....	96
5.6	Enhancement of Parking Angle Detection.....	98
5.7	Summary and Recommendations .....	99
6	APPLICABILITY TO PRODUCTION VEHICLES AND SUMMARY ....	101
6.1	Cost of Installation.....	101
6.2	Applicability to Commercial Vehicles and Enhancements Produced ....	102
6.2.1	Installation on Commercial Vehicles .....	102
6.2.2	Enhancement of Parking Spot Detection .....	105
6.3	Reflectivity Issues .....	106

6.4 Point vs Plane Mapping .....	107
6.5 Environmental Issues, Limits, and Properties to Consider .....	108
6.6 Conclusions.....	110
Appendix A: TABLES OF EXPERIMENTAL RESULTS.....	112
Appendix B: SYSTEM SPEC LIST .....	118
Appendix C: LIDAR-LITE DATA SHEET .....	119
REFERENCES .....	122

## LIST OF TABLES

Table 1: Results of LIDAR algorithm detection vs. ground truth data (Thornton, Redmill, & Coifman, 2014) .....	39
Table 2: Summary of sensor technologies available for parking detection .....	48
Table 3: LIDAR-Lite Specifications (Pulsed Light, 2015).....	57
Table 4: Experimental runs .....	69
Table 5: Experimental results .....	77
Table 6: Probability Calculation - Method 1 .....	79
Table 7: False Positive and False Negative Probability Calculations - Method 2.....	81
Table 8: Probability of correctly mapping a parking lot after a number of runs – Method 3 .....	84
Table 9: Confidence for 90° and parallel parking (best case scenario).....	85
Table 10: Confidence for 60° parking (worst case scenario) .....	86
Table 11: Total cost the suction cup and window mount systems.....	101
Table 12: Tests performed for parallel parking, at 5 mph .....	112
Table 13: Tests performed for parallel parking, at 10 mph .....	112
Table 14: Tests performed for 45° parking, at 5 mph .....	113
Table 15: Tests performed for 45° parking, at 10 mph.....	114
Table 16: Tests performed for 60° parking, at 5 mph .....	114
Table 17: Tests performed for 60° parking, at 10 mph.....	115
Table 18: Tests performed for 90° parking, at 5 mph.....	116
Table 19: Tests performed for 90° parking, at 10 mph.....	116
Table 20: Tests performed for 90° parking, at 15 mph.....	117



Table 21 System spec List ..... 118

## LIST OF FIGURES

Figure 1: Gathering parking spot information .....	3
Figure 2: Installing several ultrasonic sensors on the latest cars. The arcs represent the ultrasonic sensors and their reach (Kohler, Connette, & Verl, 2013).....	8
Figure 3: Ultrasonic beam width uncertainty, measuring a narrower empty parking spot. 9	
Figure 4: Classification of surface shape for right angle edge side and rounded edge sides (Park, Kim, Seo, Kim , & Lee, 2008) .....	11
Figure 5: Experimental (a) Setups A, and (b) B (Abdel-Hafez, Al Nabulsi, Jafari, Al Zaabi, Sleiman, & AbuHatab, 2011) .....	12
Figure 6: A diagram depicting the various scenarios and events involved in the detection of parking space using mobile sensors (Mathur, et al., 2010) .....	15
Figure 7: Schematic diagram explaining the overall architecture of the system (Mathur, et al., 2010) .....	16
Figure 8: (a) An image of the ultrasonic sensor side-mounted on a car (b) the java applet used for recording ground truth from images. (c) The map of the data collection area (Mathur, et al., 2010) .....	17
Figure 9: Dips in the sensor reading as a sensing vehicle drives past (a) two parked cars with some space between them, and (b) two very closely spaced parked cars (Mathur, et al., 2010) .....	18
Figure 10: Devices installed in roadside parking spaces. (a) Sensor nodes, (b) Router (Zhang, Tao, & Yuan, 2014).....	20
Figure 11: Three axes magnetic signature of a parking space (Zhang, Tao, & Yuan, 2014) .....	21
Figure 12: Depictions of the management system. (a) Sensor nodes installed in parking spots. (b) Topology of the network (Zhang, Tao, & Yuan, 2014).....	23
Figure 13: (a) 3-layer framework of WSN-based system, (b) the architecture of the system ( Tang, Zheng, & Cao, 2006).....	27
Figure 14: Rotation of the laser sensor .....	29

Figure 15: IHI 3D Laser Radar (IHI Corporation, 2010).....	30
Figure 16: Detection algorithm overview (Ono, Kagesawa, & Ikeuchi, 2002).....	31
Figure 17: Detection results (a) by depth-curve method, (b) by height-curve method (Ono, Kagesawa, & Ikeuchi, 2002) .....	32
Figure 18: LIDAR point cloud example (Thornton, Redmill, & Coifman, 2014).....	34
Figure 19: The three stages of the algorithm (Thornton, Redmill, & Coifman, 2014).....	35
Figure 20: (a) Single LIDAR scan producing raw data points, detecting the ground and curb. (b) Parked car detected and curb location estimated using an estimate from a preceding time sample (Thornton, Redmill, & Coifman, 2014).....	36
Figure 21: (a) Opposing lanes viewed by LIDAR and (b) object and occlusion detection by the algorithm. (c) Endpoint occlusion scenario and (d) object and occlusion detection by the algorithm. (e) Occluded gap between parked cars and (f) object and occlusion detection by the algorithm (Thornton, Redmill, & Coifman, 2014).....	37
Figure 22: (a) Gaps between parked vehicles, (b) lengths of vehicles, and (c) height of vehicles vs. distance travelled (Thornton, Redmill, & Coifman, 2014) .....	38
Figure 23: Determining the parking lot structure automatically using (a) LIDAR data and an aerial snapshot of a parking lot, (b) projected vector structure information (Tong, Cheng, Li, Wang, & Du, 2014).....	41
Figure 24: Examples of challenges faced in the parking lot extraction process: (a) A parking lot with several dominant lane-markings, (b) a full parking lot, (c) low quality line markings (Tong, Cheng, Li, Wang, & Du, 2014) .....	42
Figure 25: (a), (b), and (c) Parking lots generated by the proposed method. (d), (e), and (f) Parking lots generated by the image-based approach (Tong, Cheng, Li, Wang, & Du, 2014) .....	43
Figure 26: (a), (b), and (c) Reference lines for parking lots generated by the proposed method. (d), (e), and (f) Parking lots generated by the image-based approach. Red lines represent the parking spot limits, while green lines represent the vehicle central axis (Tong, Cheng, Li, Wang, & Du, 2014).....	44
Figure 27: Correct (red), missing (blue), and false (green) lines in the extracted lot structure (a), (b), and (c) Parking lots generated by the proposed method. (d), (e), and (f)	

Parking lots generated by the image-based approach (Tong, Cheng, Li, Wang, & Du, 2014) .....	45
Figure 28: Laser sensor satisfying all technical requirements .....	50
Figure 29: Integration of various data sources.....	51
Figure 30: Use case description .....	52
Figure 31: Illustration depicting the distance measurement principle (Kikuta, Iwata, & Nagata, 1986).....	54
Figure 32: Laser range sensor assembly .....	58
Figure 33: Laser range sensor with servo motor assembly.....	59
Figure 34: System description overview.....	60
Figure 35: Entire sensor setup (a) for the pivoting sensor, (b) for the water resistant sensor, and (c) mounted on the probe vehicle.....	61
Figure 36: General overview of the algorithm.....	62
Figure 37: Spot Count Algorithm .....	62
Figure 38: Raw Data. Driving at 5 mph, scanning 90° parking spots .....	64
Figure 39: Ground Truth Data from Onboard Camera .....	65
Figure 40: Data after ignoring the secondary and tertiary row of cars .....	65
Figure 41: Solution of Matlab algorithm counting the number of closed/open spots for 90 degree parking, at 5 mph.....	66
Figure 42: Parking lot layouts.....	68
Figure 43: Routes followed for 90° parking .....	70
Figure 44: Routes followed for parallel parking.....	70
Figure 45: (a) Sample representation of the 2D experiment and (b) desired Cartesian plot output .....	72
Figure 46: 3D system layout.....	73

Figure 47: (a) Results of testing under adverse weather conditions, and (b) ground truth data .....	88
Figure 48: Sample run with pivoting sensor .....	89
Figure 49: Black car parked at the start of the parking lot.....	90
Figure 50: Scanning a black vehicle at 5 mph, (a) with the pivoting sensor and (b) with a stationary sensor.....	91
Figure 51: Scanning a black vehicle at 10 mph, (a) with the pivoting sensor and (b) with a stationary sensor.....	92
Figure 52: Experimental result of scanning a vertical plate .....	93
Figure 53: (a) Setup and (b) experimental result of scanning a vertical plate with a hole	94
Figure 54: Picture of 3D scanned vehicle .....	95
Figure 55: Laser range sensor 3D scanning vehicle by the “Frame Method” .....	95
Figure 56: Laser range sensor 3D scanning vehicle by the “Points Method” .....	97
Figure 57: Possible parking angle detection .....	98
Figure 58: Bluetooth shield installed on Arduino microcontroller .....	102
Figure 59: Diagram of Bluetooth integration.....	103
Figure 60: 3D drawing of Bluetooth system.....	103
Figure 61: Final system mounted on a car window .....	104
Figure 62: Example of black car that is not accurately detected by the sensor: (a) Ground truth from video and (b) sensor readings .....	107
Figure 63: (a) Video and (b) data of sensor overshooting vehicles .....	108
Figure 64: (a) Motorcycle parked, and (b) picked up by sensor .....	109

## LIST OF EQUATIONS

Equation 1: Ultrasonic beam width calculation (Park, Kim, Seo, Kim , & Lee, 2008).....	8
Equation 2: Wavelength calculation .....	8
Equation 3: Calculating the distance from the vehicle .....	10
Equation 4: Calculation of the distance .....	54
Equation 5: From Polar to Cartesian coordinate system.....	71
Equation 6: Probability calculations for open and closed spots. Case where ground truth numbers greater than experimental values.....	78
Equation 7: Probability calculations for open and closed spots. Case where ground truth numbers smaller than experimental values .....	78
Equation 8: False Positive and False Negative Probability Calculations .....	81
Equation 9: Confidence calculation .....	83

## SUMMARY

To gain a better understanding of the impact of parking spaces on traffic congestion, road infrastructure, time spent searching for parking and ultimately CO<sub>2</sub> emissions, several parking surveys have been undertaken. Traditionally these surveys were performed by individuals manually logging parking lot information, thus limiting spatial and temporal coverage due to high labor costs. As a result, the need for automating the data collection process for open parking spaces is paramount when one starts looking into using parking lot information in real-time applications and across a large area such as a city, state, or even an entire country. Some studies have investigated this automation process by installing ultrasonic sensors, 2D LIDARs, vision sensors, parking lot cameras, or sensors for individual parking spots in a lot. Most of these methods generated promising results, but were either expensive or not suitable for real-time processing.

This thesis describes an affordable method to detect parking spots in real-time by installing a low cost, off-the-shelf laser range sensor onto a probe vehicle. Several algorithms will investigate the effect of having a stationary sensor and enabling a vertical motion of the sensor, with hopes of obtaining 3D images of a parking lot. The experiments are conducted at different speeds and for different parking configurations, in normal and adverse weather conditions. The results were compared to onboard ground truth camera recordings of the experiments. Statistical analyses were also performed to determine how effective a laser range sensor is in mapping a parking lot in one run, and how many runs are necessary to map the parking lot with a certain confidence.

Results show that the stationary laser range sensor maps parking spots with high accuracy, successfully generating 2D and 3D layouts of the parking configuration. Moreover, it has been shown that the sensor's accuracy does not diminish for adverse weather conditions. The vertical motion of the sensor on the other hand helps with detecting some black cars, which are not as efficiently identified by the stationary sensor.



# CHAPTER 1

## INTRODUCTION

### 1.1 Effect of Time Wasted Looking For Parking on Traffic Congestion

An urban mobility report published by the Texas A&M Transportation Institute estimates that \$121 billion dollars were lost in the United States in 2011 because of traffic congestion. This was mainly due to 2.9 billion gallons of wasted fuel, and 5.5 billion lost man-hours. Moreover, the study shows how congestion costs are increasing as the years go on: the cost of lost time and wasted fuel added up to \$24 billion in 1982, \$94 billion in 2000, and rose up to \$121 billion in 2011 (Schrank, Eisele, & Lomax, 2012).

Another study by Shoup observed parking activities in a business district in Los Angeles. He found that over the course of a year, motorists searching for parking burned 47,000 gallons of gasoline, emitted 730 tons of CO<sub>2</sub>, and covered a distance of 38 trips around the globe (Shoup, 2006). One could imagine that scaling these numbers to match the whole world instead of a small district in LA would generate worrisome data.

Similarly, as Ono et al. explain, traffic congestion is increased because of parked cars on the side of the road. That is why they believe road administrators would be interested in measuring the actual effect of parked vehicles. The authors also claim that traffic congestion would decrease if a percentage of these parked cars can be decreased (Ono, Kagesawa, & Ikeuchi, 2002).

## 1.2 The Need for Gathering Parking Spot Information

The issue with parking and its negative impact on congestion is not because of the lack of parking spots, but rather due to insufficient information regarding these spots. This information can range from GPS data, time range availability, and cost. A number of papers explore the different solutions to this lack of parking spot information. These solutions include using ultrasonics currently installed on vehicles, or vision sensors, algorithms and models, wireless sensor networks, and anisotropic magnetoresistive sensors. Additionally, other papers examine current LIDAR sensor technologies being actively researched. In (Ono, Kagesawa, & Ikeuchi, 2002) a laser sensor is installed to generate a geometric model of a town, while Thornton et al. install a 2D LIDAR onto a probe vehicle and attempt to generate a 3D point cloud representation of parked cars on the side of the road (Thornton, Redmill, & Coifman, 2014).

Figure 1 below shows how parking spot information can be obtained. A sensor vehicle (Car A) should scan a parking lot for available parking spots as it is leaving or driving by the lot (Steps 1 to 3). Parking availability data is transferred to a central server, where it is analyzed (Step 4), and then forwarded to a separate vehicle (Step 5) about to start looking for parking (Car B). Using this data, the second vehicle (Car B) can find a parking spot more efficiently. This loop is repeated for each vehicle leaving or driving by a parking lot (Steps 1 to 3), and each vehicle looking for parking (Step 5).

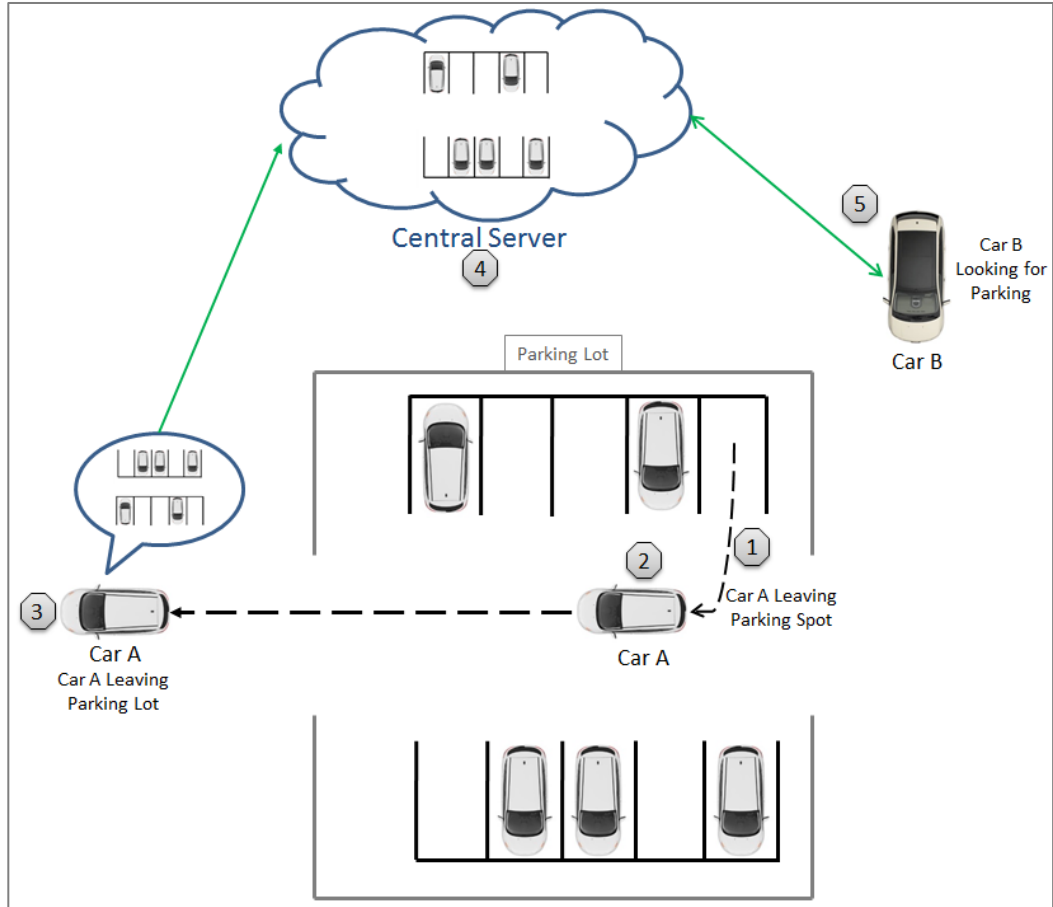


Figure 1: Gathering parking spot information

### 1.3 Thesis Organization

In this thesis, we will inspect the different methods proposed by researchers and engineers, and examine some efforts to combine different technologies in order to successfully map parking lots. Furthermore, the accuracy and applicability of these technologies for parking spot detection will be compared.

A new parking detection system using an affordable off-the-shelf laser range sensor will also be evaluated: How does a laser range sensor compare to the different

technologies being actively researched? This thesis will attempt to answer some questions that would help evaluate the system's accuracy, applicability in today's car industry, and limitations: Is the system's efficiency limited by a high market price, or could it replace current sensor setups used in production vehicles? Would the sensor be affected by inclement weather, or can it maintain a high accuracy regardless of outside conditions? Can the sensor be used for other applications, and is there a way to enhance the current available technology?

In Chapter 2, a general overview of the available literature will be presented, giving a brief description of the different sensor systems available. Previous laser technologies developed for different applications will also be discussed, along with hybrid innovations utilizing a combination of sensors and algorithms. A description of an ideal parking sensing system will be given in Chapter 3. Moreover, this chapter will focus on detailing the laser range sensor system researched, reviewing the general setup along with the hardware used and algorithms employed. Chapter 4 will go over the experimental setup and additional experiments performed, whereas the results of the experiments will be discussed in Chapter 5. Finally, the cost of installation, applicability to commercial vehicles, and limitations of the system will be presented in Chapter 6.

## **CHAPTER 2**

### **LITERATURE REVIEW**

#### **2.1 Available Parking Applications and Testing with Other Sensors**

With an increasing demand for parking availability and assistance, applications and technologies have been developed to facilitate parking-related activities. These advancements can range from existing “apps” purchasable on mobile devices to sensor technologies installed for various parking sensing requirements.

##### **2.1.1 Parking Applications and Tools to Facilitate the Parking Experience**

Some mobile parking applications are available to the public. These “apps” such as “Parker”, “ParkME”, and “BestParking” usually rely on individual sensors installed for each specific parking spot in garages and outside metered parking lots. They may also rely on parking models, which predict parking availability based on historical data, statistical analysis, and prediction algorithms (Klappenecker, Lee, & Welch, 2014). While these “apps” vigorously market their accuracy and precision when it comes to parking prediction, expanding the applications’ geographical reach requires implementing sensors to individual parking garages and budget a city’s plan that will allow for these sensors to be installed. In the City Council Report of Santa Monica in 2011, 6100 parking meters fitted with ground sensors were installed throughout the city, for a total cost of \$4,500,000 (with an additional \$612,000 allocated annually for operating costs)

(Decavalles-Hughes & Ching, 2011). This would equate to a staggering \$838.03 per parking spot (\$737.7 without maintenance costs).

To evaluate the efficiency of such systems, a simple example can be considered:

*The U.S. Department of Transportation states that each driver is on the road for an average of 13,476 miles per year (Federal Highway Administration, 2015). That equates to about 37 miles a day. Let us assume that only 1 mile out of the 37 miles driven covers some parallel street parking. Since each parallel parking spot has a length of about 24 feet ( $4.54 * 10^{-3}$  miles), then each car drives past about 220 spots a day. If probe cars were fitted with adequate parking spotter sensors, we would theoretically need 28 cars to cover the 6100 spaces fitted with parking meters in Santa Monica.*

*Santa Monica is about  $15.9 \text{ mi}^2$ . Assuming 1/4th of that area is allocated for parking ( $3.975 \text{ mi}^2$ ). A standard parking spot covers  $162 \text{ ft}^2$ , which is about  $5.81 * 10^{-6} \text{ miles}^2$ . Thus there would be about 684,082 parking spots in total in Santa Monica.*

*The above-mentioned budget of \$4,500,000 therefore only covers 0.89% of all parking spots. On the other hand, we would need about 3109 cars fitted with parking spotter sensors to cover the 684,082 total spots (assuming no two cars drive past the same parking spot). To ensure a maximum efficiency, 5000 vehicles can be considered instead. If each probe car is fitted with 2 \$150 sensors, then the total budget to map all the parking spots of Santa Monica would be about \$1,400,850.*

*The occupancy of parking spots throughout the entire city of Santa Monica can therefore be accurately determined with only a third of the city's Parking budget (\$1,400,850 as opposed \$4,500,000).*

In that case, a fleet of vehicles equipped with accurate parking spotter sensors and communicating with a server should be deployed. Compared to fitting individual spots with sensors, this method is much more cost effective, efficient, and easier to implement.

## **2.1.2 Ultrasonic Sensors**

### **2.1.2.1 Overview of Ultrasonic Sensors**

Today's vehicles are equipped with various hi-tech sensors to measure several car properties and environmental factors. For instance, the most common types of sensors are speed/timing sensors (registering engine speed among other timing properties), position sensors (used for steering wheel angle and engine throttle plate angle), temperature sensors (to retrieve coolant, engine, fuel, and environment temperatures), and pressure sensors (Fleming, 2008).

Recently, car manufacturers began implementing ultrasonic sensors to detect obstacles while backing up or driving at low speeds, as well as offer parking assist functions to drivers. While these sensors are convenient for low speed applications and large object detection (other vehicles), their efficiency is questionable since frequencies are typically low (around 50 Hz), with a limited range (2-4 m), and might be affected by severe weather conditions (Fleming, 2008). Moreover, because of their limited angular coverage, several ultrasonic sensors need to be implemented on each side of a car, as seen in Figure 2.



**Figure 2: Installing several ultrasonic sensors on the latest cars. The arcs represent the ultrasonic sensors and their reach (Kohler, Connette, & Verl, 2013)**

Park et al. explain that the ultrasonic beam width ( $\pm \theta_0$ ) is usually uncertain: this would result in an object's width being represented larger than it actually is. If an empty parking spot is surrounded by parked vehicles on both sides, or limited by a beam structure (indoor garage), then these objects' width would be measured to be greater than they are. Empty parking spaces are therefore measured to be narrower than they are (Figure 3). This issue can be resolved by increasing the center frequency  $f_r$  (mean of the lower and upper cutoff frequencies), or increasing the diameter of the transmitter  $a$ , since:

$$\theta_0 = \sin^{-1} \left( \frac{0.61 * \lambda}{a} \right)$$

**Equation 1: Ultrasonic beam width calculation (Park, Kim, Seo, Kim, & Lee, 2008)**

$$\lambda = c / f_r$$

**Equation 2: Wavelength calculation**



Consequently, as the center frequency  $f_r$  increases, the wavelength ( $\lambda$ ) decreases, resulting in a smaller beam width  $\theta_0$ . On the other hand, a reduced  $\theta_0$  would decrease the incidence angle, producing an ultrasonic beam with multiple paths, possibly leading to measurement errors (Park, Kim, Seo, Kim, & Lee, 2008).

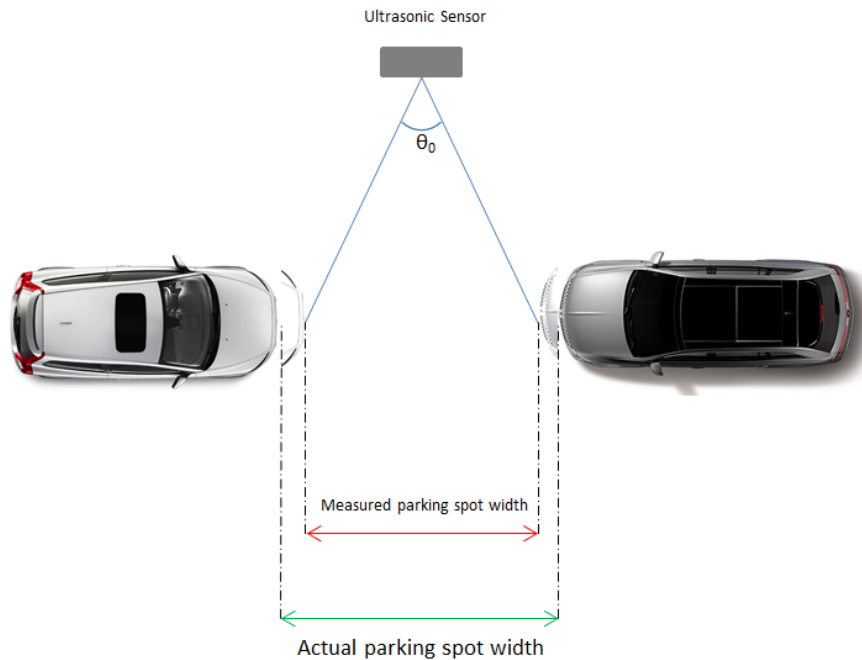


**Figure 3: Ultrasonic beam width uncertainty, measuring a narrower empty parking spot**

The authors proceed to evaluate ultrasound sensors, utilizing multiple echoes to build more accurate parking maps. Moreover, they suggest using a diagonal sensor since it provides the benefit of mapping the side of parking spots.

Using the Time of Flight (TOF) method, Park et al. explain how the distance  $R$  from a vehicle is computed:

$$R = \frac{c \cdot t_0}{2}$$

**Equation 3: Calculating the distance from the vehicle**

In Equation 3,  $c$  is the speed of sound, and  $t_0$  is the time it took for the echo to be sent out from the sensor and received. The same method can also be used when installing multiple sensors (Park, Kim, Seo, Kim, & Lee, 2008).

In Figure 4, Park et al. try to estimate the shape of the surface detected by the ultrasonics. Their method is simple: the ultrasonic sensors can either identify a plane or an edge. As seen in Figure 4.a, if the difference between the distances retrieved from echo2 and echo1 is smaller than a certain threshold, then the surface is a plane. Otherwise, the surface is an edge. This method works well for sharp edges, but the rounded edges of cars are problematic. Figure 4.e and Figure 4.f show how the edge surface is estimated to be a plane since the aforementioned distance difference is smaller than the threshold.

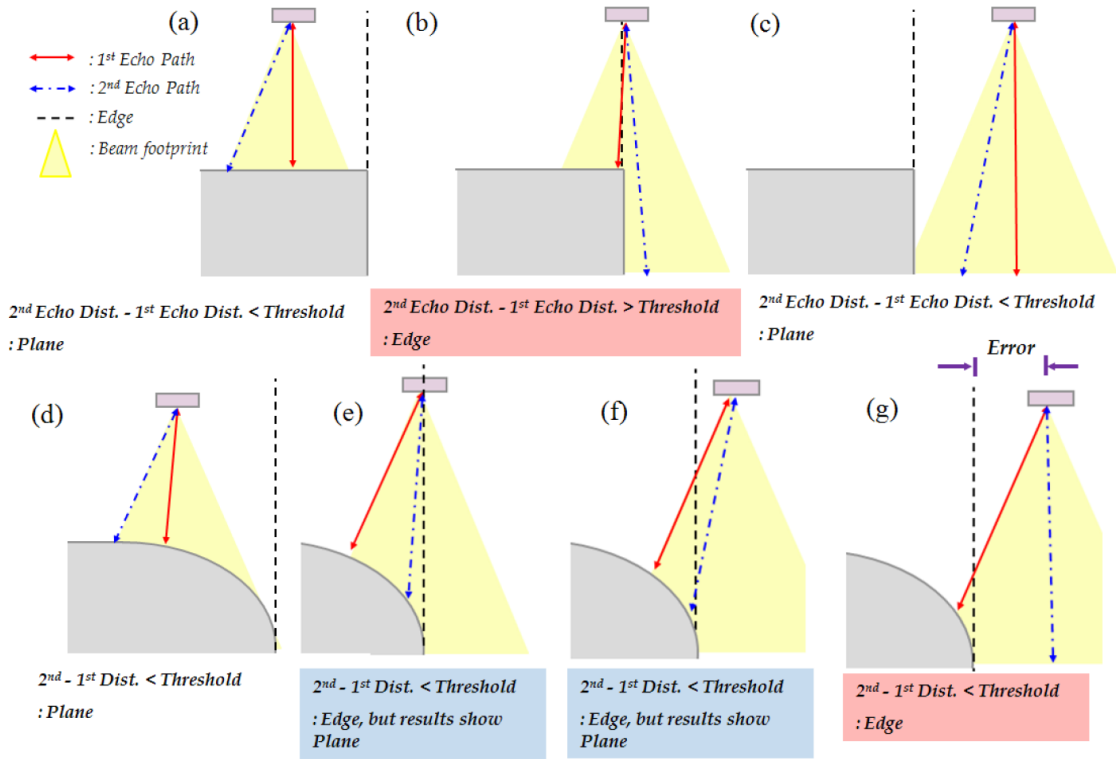


Figure 4: Classification of surface shape for right angle edge side and rounded edge sides (Park, Kim, Seo, Kim, & Lee, 2008)

What if there is a scenario where the actual ultrasonic sensors currently installed on vehicles are faulty and not operating correctly? Abdel-Hafez et al. worked on implementing a “fault detection and identification (FDI) routine” to evaluate the reliability of a car’s ultrasonic sensors. The authors generate a list of possible errors that might occur, and the probability of each hypothesis is updated as sensor data is retrieved. As the probability of the hypotheses is updated, the correct hypothesis is identified when it approaches a value of 1 (Abdel-Hafez, Al Nabulsi, Jafari, Al Zaabi, Sleiman, & AbuHatab, 2011).

As seen in Figure 5, the authors set up 4 ultrasonic sensors, each having a frequency of 40 kHz, and range of 0.03-3 m on the side of a robot. The first setup shows the sensors aligned vertically (Figure 5.a), whereas the robot was angled for the second setup (Figure 5.b).

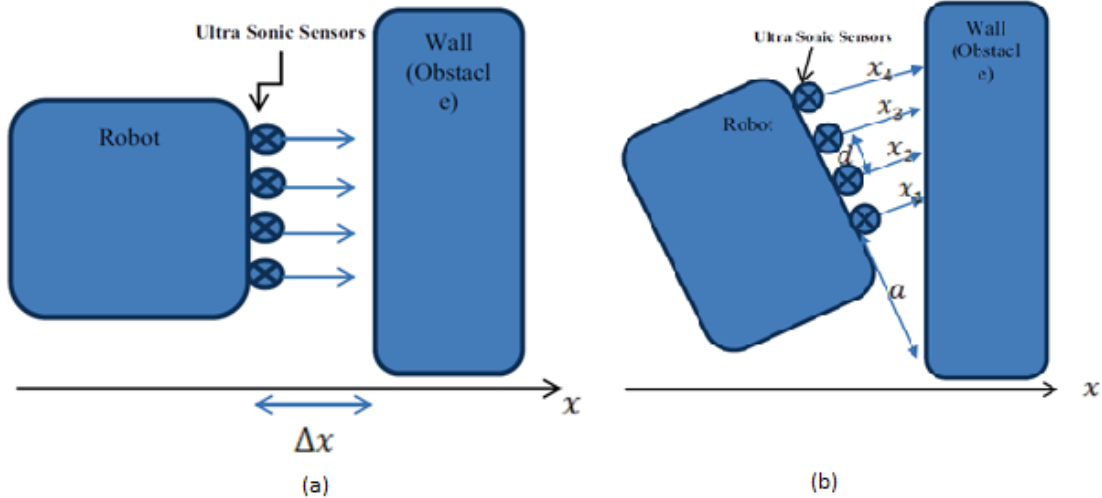


Figure 5: Experimental (a) Setups A, and (b) B (Abdel-Hafez, Al Nabulsi, Jafari, Al Zaabi, Sleiman, & AbuHatab, 2011)

On each sensor, faults of 10, 5, 0, -5 and -10 cm were hypothesized. It was also assumed that only one sensor will be faulty at a given time. The algorithm Abdel-Hafez et al. generated assumes all 21 hypotheses to have an equal probability. As data is gathered, each hypothesis's probability is updated. A fault is signaled as a probability approaches a value of 1, signaling a correct hypothesis is identified.

The authors began by performing tests to ensure that the algorithm is working properly: since no faults were introduced, a probability of 1 should be computed for the case where the hypothesis states that no fault is detected. Abdel-Hafez et al. then tested

the algorithm for the first case where the robot is not angled, having a 10 cm bias for sensor 2. Throughout their experiments, the algorithm correctly detects the bias as the probability that the hypothesis is correct converges to 1. Abdel-Hafez et al.'s system also checks the probability associated with a no fault hypothesis and with a 10 cm bias on sensor 1. It was determined that the probability converges to 0, indicating a wrongful hypothesis is detected (Abdel-Hafez, Al Nabulsi, Jafari, Al Zaabi, Sleiman, & AbuHatab, 2011).

The algorithm was then tested for the inclined robot, with a 10 cm bias induced for sensor 2. The authors notice that the probabilities associated with a no fault hypothesis and a -10 cm bias on sensor 3 converge to 0. However the probability associated with a 10 cm bias on sensor 2 converges to 1, proving that the algorithm again works in this situation.

This FDI algorithm correctly identifies sensor faults, and is essential for vehicle ultrasonic sensor applications (Abdel-Hafez, Al Nabulsi, Jafari, Al Zaabi, Sleiman, & AbuHatab, 2011).

#### 2.1.2.2 Experimental Implementation of Ultrasonic Sensors

“ParkNet” is a mobile system which provides parking lot information based on probe cars that collect and transmit information while driving by parking spots. To determine parking spot availability, a side mounted ultrasonic sensor and GPS receiver are used in parallel. The gathered information is then sent to a central server that provides a real-time map of the parking lot for customers (Mathur, et al., 2010).

The authors emphasize the benefits of installing the sensors on government vehicles or taxi. Their system consists of an ultrasonic sensor attached to the side of a probe vehicle, consistently retrieving the distance from the sensor and reporting GPS position to a mobile system. The collected information is linked together through environmental fingerprinting, which uses landmarks to correctly identify the GPS data. Mathur et al. explain that the price savings occur because they assume that the status of parking spots does not vary greatly with time; hence continuous sensing from pavement installed sensors is highly unnecessary (Mathur, et al., 2010).

Experimentally, the authors show through 500 miles of driving over 2 months that parking spots are identified correctly 95% of the time and parking lots are mapped with 90% accuracy. Future plans are also made for implementing ParkNet in a city such as San Francisco: by monitoring 500 taxicabs using GPS, Mathur et al. show that installing ParkNet systems would be 10 to 15 times more cost effective than having individual sensors for every parking spot (Mathur, et al., 2010). This falls in line with the Santa Monica example taken in Chapter 2.1.1.

Mathur et al. explain that parking information regarding lots can be easily obtained from parking gate operators. However information about roadside parking proves much more difficult since an efficient sensing system has not been installed yet. Eventual implementation of such systems would allow concerned government agencies to correctly place and price parking meters, and better manage traffic congestion.

As explained previously, sensors have already been installed in asphalt to monitor individual parking spots. A San Francisco project employs this method and covers 25%

of parking spots, costing several million dollars. While this solution may work in the short term, its drawbacks outweigh the advantages: these projects usually have extremely high costs, parking availability can only be determined for sensor-fitted spots, wireless relay nodes need to be installed on public property, and high maintenance costs need to be accounted for.

The authors also explore the previously mentioned idea of modifying ultrasonic sensors already installed on cars to report vacant or closed parking spots.

Some of the design objectives and necessities that this type of project requires are: finding low cost sensors, anticipating a low vehicle participation rate, being able to identify parking spot orientation based on collected data, and eventually wirelessly send out data to main servers (Figure 6). Mathur et al. also believe this data can assist parking enforcement.

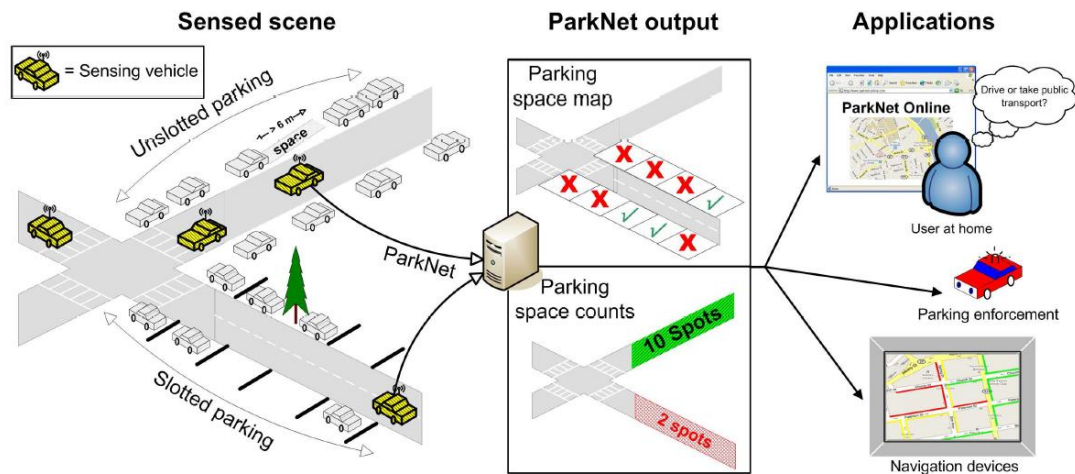


**Figure 6:** A diagram depicting the various scenarios and events involved in the detection of parking space using mobile sensors (Mathur, et al., 2010)

The vision is that several vehicles equipped with these sensors could transmit data to a server using a cellular or Wi-Fi network. This data could be used to generate parking layout maps and inform customers of available parking spots.

The authors explain that they chose ultrasonic sensors because of their cheap price, higher efficiency in the nighttime, and their extensive use in the automotive market. The sensors were mounted on the passenger side of cars, and a camera was installed as a ground truth source. The sensors emitted sound waves every 50 ms, with a maximum range of 6.5 m. The data is then combined with GPS data and analyzed by probabilistic detection algorithms, as seen in Figure 7 and Figure 8 (Mathur, et al., 2010).

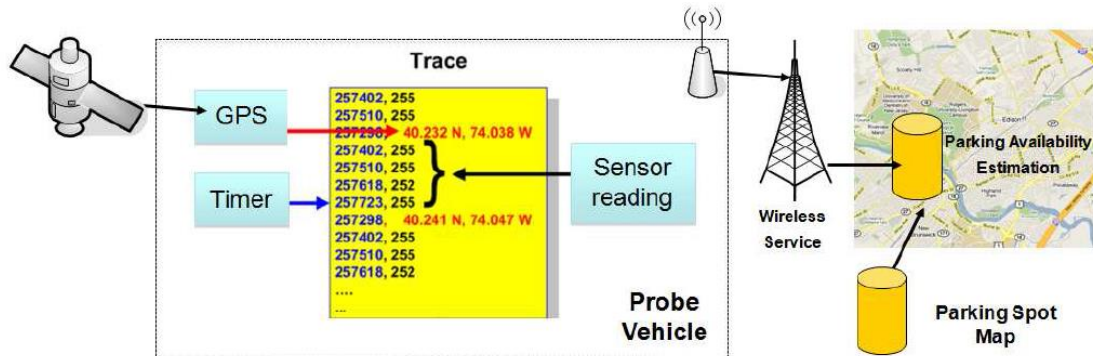


Figure 7: Schematic diagram explaining the overall architecture of the system (Mathur, et al., 2010)





**Figure 8: (a) An image of the ultrasonic sensor side-mounted on a car (b) the java applet used for recording ground truth from images. (c) The map of the data collection area (Mathur, et al., 2010)**

This system was tested on 3 probe cars, collecting data for over 2 months around a parking lot in New Jersey. For that period of time, around 500 miles of data was gathered. Mathur et al. note that the data collection process was not altered in any way, thus drivers had no control over the ultrasonic sensor data. Also, ground truth information was obtained by attaching a gaming webcam, and ultrasonic data was compared to that information.

The GPS is used to set up boundaries for the testing application: if the probe car enters a virtual box bounded by GPS coordinates, the application is launched and the data collection process is started. On the other hand, if the probe car leaves this bounding box, the application is stopped.

The authors' detection algorithm is similar to the one explored later in this thesis (Chapter 3.3.3). Figure 9 shows typical ultrasonic readings detecting two cars parked far away from each other (Figure 9.a), and two other cars parked closer (Figure 9.b) to one another.

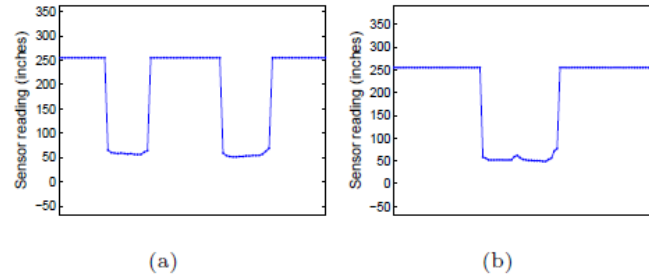


**Figure 9: Dips in the sensor reading as a sensing vehicle drives past (a) two parked cars with some space between them, and (b) two very closely spaced parked cars (Mathur, et al., 2010)**

In (Mathur, et al., 2010), some major drawbacks of the ultrasonic sensors are pointed out: ultrasonic sensors emit sound waves with a wide range of detection. That is why some tight spaces between cars might not be picked up, as seen in Figure 9.b and explained in Chapter 2.1.2.1. The sensor might therefore detect objects that are not aligned but angled with respect to the sensor. Some of the other system limitations that the authors mention are: the sensor's power source, which added noise to the sensor data. The tougher detection of parking spots on a multilane road was also discussed, but Thornton et al.'s paper explored the method of detecting vehicles on a multiple lane road using an occlusion method (Thornton, Redmill, & Coifman, 2014). Moreover, the probe car's speed used in (Mathur, et al., 2010) needed to be limited to 33 mph: the frequency of the ultrasonic sensor might not be high enough to detect parked vehicles at high traveling velocities.

### **2.1.3 Vision Sensors**

More complex sensors can also be used to locate parking spots and determine their availability. Vision sensors for example, which require accurate camera footage, can be installed onto a probe car to study its surroundings (Son, Kim, & Sohn, 2015), (Makris, Perrollaz, & Laugier, 2013).

Son et al. explain that localization can be performed using multiple vision sensors, necessary for any autonomous driving applications (Son, Kim, & Sohn, 2015). Makris et al. go over an object class recognition method in their paper, which consists of combining image feature detection and depth information to create a probabilistic model of locating a car at a given distance (Makris, Perrollaz, & Laugier, 2013). By running the experiment in an urban environment, and integrating the two information types, the authors manage to improve the efficiency of using vision sensors.

Both papers explain that multiple issues may arise when using said sensors: large variations in illuminations, viewpoint variations, partial occlusions, unintentional sensor displacement, background noise and most importantly, large computational complexity (Son, Kim, & Sohn, 2015), (Makris, Perrollaz, & Laugier, 2013).

### **2.1.4 Anisotropic Magnetoresistive (AMR) Sensors**

Zhang et al.'s paper looks into using anisotropic magnetoresistive (AMR) sensors to develop new algorithms for detecting parking occupancy. After explaining the logic behind their algorithm, the authors test out their sensors in field tests. 82 sensors were

installed over spots in a parking lot and solar powered routers to transmit data were then attached to light poles (Figure 10). After continuously running all 82 sensors for 6 months, Zhang et al. noted an accuracy of about 98% (Zhang, Tao, & Yuan, 2014).

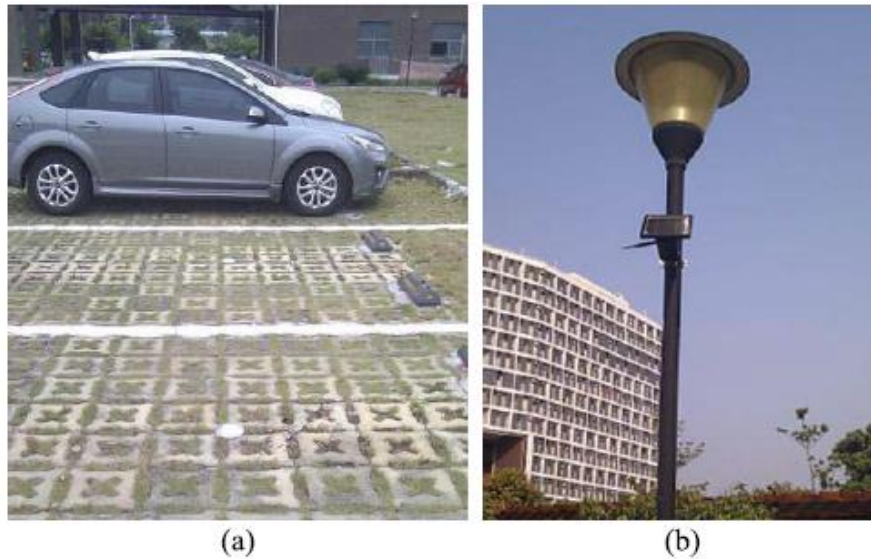


**Figure 10: Devices installed in roadside parking spaces. (a) Sensor nodes, (b) Router (Zhang, Tao, & Yuan, 2014)**

Previous studies have been conducted on AMR sensors which also showed highly accurate results: 99% accuracy for vehicle detection, and 90% accuracy for vehicle length and speed estimation. Other practical uses for AMR sensors have also been explored, mainly vehicle position estimation by change in the magnetic as the car drives away from the sensor.

As Zhang et al. explain, wireless AMR sensors are characterized by their low cost and power requirements, high accuracy, and small size. To measure the geomagnetic field around a specific axis, adaptive threshold detection algorithms are used. The

parking activity is divided into 3 steps: entering, parking and exiting. As seen in Figure 11, the magnetic field is stable before the car approaches, disturbed as the car enters and leaves, and is stable but detects a stable disturbance as the car is parked (Zhang, Tao, & Yuan, 2014).

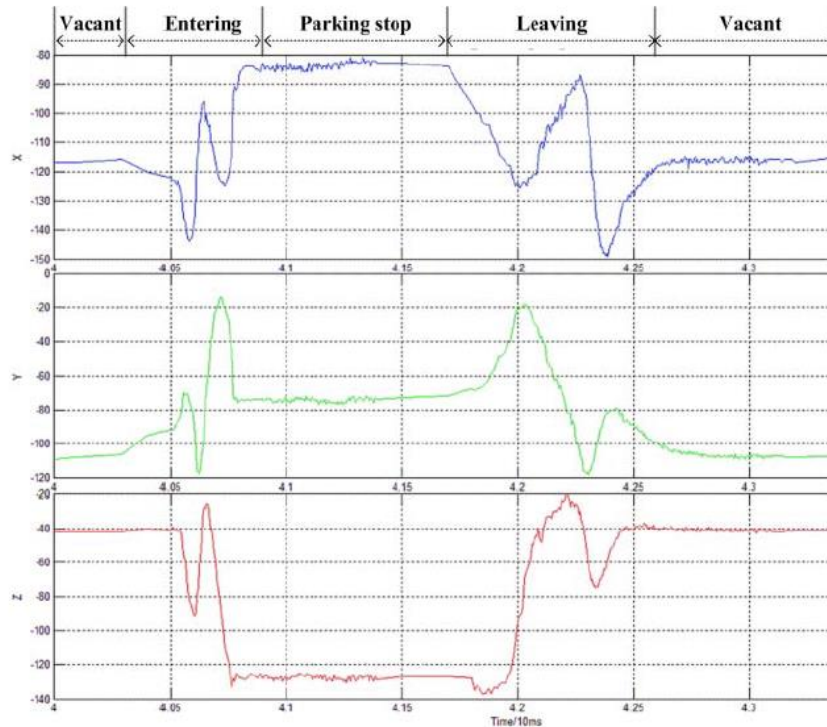


**Figure 11: Three axes magnetic signature of a parking space (Zhang, Tao, & Yuan, 2014)**

Some drawbacks from this method are also highlighted in the paper: in low Signal-Noise-Ratio (SNR), there is no real way of distinguishing between interference noise and a parking vehicle. Furthermore, different parking spots have varying geomagnetic fields. This makes selecting a certain uniform threshold for this application erroneous. These facts, coupled with the low success rate of analyzing the wave patterns limit the application of AMR sensors for parking detection.

Some sensors are commercially available such as the SENSIT system, which uses infrared and magnetic sensors, with accuracy close to 100%. These systems require individual sensors to be installed for each parking spot. As seen in Chapter 2.1, these setups are not cost effective. Zhang et al.'s paper focuses on two main criteria not explored previously: proposing a new algorithm for vehicle detection based on analyzing the characteristics of the geomagnetic signal disturbance. This method should be immune to interference signals. The authors also looked into the interval when a car leaves a parking spot, which should have the inverse signal signature of a car entering a parking spot (Zhang, Tao, & Yuan, 2014).

Figure 12 shows a graphical client interface where customers can see the status of the parking lot and locate which spot is vacant (green spots). This figure also shows the wireless network set up between sensors and servers. To verify the validity of the entire set up, the experiment was run for 6 consecutive months and was found to have an accuracy of 98.9%.

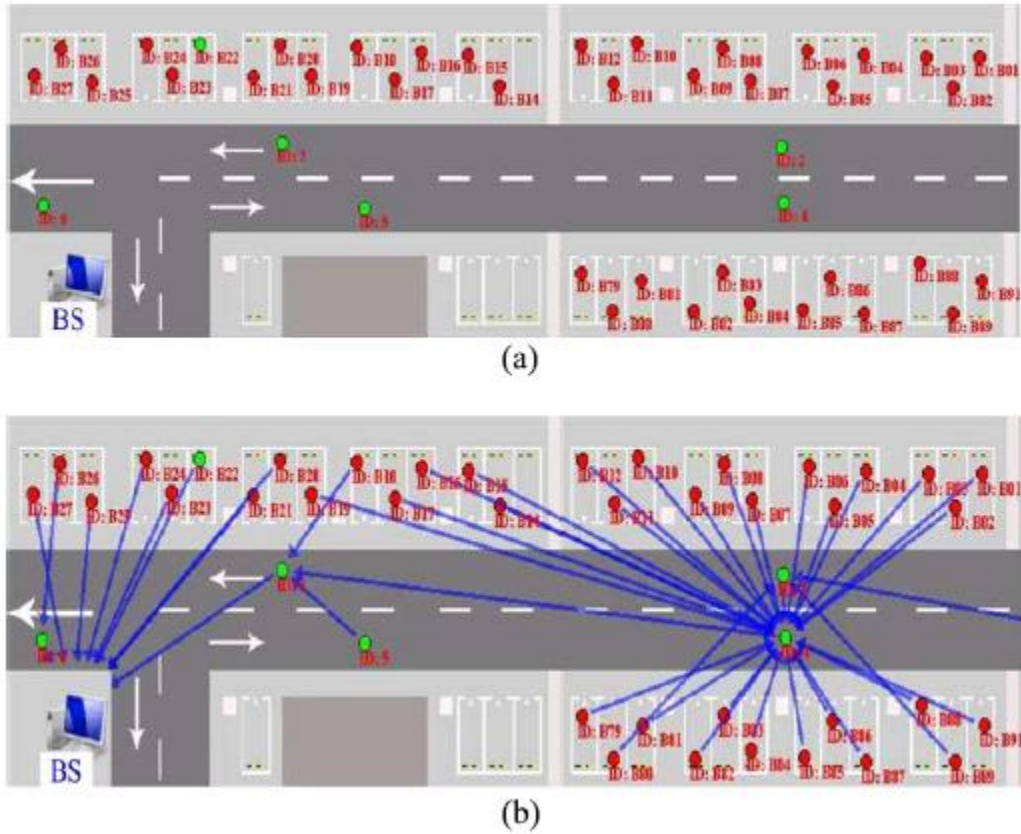


Figure 12: Depictions of the management system. (a) Sensor nodes installed in parking spots. (b) Topology of the network (Zhang, Tao, & Yuan, 2014)

The system seems very accurate and applicable to parking lots. It is nevertheless important to note that, as highlighted before, this type of setup necessitates installing individual sensors for each parking spot, thus limiting the scope of applicability.

### 2.1.5 Using Models to Predict Parking Spot Occupancy

Klappenecker et al. devise a method for predicting the number of free parking spaces by modeling a lot using a continuous Markov chain, following Caliskan, Barthels, Scheurmann and Mauve. Through a Vehicular Ad Hoc Network (VANET), information about the parking lot such as capacity, parking rate, occupied spaces, and vehicle arrival/departure is obtained. This entails using fewer sensors than sensors for individual parking spots, then transmitting the data through a vehicular ad hoc network or a mobile cellular network. The advantage of Klappenecker et al.'s method is utilizing a vehicle's navigation system to compute the probability of an available parking spot as the car enters the lot (Klappenecker, Lee, & Welch, 2014).

Since the information provided is historical, the question becomes: *how to predict the availability of a parking space in a correct and efficient way?* In (Klappenecker, Lee, & Welch, 2014) a continuous-time Markov chain is implemented to predict the probability distribution of the number of occupied spots in a parking lot. The information that would be required by the algorithm is: the total number of parking spaces in a lot, the number of occupied spaces, the arrival rate of the vehicles (modeled by Klappenecker et al. using a Poisson distribution), the parking rate (exponential distribution), and the relative time.

The authors explain their methodology and thought process for constructing the algorithm, and test it for two different scenarios. For the first example, the parking lot is estimated to have: a total of 1000 spots (where 900 are occupied), an arrival rate of .3268



cars per second, and a parking time of 3060 seconds (Klappenecker, Lee, & Welch, 2014).

The first scenario is having a high number of cars arrive at an already rather full parking lot. The second scenario involves cars still reaching a full parking lot, but with lower frequency than in the first scenario.

The authors generate probability distribution curves of the occupancy number, 1, 4 and 16 minutes after the parking lot information is transmitted. For the first scenario, Klappenecker et al. notice that the probability that the parking lot is completely full decreases from about 0.067 % to 0.02 % from 60 seconds to 16 minutes after the initial parking request, but remaining around  $10^{-2}$  % the entire time.

For the second scenario, the lot is completely full (1000 closed spots), but only 0.2124 cars drive into the lot. Klappenecker et al. notice that a minute after the information is sent, the probability that the lot remains completely full is less than 0.025. In addition, after 16 minutes, that probability drops down to less than  $10^{-5}$ .

Klappenecker et al. evaluate a model described by Caliskan et al., which focuses on larger lots such as airport and mall parking. They showed that accurate predictions can be made with regards to future parking occupancies. The major limitation of this model is the need to keep an accurate track of the number of cars entering a lot, and a constant update on its occupancy. Moreover, some of the assumptions taken by the authors might not hold if admission is not strictly enforced, parking data is erroneous, or a single reported parameter is not available.

### 2.1.6 Wireless Sensor Networks

The basis of Wireless Sensor Networks (WSN) usually involves implementing hardware and software updates to a parking lot, as seen briefly in Chapter 2.1.2.2. On the hardware side, the goal is to deploy low-cost sensors throughout the lot with the aim of detecting and tracking vehicles, and possibly mapping entire lots for parking management applications (Zhang, Tao, & Yuan, 2014). These sensors are usually acoustic, light and sound sensors, such as the sensor systems covered previously. The novelty behind WSN is the software implementation. Many papers have explored this option and detailed their findings ( Tang, Zheng, & Cao, 2006), (Gu, Zhang, Yu, & Liu, 2012), (Srikanth, Pramod, Dileep, Tapas, Patil, & Sarat, 2009), (Yang, Portilla, & Riesgo, 2012), (Chinrungrueng, Sunantachaikul, & Triamlumlerd, 2007) . As explained by Tang et al., the goal behind the software is to transmit sensor information to a main database. This data can then be evaluated in real time by algorithms and applications to actively manage the parking lot, as well as generate some useful statistics, and facilitate parking for customers ( Tang, Zheng, & Cao, 2006).

Tang et al. specify the hardware they use (Motes, Sensor Boards and Gateways) and also explain the event-based architecture they followed, as seen in Figure 13.

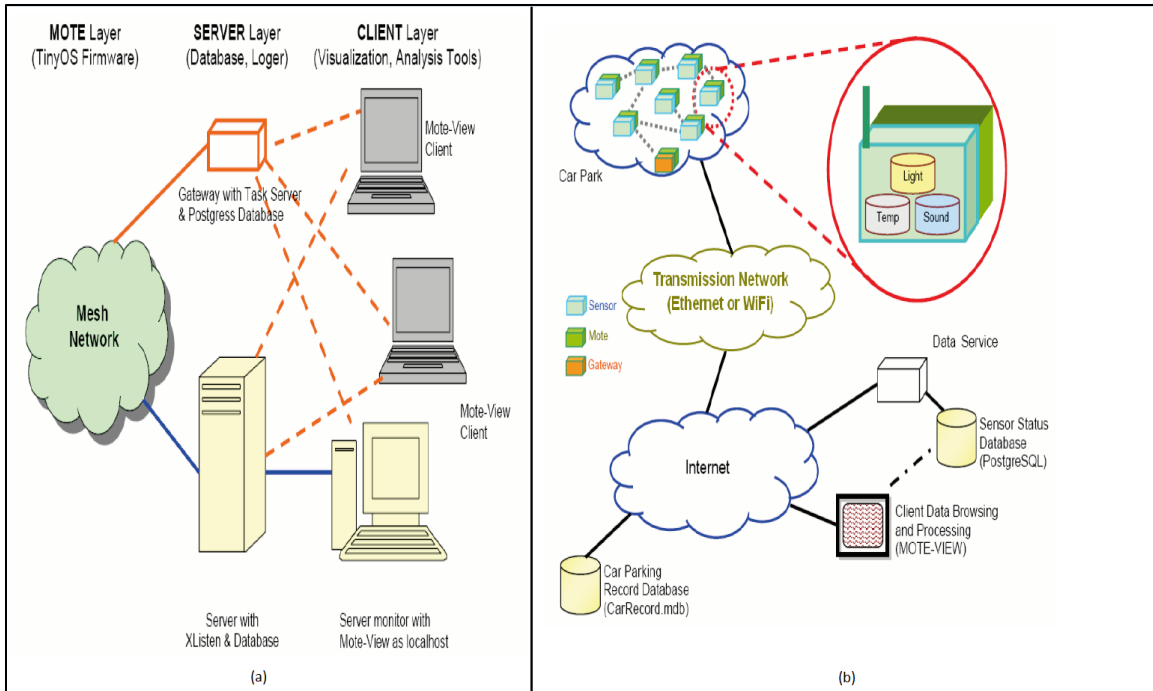


**Figure 13: (a) 3-layer framework of WSN-based system, (b) the architecture of the system ( Tang, Zheng, & Cao, 2006)**

The authors tested their system on a prototype model of a parking lot and obtain positive results; for example sensors were able to locate parked cars and update the parking spot status in the database. The number of available parking spots and a light indicator signaling that event were also among the features the WSN was tested for.

Many papers have been written on Wireless Sensor Networks ( Tang, Zheng, & Cao, 2006), (Gu, Zhang, Yu, & Liu, 2012), (Srikanth, Pramod, Dileep, Tapas, Patil, & Sarat, 2009), (Yang, Portilla, & Riesgo, 2012), (Chinrungrueng, Sunantachaikul, & Triamlumlerd, 2007). Thus we can assume that the technology is highly implementable and tested. But as mentioned previously, these Wireless Sensor Networks need to be implemented and tested for each individual parking lot. This places a limit on the scope of tested lots.

### **2.1.7 Overview of Sensor Technologies**

Several sensor technologies and prediction algorithms have been researched and applied for parking spot detection. This chapter covered the most effective technologies, such as wireless sensor networks, ultrasonic, video, and AMR sensors. Each technology had its advantages and drawbacks: ultrasonic sensors for example are cheap and easy to implement, but possess low frequencies and efficiencies. Vision sensors on the other hand are effective and can be used for multiple applications (parking occupancy detection and autonomous driving), but are computationally complex and depend heavily on lighting conditions.

## **2.2 The Need for Laser Sensors**

The sensors discussed in Chapter 2.1 each exhibit several drawbacks that would limit their efficiency in parking spot detection. This thesis will therefore focus on testing an alternative technology using laser sensors which are accurate, have long range, and fast frequencies.

### **2.2.1 Available Laser Sensor Technology**

#### **2.2.1.1 Laser Sensor Implementation**

In their paper, Ono et al. use a laser range finder vertically mounted on a probe car, and describe their method of parked-vehicle detection. Since their ultimate goal is

mapping a “geometric model” of a town, they plan on reconstructing a 3D set of points representing actual road side scenarios, possibly generating information on town activities in Japan (Ono, Kagesawa, & Ikeuchi, 2002).


The authors put in place three requirements that the sensor must follow: It should be accurate enough to obtain a geometric model of the town, the laser sensor should be safe and not harmful to pedestrians, and it should scan on a line. Ono et al. explain that the third requirement is important since a line sensor, as opposed to a 2D laser sensor (Thornton, Redmill, & Coifman, 2014), has a higher accuracy and frequency since it does not measure distances in a 2D plane, and therefore requires less computational power. However, to get a more accurate 2D representation of parked cars, the laser range sensor can be rotated about its horizontal axis (Figure 14). The measured distances can then be adjusted accordingly, and a 2D map can be generated (Ono, Kagesawa, & Ikeuchi, 2002).

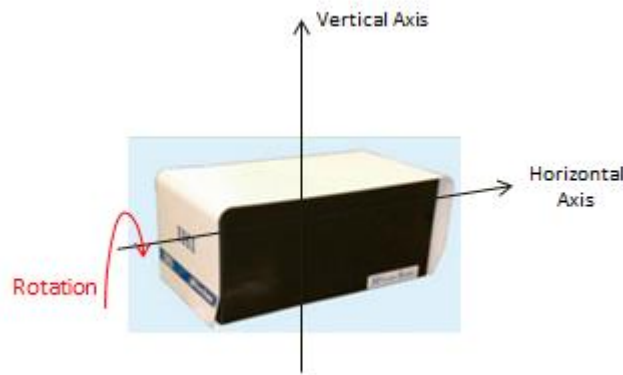


**Figure 14: Rotation of the laser sensor**

The sensor used in Ono et al.’s experiments is an “IHI range sensor”, initially developed to detect pedestrians at intersections, rendering it safe for the public. Its accuracy is about  $\pm 50$  cm, leading the authors to experiment with a “line sensing

system”. Moreover, the sensor weighs 14 kg with dimensions of 560 mm x 240 mm x 280 mm (Figure 15), suggesting that it is a bulky and cumbersome attachment to the probe vehicle.

Item		Specification	Appearance of Laser radar head
Detection object		Vehicle (incl. two-wheeled motor vehicle), pedestrian, bicycle, and obstacle, etc.	 <p>Dimensions : 560mm x 240mm x 280mm Weight : 14kg</p>
Content of detection		Detection of position and speed and judgments of type	
Range of measurement	range horizontal picture corner (degree)	90	
	vertical picture corner (degree)	60	
	ranges (m)	200(Max)	
Detection time(s)		0.1~3	
Positional detection accuracy (m)		± 0.1	
speed detection accuracy	speed (km/h) of object	0~120	
	measurement speed (km/h) at detection time	± 5	
Light source		nearinfrared laser diode(IEC60825-1 Class1)	

**Figure 15: IHI 3D Laser Radar (IHI Corporation, 2010)**

Since the frequency of the sensor is low, and the distance between the probe car and the parked vehicles is variable, experimental readings were not conclusive. As an example, Ono et al. explain that without vertical line sensing, the range sensor could not differentiate between parked cars and objects on the street, and could not detect black vehicles because of its low power (Ono, Kagesawa, & Ikeuchi, 2002).

As the probe vehicle is moving at speeds upward of 30 km/h (18.6 mph), vertical line sensing can be performed by generating one vertical line depth image every 10 ms, resulting in an interval of 10 cm between two vertical scan lines.

To obtain a depth image of the experimental situation, the authors propose normalizing the sequence of the one-line depth images so that each line image is assigned to an exact position in the real world depth image.

Since black vehicles might not be detected by their sensor, Ono et al. could not truncate undesirable points and focus on specific distances. Instead, they had to devise two algorithms to count the number of parked cars (Figure 16): using a depth-curve method and a height-curve method (Ono, Kagesawa, & Ikeuchi, 2002). Figure 17 shows the results of both detection methods.

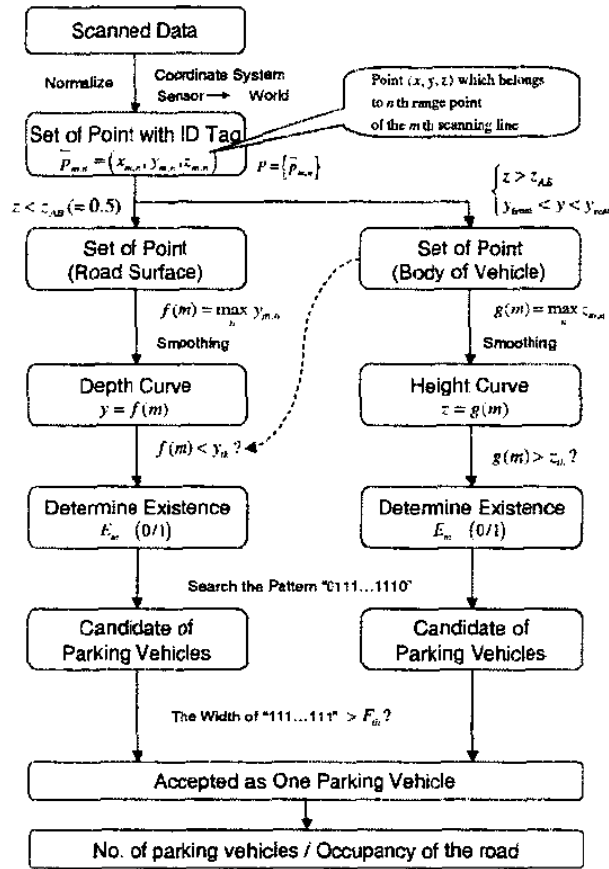


Figure 16: Detection algorithm overview (Ono, Kagesawa, & Ikeuchi, 2002)

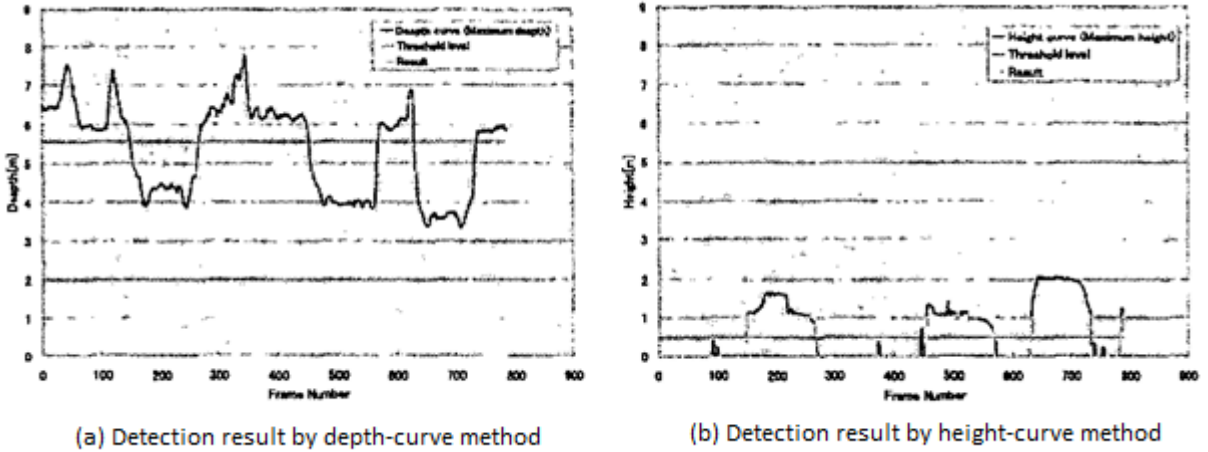


Figure 17: Detection results (a) by depth-curve method, (b) by height-curve method (Ono, Kagesawa, & Ikeuchi, 2002)

To test their setup and logic, Ono et al. performed two outdoor experiments, with varying speeds and densities of traffic. Because of their method, they must assume that the probe car drives in a straight line at either 10 or 20 km/h (Ono, Kagesawa, & Ikeuchi, 2002). After applying their algorithm, the authors were able to detect a total number of 107 vehicles with no errors.

Nevertheless, some drawbacks can be observed from Ono et al.'s paper. The sensor used would not be easily attached to probe vehicle since it weighs 14 kg with dimensions of 560 mm x 240 mm x 280 mm. Furthermore, the sensor's sensitivity is not ideal ( $\pm 50$  cm) for the parking detection application. The authors are also manually counting parked vehicles (neglecting open spots), and do not seem to have an algorithm that automatically computes the actual number of parked cars. This suggests that the counting process could not be automated and information is not transmitted to a cloud/server for parking applications. This analysis is mainly for offline research and statistical analysis for traffic congestion management, as mentioned previously.



Additionally, Ono et al. needed to use detection algorithms such as depth-curve and height curve methods to detect all vehicles. Finally, experiments were only performed for parallel parked vehicles, at 10 and 20 mph (one run each). Other parking layouts (45, 60 and 90 degree parking) were not evaluated, and the probe vehicle speed was not varied appropriately.

#### 2.2.1.2 2D Lidar Implementation

Another study by Thornton et al. uses a 2D LIDAR sensor to automate data collection for parallel parked vehicles around a university campus. The LIDAR provides a precise point cloud of the surrounding environment at high frequency. Thornton et al. employ an algorithm that uses this point cloud to locate vehicles parked on the side of a street, and determine their height and length (Thornton, Redmill, & Coifman, 2014).

For example, curb location and objects on the side of the road are evaluated. Then vehicle sizes, gaps between vehicles, and parking lot occupancy are measured.

Thornton et al.'s sensing system costs about \$10,000 per unit, while they suggest that the cost for fitting a parking lot with the appropriate sensors can be around \$60,000. Their probe vehicle is equipped with 2 main sensors: a 2D LIDAR and a differential global positioning system receiver (DGPS). Additionally, inertial navigation corrections are performed by an onboard speedometer and a yaw gyroscope (Thornton, Redmill, & Coifman, 2014).

The LIDAR scans in a vertical plane at a frequency of 37 Hz covering  $180^\circ$  with a resolution of  $0.5^\circ$ , and has a range of 81 m, with a resolution of 0.01 m. Since the 2D LIDAR is mounted on the driver's side, it measures parallel parking on the opposite side of the road, generating a 3D point cloud, as seen below:

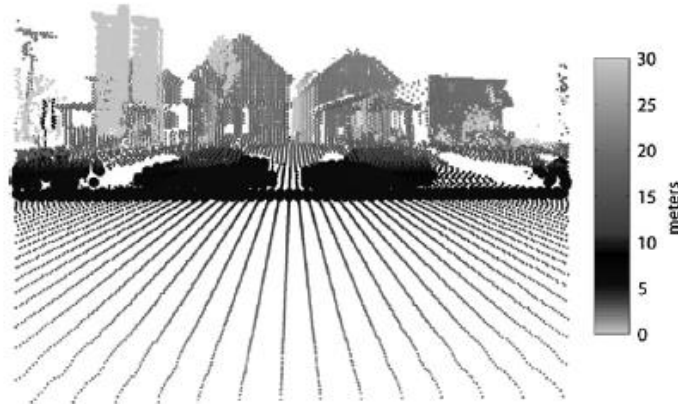


**Figure 18: LIDAR point cloud example (Thornton, Redmill, & Coifman, 2014)**

Cars passing by the side of the vehicle must be occluded since they are not part of the parking lot setup. The complexity of this occlusion step depends on the direction to which the car is driving, its speed and distance from the probe car.

This paper also describes a method of “sectioning” the parking lot strip into a number of spots depending on the width of each parking spot.

As seen in the chart below (Figure 19), the algorithm Thornton et al. developed is divided into three stages: firstly, the position of the probe vehicle is estimated for each LIDAR scan, the data is processed and specifies whether an object is detected, and locates the far side curb. The second stage involves integrating information from successive LIDAR scans to segment vehicles from the background and from one another.

Following the occlusion step, Thornton et al.'s algorithm marks the location of each vehicle, and measures its height, length, and heading. Finally, the vehicle info is assigned to road segments and lanes, noting the occupancy of each parking lot and other vehicle information (e.g. vehicle-to-vehicle gap).

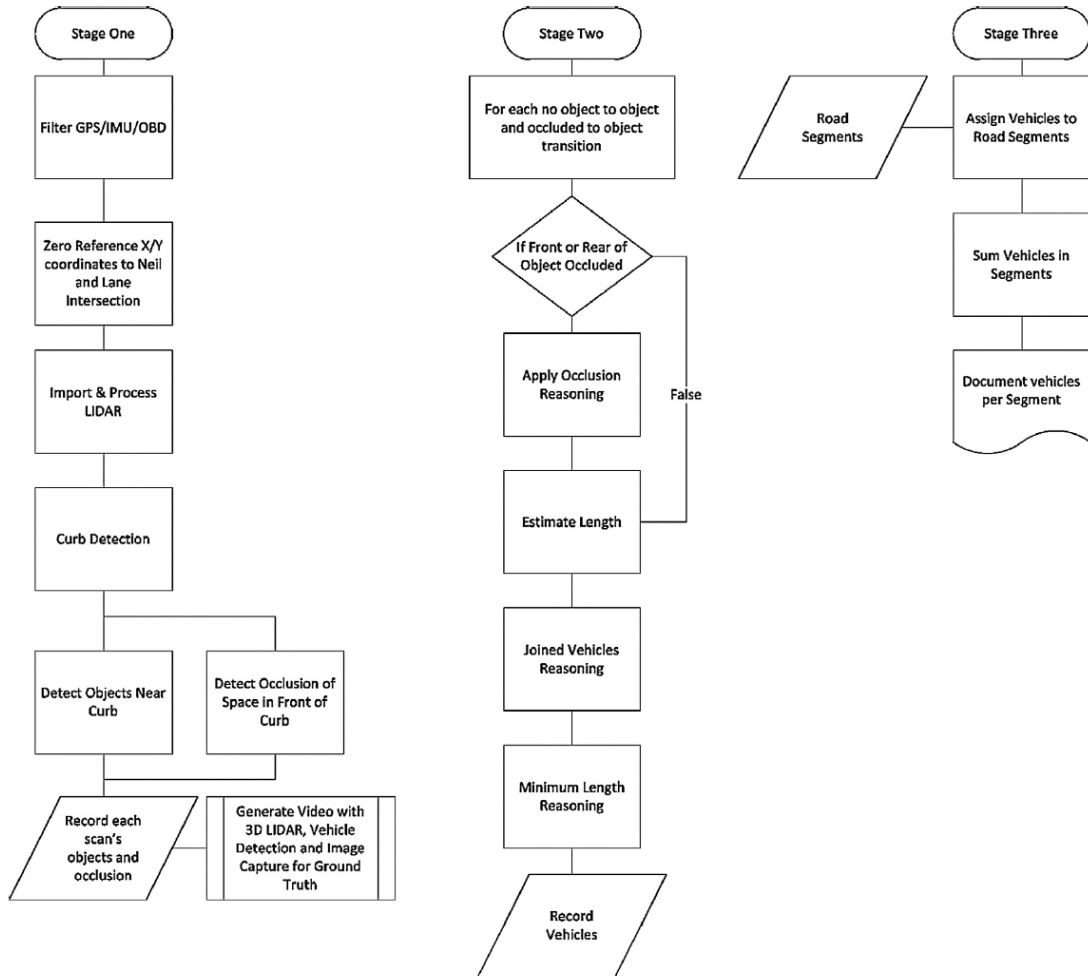
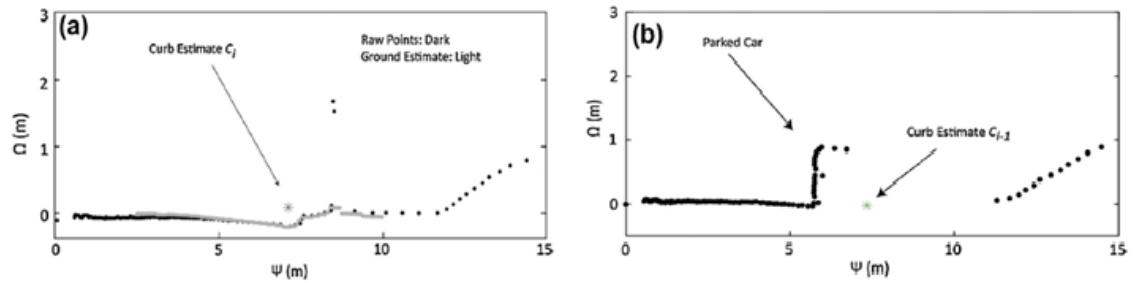


Figure 19: The three stages of the algorithm (Thornton, Redmill, & Coifman, 2014)

After compensating for tilt and other environmental factors, Thornton et al. are able to generate the graphs in Figure 20. They represent the LIDAR data from a single scan with and without a parked car.



**Figure 20: (a) Single LIDAR scan producing raw data points, detecting the ground and curb. (b) Parked car detected and curb location estimated using an estimate from a preceding time sample (Thornton, Redmill, & Coifman, 2014)**

After the curb is located, object and occlusion detection for each scan is performed. The second stage of the algorithm is integrating information across scans. This entails looking at each individual scan, and analyzing where a potential vehicle is spotted (Thornton, Redmill, & Coifman, 2014).

As seen in Figure 21, 3 cases are examined and explained. The first case is where the probe car is driving on the opposite side of the parking lane, without an occluded vehicle present. The second case is where a vehicle drives by the probe car. And finally the last case demonstrates how the gap between two parked cars might not be seen if it is occluded by a moving vehicle.

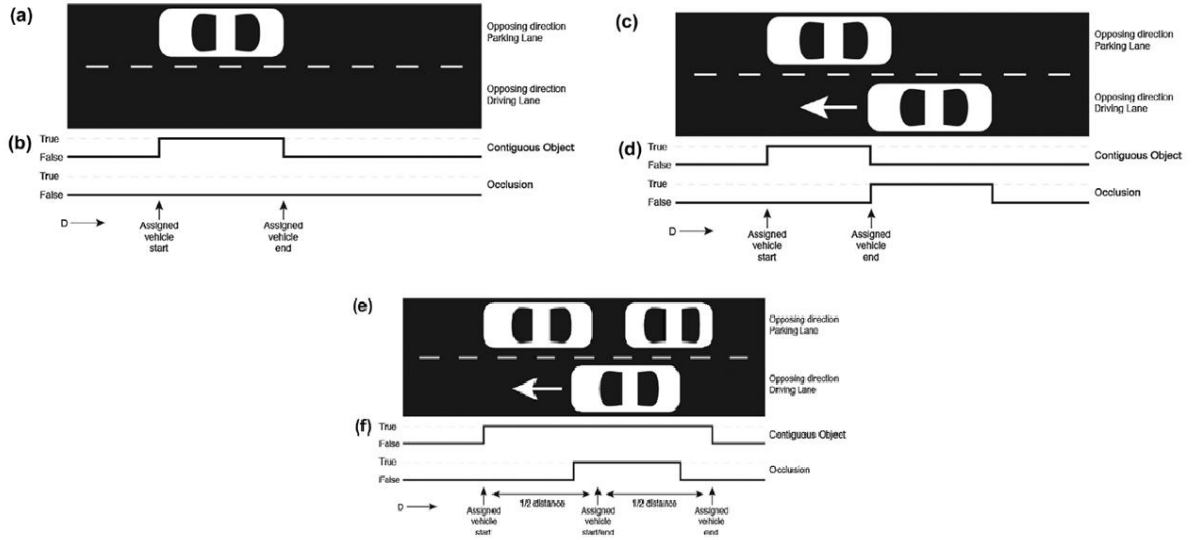


**Figure 21: (a) Opposing lanes viewed by LIDAR and (b) object and occlusion detection by the algorithm. (c) Endpoint occlusion scenario and (d) object and occlusion detection by the algorithm. (e) Occluded gap between parked cars and (f) object and occlusion detection by the algorithm (Thornton, Redmill, & Coifman, 2014)**

The next step in this second stage is length estimation. Assuming the width of a car is between two values, smaller occlusions (such as trees and fire hydrants) can be ignored since they do not represent a car. However this risks overseeing motorcycles, but the frequency of occurrence is usually very low. For large adjacent-object lengths, Thornton et al. assume that the space between parked vehicles was not detected. This led the authors to divide the adjacent space by an assumed generic car width value to get an approximate of the number of cars parked on the side of the road.

Figure 22 shows the results of vehicle lengths and heights, their location with respect to the distance traveled, and gaps between parked vehicles.

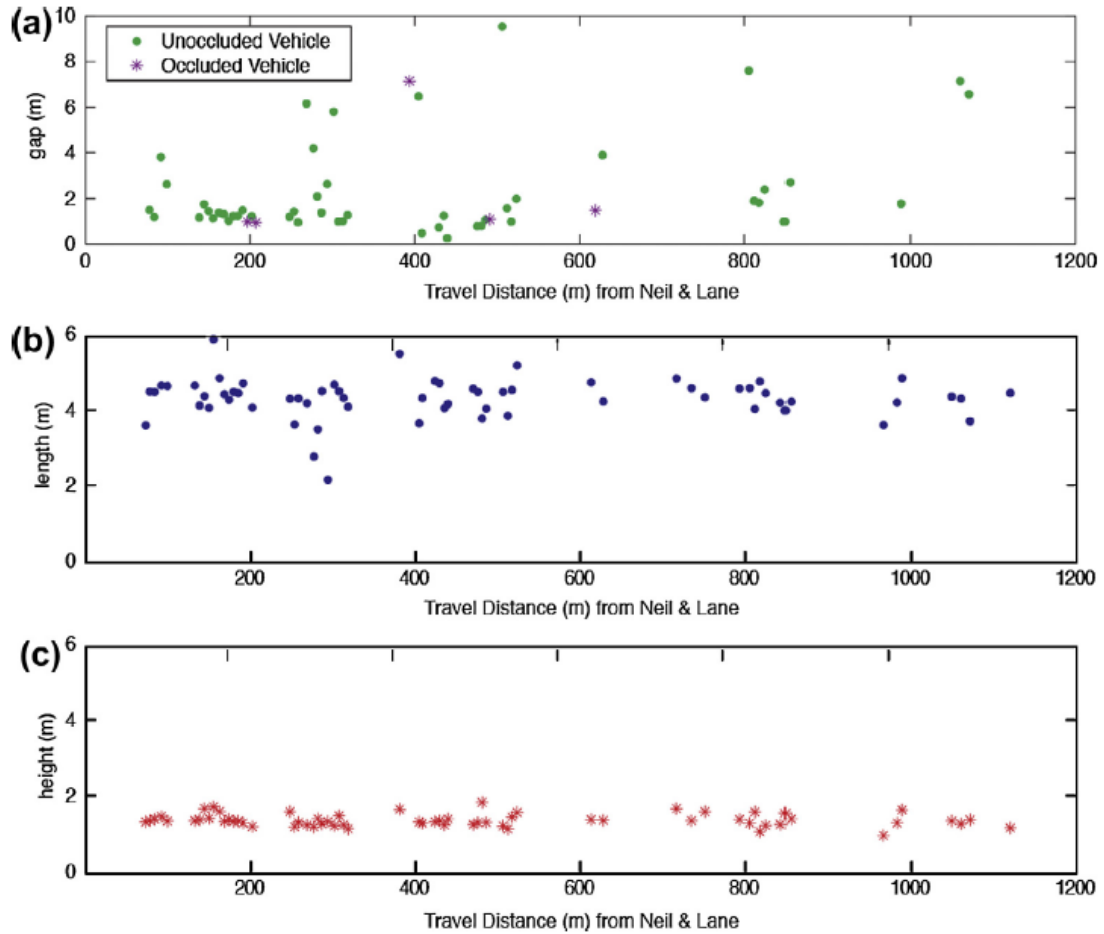


Figure 22: (a) Gaps between parked vehicles, (b) lengths of vehicles, and (c) height of vehicles vs. distance travelled (Thornton, Redmill, & Coifman, 2014)

In the third part of the algorithm, Thornton et al. used Differential GPS (DGPS) data to determine which vehicles are in a parking zone and need to be counted, and which vehicle should be ignored. However the authors also go over two methods not necessitating DGPS data: increasing the tolerance used when locating a car using the LIDAR, or using landmarks on the road to match GPS and LIDAR data. Both options reduce the cost of the sensor system, but allow for more errors in the first case (LIDAR

only), and increasing the complexity of the algorithm in the second case (LIDAR and GPS).

Thornton et al.'s probe vehicle collected data from numerous test runs around a university campus over the course of four years and throughout different seasons. Eventually, 29 runs were chosen at random from this data base. Table 1 shows the difference of number of cars counted between experimental and ground truth data.

**Table 1: Results of LIDAR algorithm detection vs. ground truth data (Thornton, Redmill, & Coifman, 2014)**

Segment	Sum of absolute errors across runs	Total # of vehicles	Relative absolute error (%)
1	1	171	0.6
2	0	401	0
3	6	357	1.7
4	0	196	0
5	2	237	0.8
6	0	98	0
7	1	85	1.2
8	0	193	0
9	1	31	3.2
10	4	104	3.8
Total	15	1873	0.8

The authors explain that potential errors in LIDAR measurements could arise because of the change in geometry of a road, or a specific intersection design where passing cars can occlude parked cars. Out of 1873 vehicles, 15 were miscounted, yielding an error of 0.8% (Thornton, Redmill, & Coifman, 2014). Thornton et al.'s algorithm is therefore effective, and would be beneficial if installed on a public transport vehicle.

However some factors that need to be considered before adaptation are: testing in adverse weather conditions (e.g. rain), the price and bulkiness of the sensor, the difficulty of installing the system onto a probe vehicle, the complexity of the algorithm, and its ability to generate usable real time data transferable to servers or clouds.

### 2.2.2 Combining Laser Sensor Technology and Other Sensors

Tong et al.'s method for extracting a parking lot structure consists of combining LIDAR and Orthophoto (photographic map) data in three steps. Firstly, vehicle locations and their central axis are extracted from a LIDAR scan. The authors then use this axis information to bind the parking lines of a lot extracted from the photographic map. Finally, an “adaptive growth method” is employed to extract the entire parking lot structure from retrieved parking lines and vehicle central axes. Tong et al. set up two new algorithms for this application: the first is for parking lines extraction with principal orientation constraints, and the second deals with determining a parking lot structure based on parameter solution and adaptive growth (Tong, Cheng, Li, Wang, & Du, 2014).

Figure 23 below shows the idea behind finding a parking lot structure: from LIDAR and photographic map data implemented into an algorithm (Figure 23.a), a complete structure recognition is made possible. Information about the parking lot's dimensions, line orientation and occupancy can successfully be computed. Tong et al. explain that this method can offer great advances in parking policies and structures: by correctly monitoring a parking lot, superfluous parking spots and wasteful driving time spent looking for an open spot can be reduced (Tong, Cheng, Li, Wang, & Du, 2014). This might also extend to the world of autonomous driving, as parking lot information is essential when considering the final leg of a car's journey.



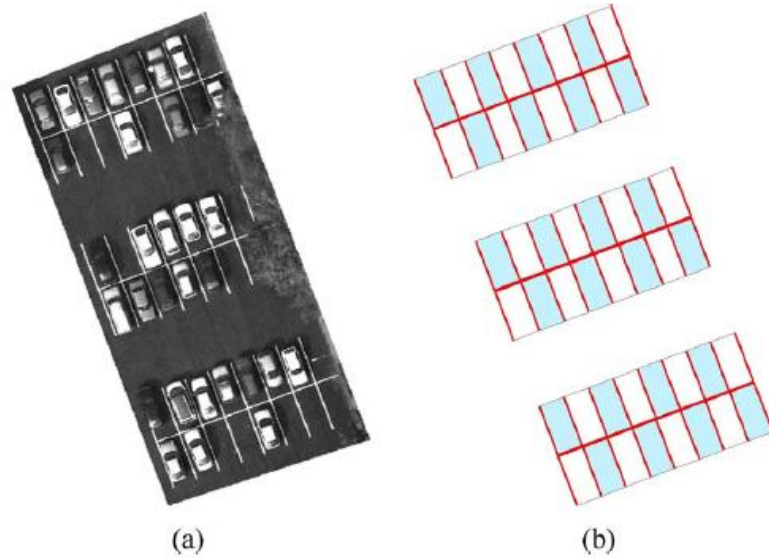


**Figure 23: Determining the parking lot structure automatically using (a) LIDAR data and an aerial snapshot of a parking lot, (b) projected vector structure information (Tong, Cheng, Li, Wang, & Du, 2014)**

As the authors explain, prior art has been developed regarding this issue, mainly by employing optical sensors to extract parking lot structures. But Tong et al. clarify that this method is hindered by “dramatic luminance variations, shadow effect, perspective distortion, and inter-occlusion among vehicles” (Figure 24). However, the proposed method in (Tong, Cheng, Li, Wang, & Du, 2014) showed promising results, and is not affected by the limiting parameters of optical sensor technology.

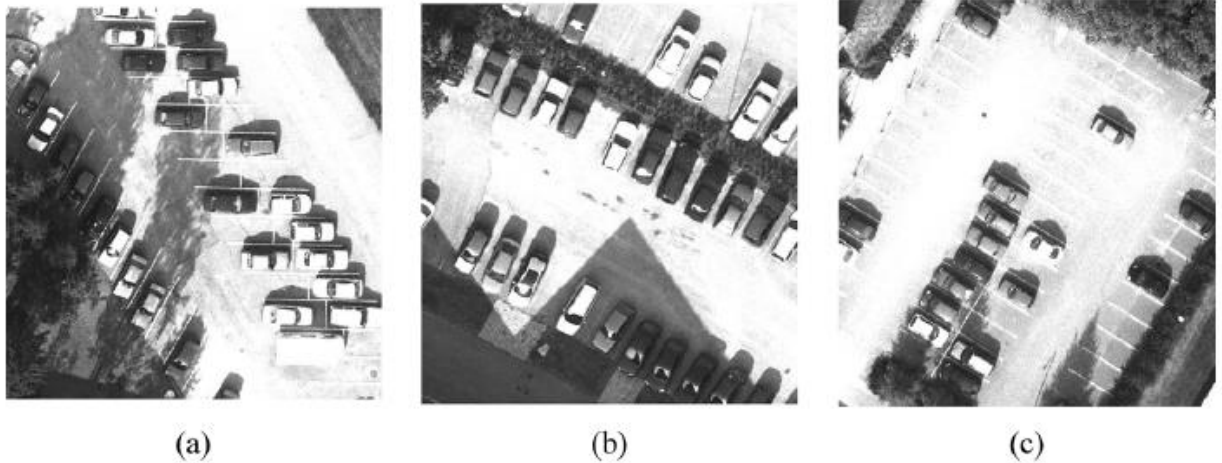


**Figure 24: Examples of challenges faced in the parking lot extraction process: (a) A parking lot with several dominant lane-markings, (b) a full parking lot, (c) low quality line markings (Tong, Cheng, Li, Wang, & Du, 2014)**

Tong et al. tested their algorithm on three types of parking lots with different structures, image qualities, shading natural elements, car distributions, parking orientations, and luminance variations. They also compared their results to image-based methods relying on segment extraction and filtering, and parking lines interpolation and expansion.

Seen in Figure 25 and Figure 26 are the results from Tong et al.'s proposed method (figures a, b and c) compared to the results from the aforementioned image-based method (figures d, e and f). They noticed that the results from the proposed method are far better than the results from the image-based approach: all three parking lots are correctly mapped and the reference lines accurately placed in Tong et al.'s approach whereas some errors are observed for the image-based method.

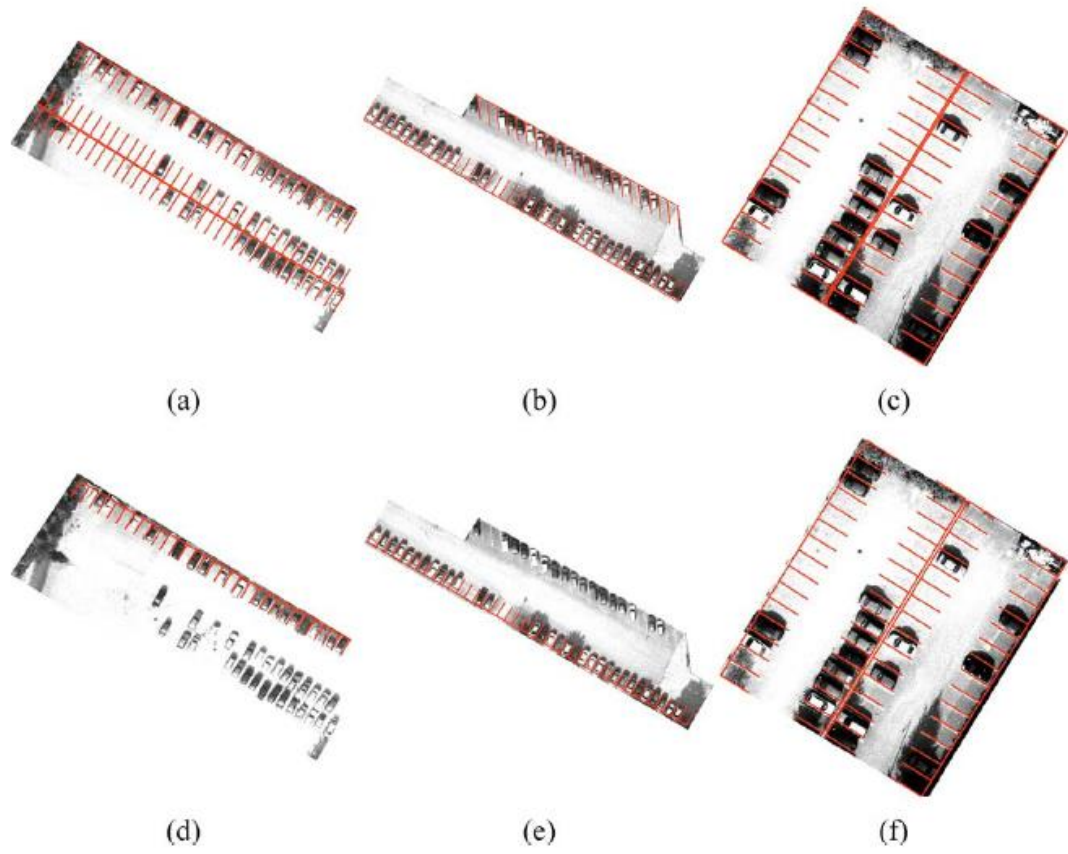


**Figure 25: (a), (b), and (c) Parking lots generated by the proposed method. (d), (e), and (f) Parking lots generated by the image-based approach (Tong, Cheng, Li, Wang, & Du, 2014)**

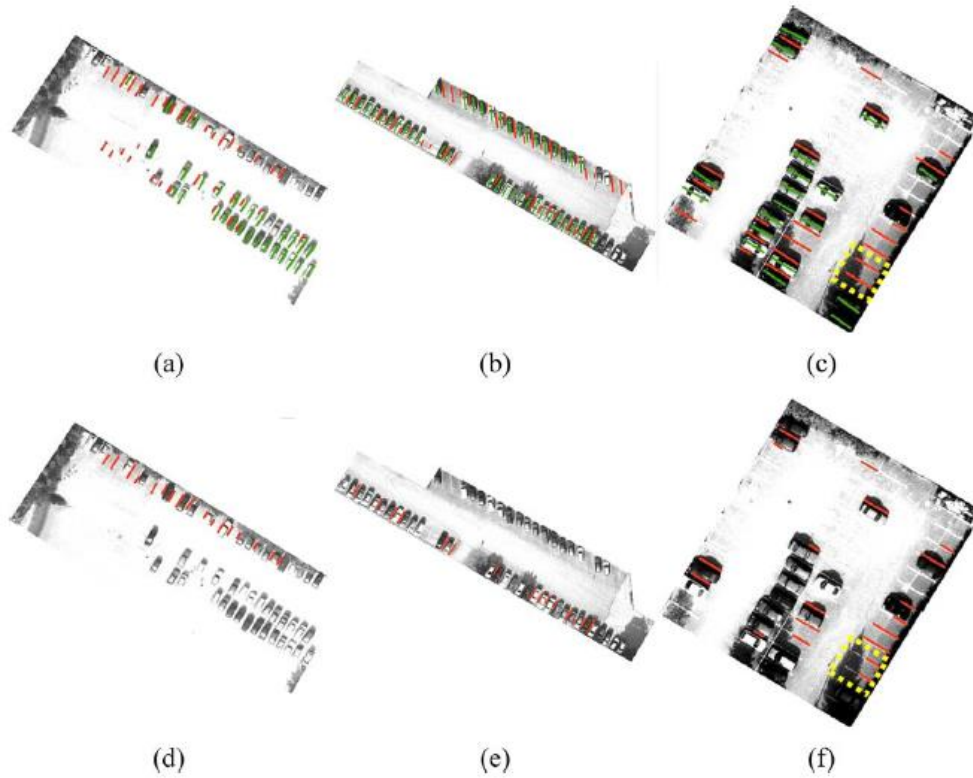


**Figure 26: (a), (b), and (c) Reference lines for parking lots generated by the proposed method. (d), (e), and (f) Parking lots generated by the image-based approach. Red lines represent the parking spot limits, while green lines represent the vehicle central axis (Tong, Cheng, Li, Wang, & Du, 2014)**

Statistical results from the experiments proved that the proposed method far outperforms the image-based method for every parking lot. At some instances, it was even shown that the image-based method could not represent parking lot at all, because of various issues such as image qualities, shading and luminance variations (Tong, Cheng, Li, Wang, & Du, 2014).

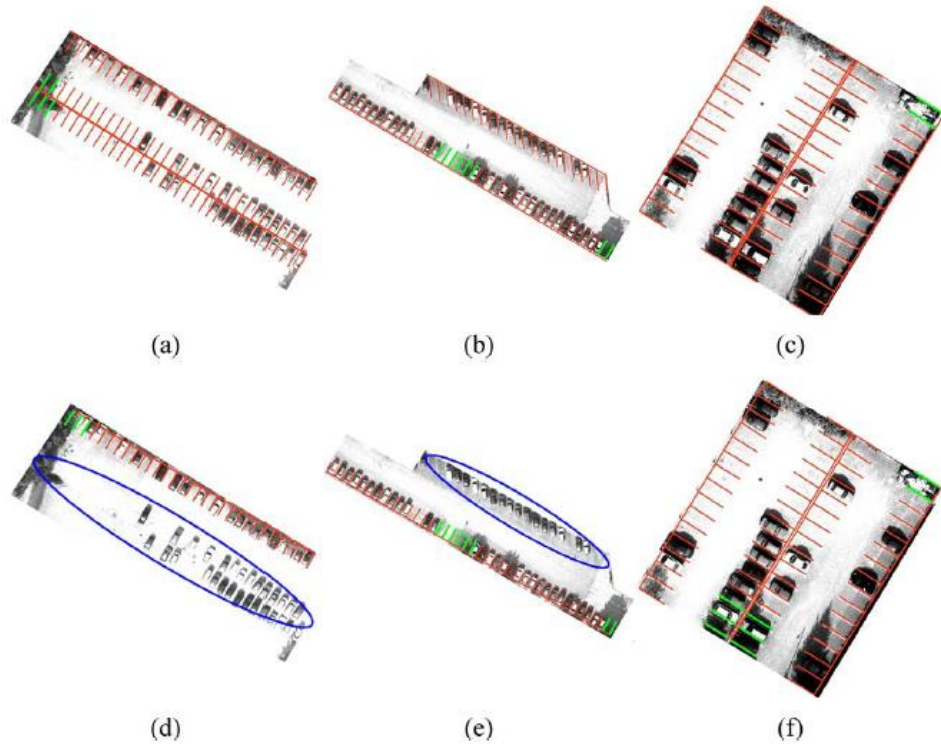


**Figure 27: Correct (red), missing (blue), and false (green) lines in the extracted lot structure (a), (b), and (c) Parking lots generated by the proposed method. (d), (e), and (f) Parking lots generated by the image-based approach (Tong, Cheng, Li, Wang, & Du, 2014)**

### 2.2.3 Overview of Laser Sensor Technology

Literature has shown that laser sensors would be a competent replacement to other sensor technologies as they help accurately detect parking spot availability and efficiently map parking lots. However, some drawbacks can be observed for each of the sensors mentioned in Chapter 2.2: The sensor used in (Ono, Kagesawa, & Ikeuchi, 2002) does not have an ideal accuracy ( $\pm 50$  cm); it also cannot be easily attached to a probe vehicle because of its weight (14 kg) and dimensions (560 mm x 240 mm x 280 mm). Similarly, the 2D LIDAR sensor used in (Thornton, Redmill, & Coifman, 2014) would

not only be cumbersome but also costly: \$10,000 per unit and \$60,000 for fitting a parking lot with the appropriate sensors.

Moreover, for parking lot mapping, parking layouts need to be extracted manually as a precondition, and the simulated information cannot be applied to detect parking availability instantaneously.

Finally, some factors need to be considered before implementing these sensors in commercial vehicles. These factors can range from testing in adverse weather conditions (e.g. rain), to minimalizing the complexity of the algorithm, and perfecting its ability to generate usable real time data transferable to servers or clouds.

### **2.3 Summary of Available Sensor Technologies for Parking Detection**

Table 2 below shows a summary of the qualities of available sensor technologies for parking detection. A technology's positive qualities are highlighted in green, whereas its drawbacks are highlighted in red.

Anisotropic Magnetoresistive (AMR) sensors are accurate and have a high frequency, but are limited by their low range and noise interference (Table 2). These sensors are installed for each parking spot, limiting their scope of applicability to specific parking lots fitted with AMR sensor technology. To enhance the applicability of sensors to detect parking availability, these sensors should be attachable to probe vehicles.

Vision sensors offer accurate data and cover large surface areas since sensors can be installed onto experimental vehicles. The price and algorithm complexity of such

systems are major drawbacks, thus limiting their implementation onto production vehicles.

Ultrasonic sensors seem promising because of their low price and ease of implementation onto probe vehicles. This hardware however is restricted by low frequencies, limited range, and poor accuracy (Table 2).

Laser sensors on the other hand possess high accuracy, long range and exceptional frequencies. Abdel-Hafez et al.'s paper brings up two important points for parking spot detection using laser sensors: since ultrasonic sensors' accuracy and range is very limited, numerous algorithms need to be implemented to ensure the soundness of the data and safety of the passengers. On the other hand, an application using an affordable laser sensor does not require intense algorithm developments. The second point this paper highlights is the possibility and added safety that algorithms might have on laser sensor applications. As car manufacturers might want to move forward with the proposed sensors, they would have the ability to generate and implement required algorithms for driver safety and added accuracy.

The laser sensors seen in literature possess the best qualities compared to other sensors, such as high accuracy and frequency, and long range. Nevertheless, these laser sensors are expensive and not easily attachable onto vehicles. Moreover, their performance under adverse weather conditions was not evaluated. Consequently, the ideal solution for parking spot detection would be a laser sensor having the qualities mentioned above (long range, high frequency and accuracy), but having a lower cost and smaller size.

**Table 2: Summary of sensor technologies available for parking detection**

		Sensor Technologies for Parking Detection			
		Laser sensors	Ultrasonic Sensors	Vision Sensors	AMR sensors
Desired Features	Accuracy	✓	✗	✓	✓
	Frequency	✓	✗	✓	✓
	Range	✓	✗	✗	✗
	Noise Interference	✓	✓	✗	✗
	Price	✗	✓	✗	✓
	Ease of Implementation (Size)	✗	✓	✗	✓
	Scope of Applicability	✓	✓	✓	✗
	Impact of Environmental Conditions	✗	✗	✗	✗



## **CHAPTER 3**

### **SYSTEM DESCRIPTION**

#### **3.1 Ideal System Requirements**

To enhance the parking experience for drivers, parking lot information should be made accessible, focusing on correctly detecting parking spot availability. In order to accurately determine this availability, several design criteria should be met. The system must be able to detect parked cars, and assess the status of a parking spot (available or occupied). Since the sensor will be installed on a probe car, it should also detect parking availability while the probe vehicle is in motion.

##### **3.1.1 Installing a laser range sensor**

Literature in Chapter 2 has shown that laser sensors would be the ideal equipment to use for parking spot detection, due to their high precision and long range (Table 2). The laser sensors used in (Ono, Kagesawa, & Ikeuchi, 2002) and (Thornton, Redmill, & Coifman, 2014) were determined to be expensive and cumbersome. The sensor installed in this thesis therefore must possess similar qualities as Ono et al. and Thornton et al.'s sensors (long range, high accuracy and frequency), but should also be affordable and easily attachable to a probe car. Laser sensors explored in literature were also not subject to different experimental conditions such as 45 and 60 degree parking angles. The sensor

used in this thesis should then scan accurately in various testing scenarios but also under inclement weather conditions. Finally, more complex and expensive laser sensors have the ability to produce accurate 3D maps of parking lots or streets. The sensor mounted on the probe vehicle in this thesis should be able to compete with these more expensive sensors, and generate similar images, using affordable off-the-shelf instruments. Figure 28 illustrates the main points required for an efficient, accurate and affordable sensor to be utilized in this thesis.

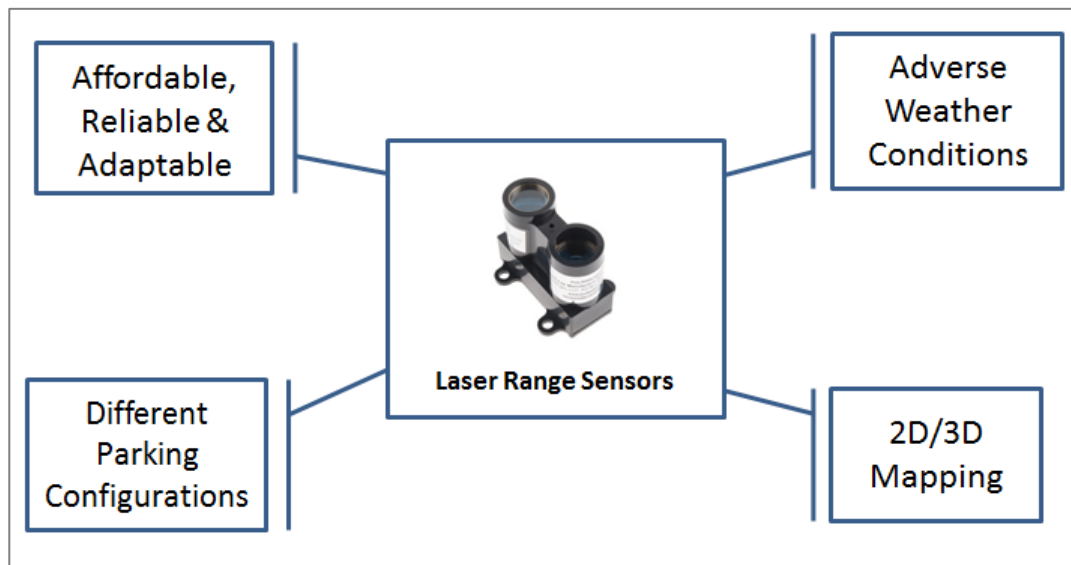


Figure 28: Laser sensor satisfying all technical requirements

### 3.1.2 Integrating other data sources

Ideally, the sensing system would also be able to integrate other sources of data for added applications or security features (Figure 29). Vehicle speed for instance, could be used to calculate the distance travelled, and generate a 3D map (explained in Chapter 4.2.2). GPS data could also be used in parallel with laser sensor data to accurately locate

the probe car based on surrounding landmarks, as done in (Thornton, Redmill, & Coifman, 2014). This would also help in detecting lots, pinpointing parking spots, and enhancing data visualization. Once parking availability is determined, that information should be made available to customers searching for parking. Hence, syncing sensor information to a cloud or central server could be integrated as well (Figure 29). This feature would improve parking applications by having different data streams feeding into one common parking detection algorithm.

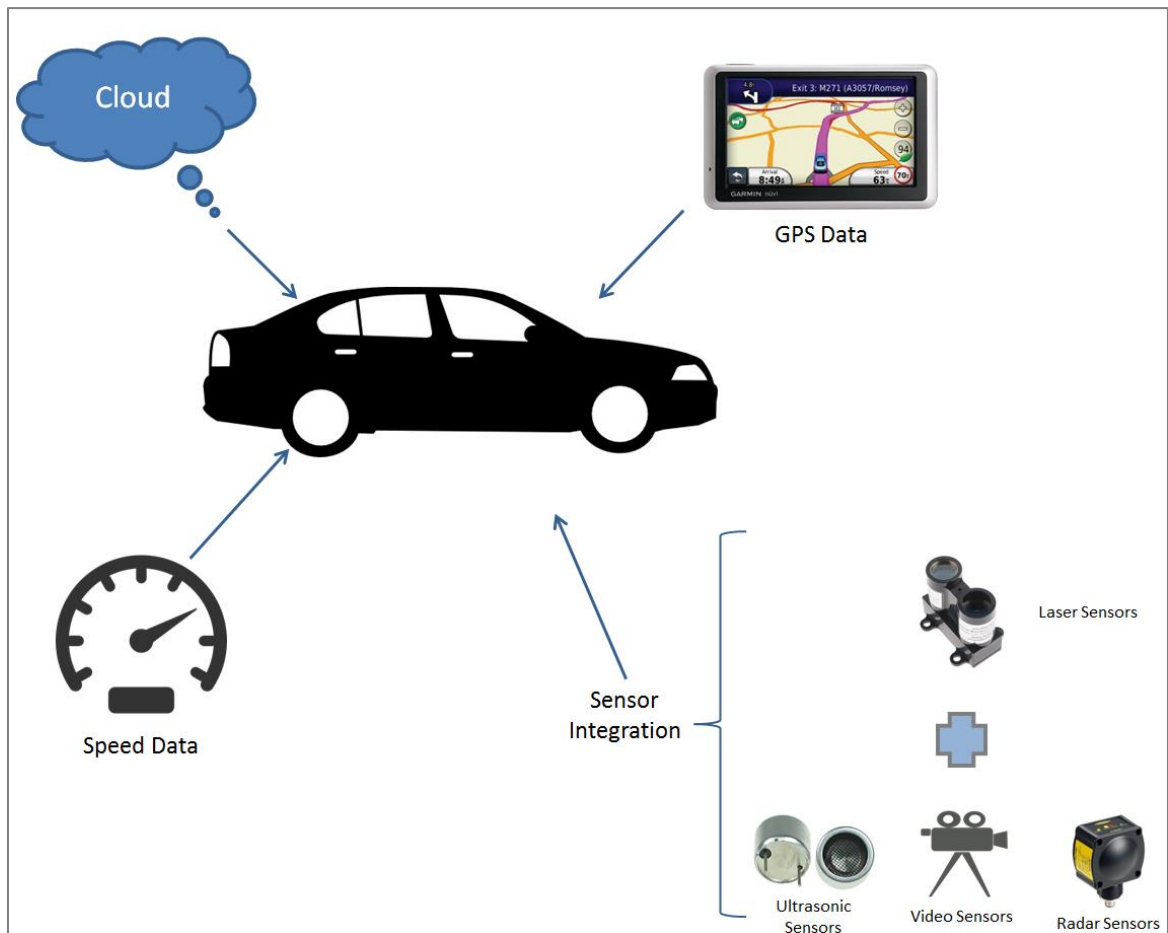


Figure 29: Integration of various data sources

### 3.1.3 Use case description

As an example of the application of this sensing system, the figure below describes a use case: how is the sensor information used?

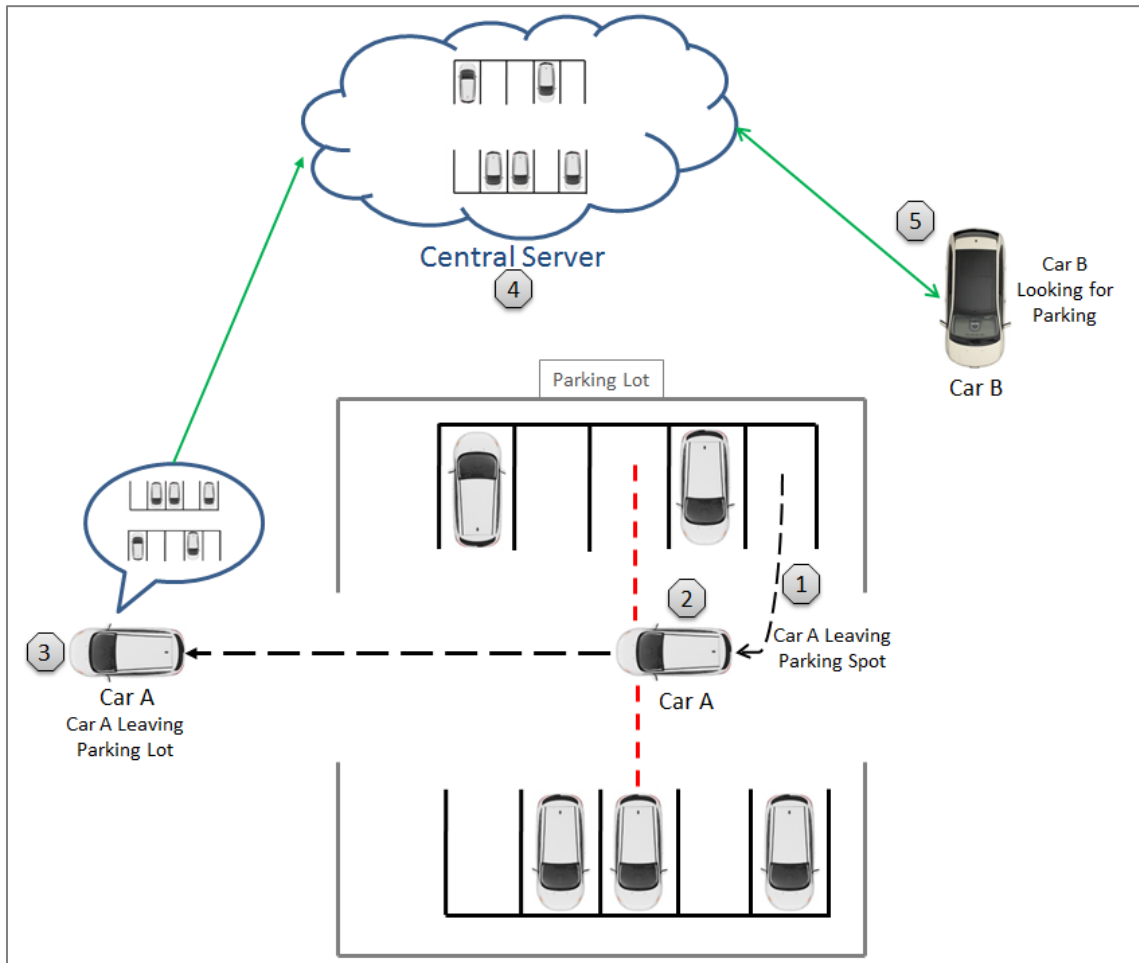


Figure 30: Use case description

After a parked vehicle leaves its parking spot (Car A in Step 1), laser sensors installed on its sides retrieve distance data (Car A in Step 2). The data can then be sent to a central server (Step 4) either instantaneously to reflect the exact status of a parking spot (Step 2), or can be aggregated and sent after leaving the parking lot (Step 3). Once data

reaches the central server, it is analyzed using detection algorithms. The evaluated data is then forwarded to other vehicles requesting assistance from the central server to locate a parking spot (Car B in Step 5). These vehicles use this data to evaluate which parking lot is ideal. As these cars are leaving a parking spot or driving by a lot (Car B), they can also scan for empty parking spots and send data back to the server, thus closing the data sharing loop. This use case shows an example of how the sensors can be used to retrieve parking availability and forward it to other vehicles looking for parking. However other use cases can be assessed. These include installing sensors onto taxis or government-owned vehicles (buses or police cars) that continuously drive through a city and therefore past parking lots. In those scenarios, the same use case explained in Figure 30 applies, however the sensing vehicles in question are not searching for a parking spot.

### **3.2 Infrared Laser Technology Overview**

Laser range infrared sensors emit an optical signal through a transmitter and measure the time it takes for that signal to “bounce off” an object and reach the receiver. This “Time-of-flight” distance measurement technique estimates the time delay by correlation. That is a signal processing approach which generates a signature match between the outgoing and incoming signals.

As Kikuta et al. explain in their paper dating back to 1986, measuring a distance with a laser diode is made possible since the wavelength of the emitted laser beam fluctuates in relation to the diode’s injection current (Figure 31). Because of the sinusoidal variation of wavelength, the phase difference between both beams oscillates;

the magnitude of this variation is related to the light wavelength shift and measuring distance. By measuring the phase variation, and knowing the wavelength shift, a distance (larger than the wavelength) can be estimated (Kikuta, Iwata, & Nagata, 1986).

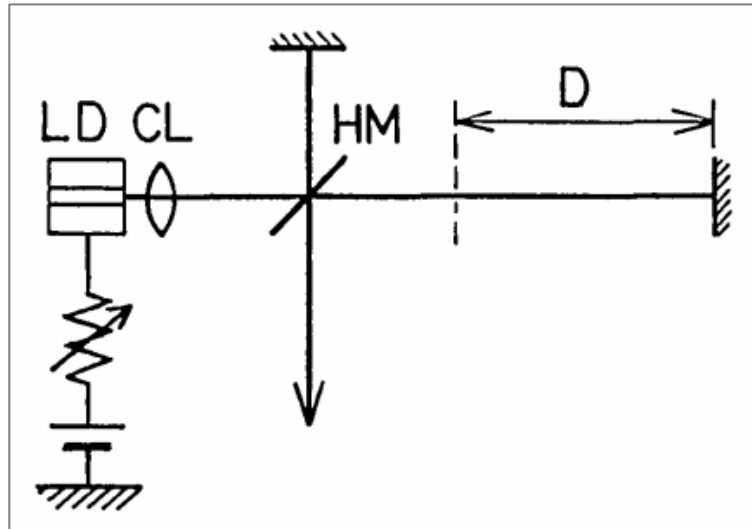


Figure 31: Illustration depicting the distance measurement principle (Kikuta, Iwata, & Nagata, 1986)

After the correlation algorithm determines the time delay, distance is computed from the known speed of light ( $2.998 \times 10^8$  m/s):

$$d = c * \Delta t$$

Equation 4: Calculation of the distance

Because of this high speed, time-based accuracy can be very high. This accuracy should be a requirement for the laser sensor used in this thesis.

### 3.3 General System Description

The requirements for the sensing system will be explored herein. The laser range sensor setup used for the experiments will also be illustrated: it combines the hardware installed and the detection algorithm used.

### **3.3.1 System Requirements**

In order to correctly map parking lots, or enhance parking spot detection, an affordable laser sensor needs to be installed. That sensor must have a reliable accuracy and should perform consistently under different weather conditions. The sensor should also be adaptable to current production vehicles, and hence must not be harmful to pedestrians. Furthermore, the algorithm used to analyze collected data must be accessible, simple, and efficient. It should also be capable of generating real-time data should it be implemented in parking “apps”.

### **3.3.2 Hardware Overview**

#### **3.3.2.1 Laser range sensor description**

Pulsed Light introduced their new infrared sensor “LIDAR-Lite” in 2014 for \$89.95, describing it as a “single chip processing solution” which requires minimal hardware. It should be noted that this sensor measures distances using a single infrared beam (described in Chapter 3.2). Therefore it is not technically classified as a “LIDAR” (combination of “Light” and “Radar”) since these sensors generate a 2D image based on a rotating laser source. As will be explained in Chapter 4.2, obtaining 2D and even 3D

images using the laser range sensor is possible but requires hardware and software modifications.

The laser range sensor in question has a reported maximum range of 40 m, although field tests showed that the sensor could detect objects as far as 35 m (which is far beyond what this application requires). With an average acquisition time of roughly 20 ms (50-70 Hz) and an accuracy of  $\pm 25$ mm (compared to the sensor used in (Ono, Kagesawa, & Ikeuchi, 2002) having an accuracy of  $\pm 50$  cm), this sensor is ideal for applications which require fast distance measurements with high accuracy (Table 3). Since it is powered by 4.75-5.5V DC, these applications include robotics, unmanned vehicles and automotive applications. This laser sensor is designated Class 1, meaning that it complies with US FDA performance standards for laser products, and is safe to look at with the naked eye (although not recommended).



**Table 3: LIDAR-Lite Specifications (Pulsed Light, 2015)**

General	Technical Specifications
Power	4.75-5.5V DC Nominal, Maximum 6V DC
Weight	PCB 4.5 grams, Module 22 grams with optics and housing
Size	PCB 44.5 X 16.5mm (1.75" by .65")
Housing	20 X 48 X 40mm (.8" X 1.9" X 1.6")
Current Consumption	<2mA @ 1Hz (shutdown between measurements), <100mA (continuous operation)
Max Operating Temp.	70° C
External Trigger	3.3V logic, high-low <a href="#">edge triggered</a>
PWM Range Output	PWM (Pulse Width Modulation) signal proportional to range, 1msec/meter, 10µsec step size
I2C Machine Interface	100Kb – Fixed, 0xC4 slave address. Internal register access & control.
Supported I2C Commands	Single distance measurement, velocity, signal strength
Mode Control	Busy status using I2C, External Trigger input / PWM outputs
Max Range under typical conditions	~40m
Accuracy	+/- 2.5cm, or +/- ~1"
Default Rep Rate	~50 Hz.

In 2015, the company upgraded the hardware to a “LIDAR-Lite v2 Blue Label”, which was selling for \$114.95. The 40 m range, 25 mm resolution and low power requirements were still some of the qualities transferred to the newer generation LIDAR. However one of the most noteworthy upgrades was the increase in measurement speed: the sensor can now operate with speeds of up to 500 readings per second. In field tests, the frequency was closer to 200 Hz, a significant improvement from the previous 70 Hz value. To illustrate this improvement in frequency, 3D mapping was attempted using the newer “LIDAR-Lite v2 Blue Label”, as shown in Chapter 4.2.2.

### 3.3.2.2 Mounting system description

To temporarily secure the laser range sensor to the probe car, a suction cup and its mount were used (Figure 32) since they allowed modifying the location and tilt angle of the sensor. A 3D printed part was attached to the mount, and the sensor was then fixed to that attachment. To power the sensor and receive its data, it was wired to an Arduino Uno microcontroller which runs on a version of C/C++ languages. For vehicle tests, the Arduino was powered via USB connected to a laptop, and sensor data was saved to an excel file on said laptop. That Arduino microcontroller was secured to the mount using Zip Ties. To obtain 2D and 3D images and evaluate the effect of pivoting the sensor, a servo motor was also attached to the mount (Figure 33). The final product and its installation on the probe car can be seen in Figure 35.

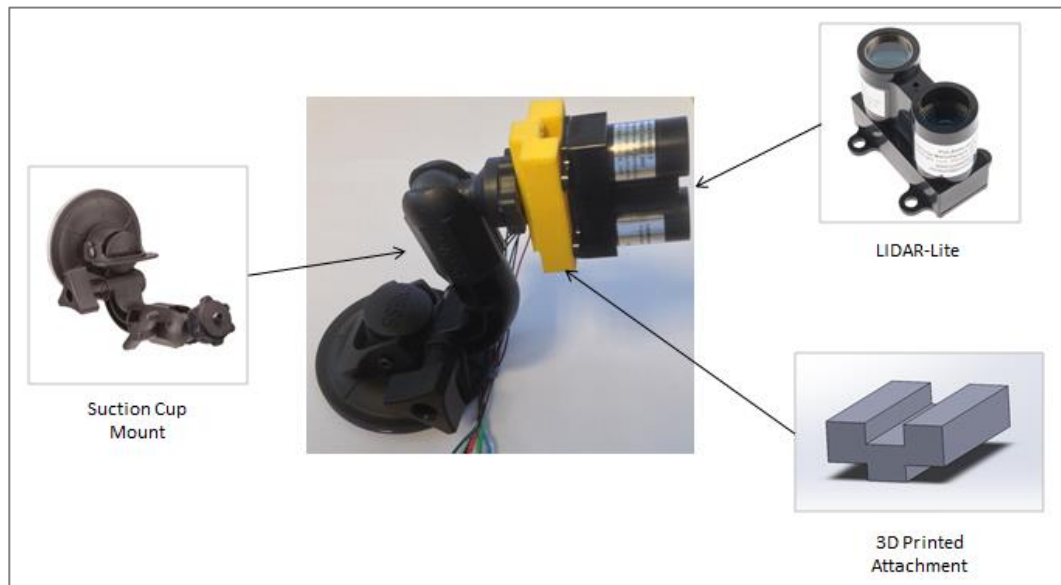


**Figure 32: Laser range sensor assembly**

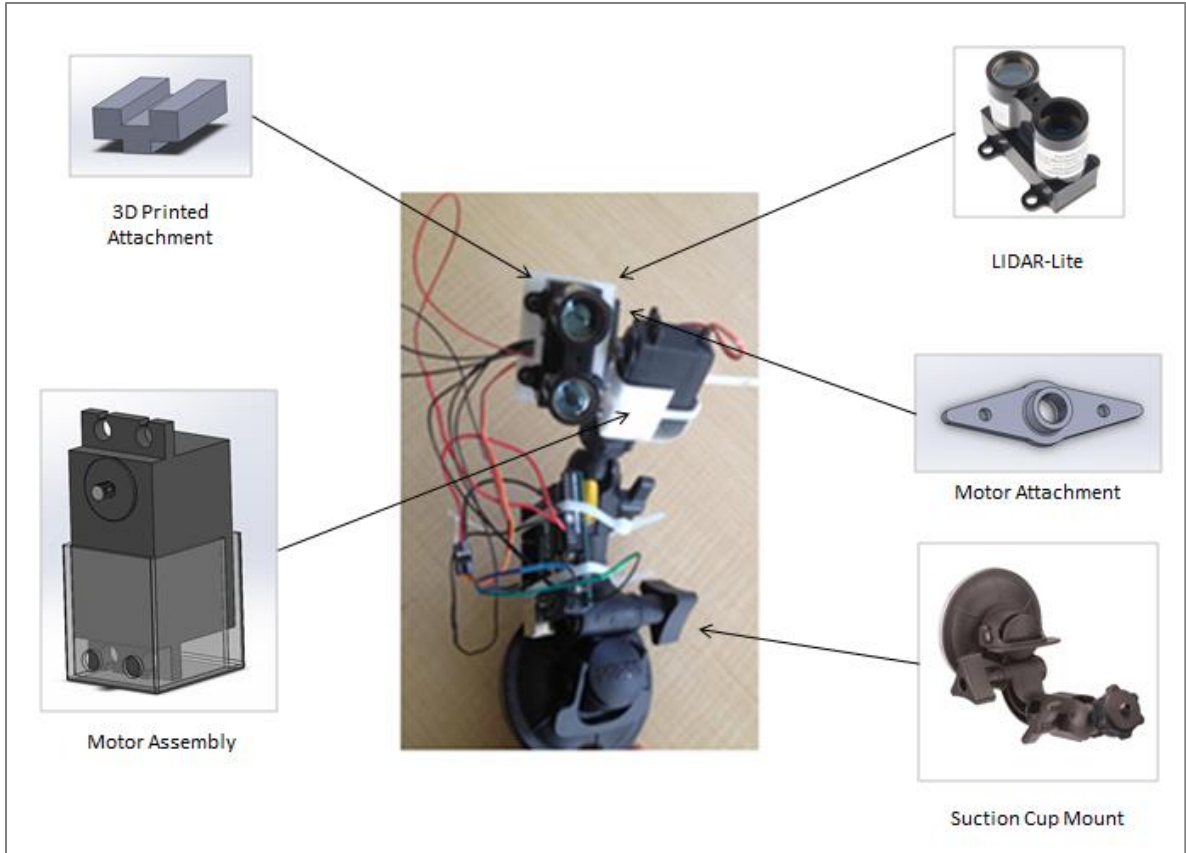


**Figure 33: Laser range sensor with servo motor assembly**

The mounts were attached to the side of the front bumper of the car. This would make it easier to possibly compare laser sensor data with the probe vehicle's factory installed ultrasonic sensors.

Figure 34 below shows an overview of the system description, along with the different steps followed throughout the measurements: in Step 1, the laser sensor setup is mounted to the probe vehicle (Item 2), which drives past parked cars. The red dashed line in Figure 34 represents the laser beam emitted from the sensor. Data is transferred from the laser range sensor and microcontroller (Item 2) to an onboard laptop (Item 4) via USB cable (Item 3). An Arduino IDE code (Step 5.a) is installed on the microcontroller to send sensor data via Serial communication to the laptop. "Processing", a program

which continuously reads the serial port of the laptop (Step 5.b), receives the incoming data and saves it to an excel file (Step 6 a). Once all experimental runs are completed, the detection algorithm (explained in Chapter 3.3.3) is run in Matlab to determine the number of available and occupied parking spots.

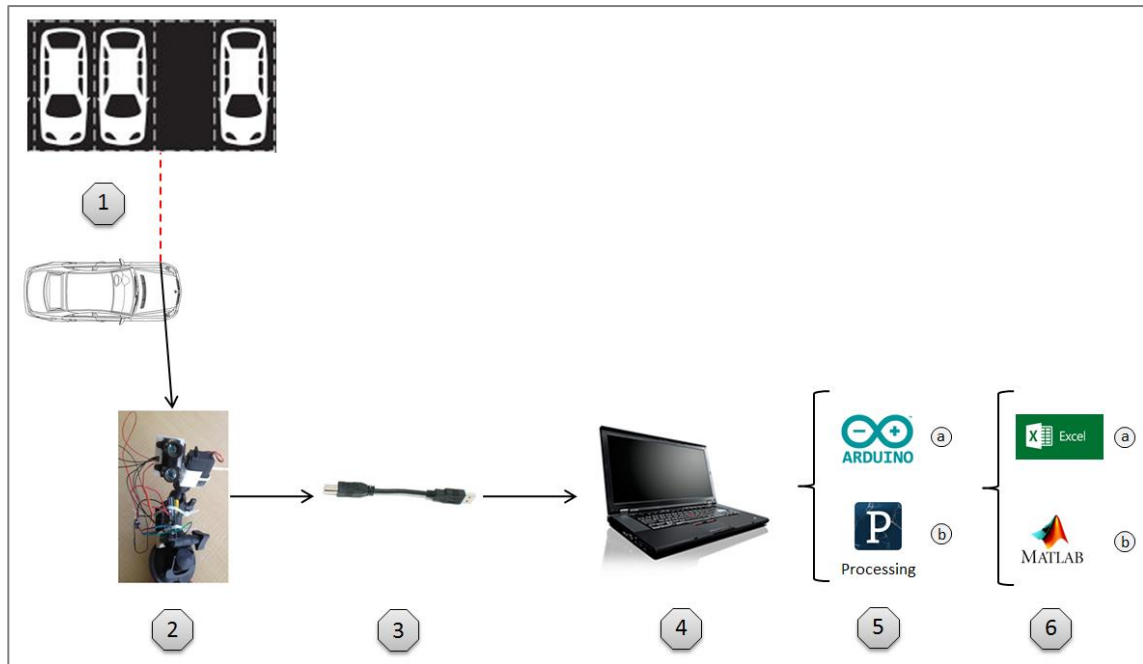


**Figure 34: System description overview**

To test the feasibility of market implementation, the laptop (in Step 4) needed to be eliminated from the system. Hence two methods for powering the microcontroller were explored: the first option would be to power the Arduino/Controller through a lithium ion battery, making the entire setup cable-free. The other option is to power the system by plugging in a USB car charger into the cigarette lighter, and running a standard USB cable to the microcontroller. In both cases, sensor data will be sent to a mobile device by Bluetooth through a Bluetooth BLE shield connected to the microcontroller. This will be discussed further in Chapter 6.2.1.

Moreover, a limitation on the sensors that should be considered before installation is performance under inclement weather such as heavy rain. Since a laser beam can detect objects through clear material, the system was waterproofed by wrapping the sensor and sensitive wires with clear freezer bags (Figure 35.b). The system was tested under heavy rain, and the results will be reported in Chapter 5.2.

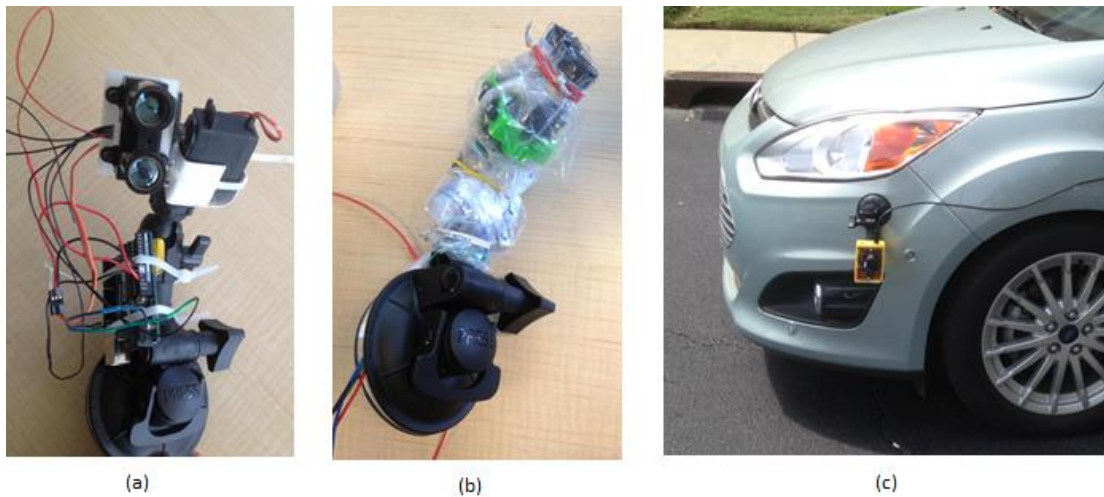


**Figure 35: Entire sensor setup (a) for the pivoting sensor, (b) for the water resistant sensor, and (c) mounted on the probe vehicle**

### **3.3.3 Detection Algorithm**

#### **3.3.3.1 Algorithm Overview**

After experimental runs were conducted for all parking angles and desired speeds, different log files containing multiple excel folders were generated. The role of the algorithm is to open these source files, evaluate the experimental data, and perform

different analyses. To explain the logic behind the algorithm, a general overview can be seen in Figure 36 and Figure 37.

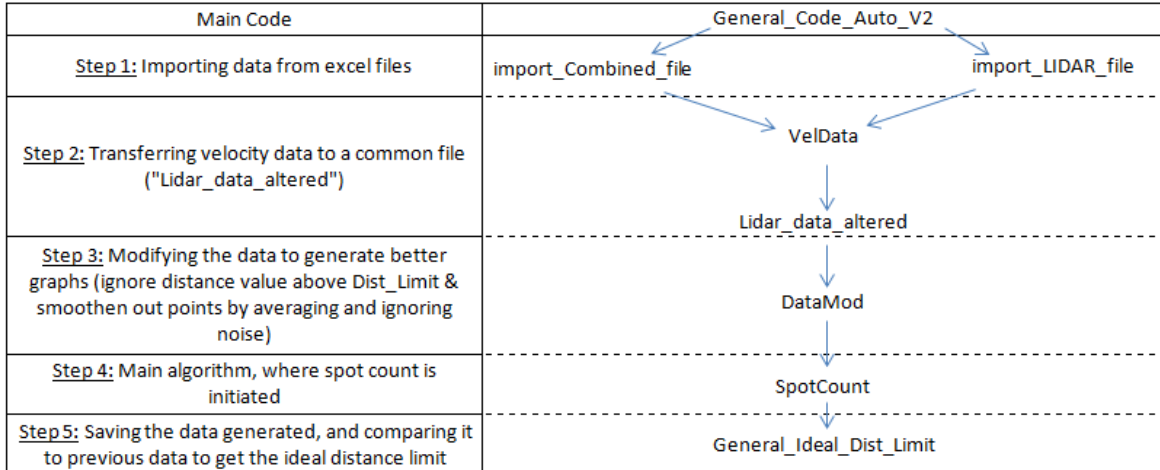


**Figure 36: General overview of the algorithm**

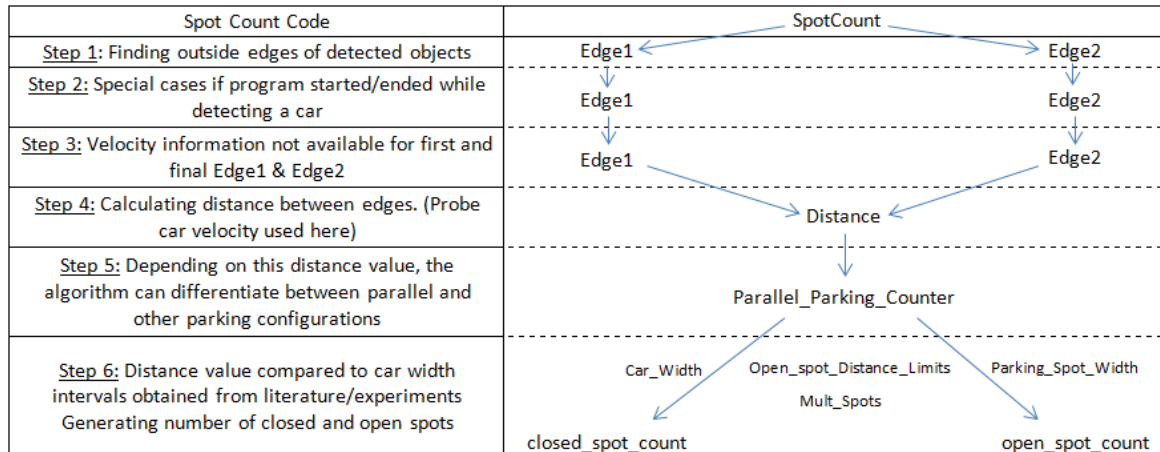


**Figure 37: Spot Count Algorithm**

These figures enumerate the different steps undertaken in the detection algorithm: Figure 36 shows a general overview of the algorithm where the main code (“General\_Code\_Auto\_V2”) is divided into steps (left column), and the order in which

the Matlab functions are used (right column). Figure 37 on the other hand focuses on a function constituting the bulk of the algorithm: “SpotCount”. Again in this figure, the logic behind this spot count algorithm is shown in the left column. The order of functions used is then shown in the right column.

### 3.3.3.2 Determining the “Ideal Distance” of Parked Vehicle from Probe Car

A main issue encountered was determining at which distance (in mm) the algorithm should expect to detect parked cars: since the laser range sensor only measures distances, the user needed to determine that distance limit visually. After doing so, a manual input into the algorithm would allow it to count the number of closed/open spots. However, an update to the code allowed the algorithm to test several distance limits, and run the code based of that value. It was observed that for the ideal distance limit, the algorithm would return a maximum number of open/closed spots. Because of that, the algorithm can now detect spot availability without any inputs from users.

The program is run as the probe vehicle begins to accelerate. Meanwhile relative time is registered, and the sensor values are reported and saved to an excel file. Figure 38 shows a plot in Matlab of raw sensor data vs. relative time. The sensor reports the distance objects are from the probe car every 20 ms with accuracy of  $\pm 0.025$  m. In Figure 38, the graph shows how far the objects detected by the sensor are, and at what point in time they are actually detected.

Since the laser sensor has a range of 40 m, as specified on its data sheet (Appendix C), a number of rows of cars in the background might be sensed. For instance,

for some of the 90 degree runs, 3 rows of cars are detected: around 1-5 m from the probe vehicle, around 10 m from the vehicle, and finally around 20 m from the vehicle. A run for 90 degree parking with the probe car driving at 5 mph is shown in Figure 39. Since we are mainly interested in the row of cars closest to the probe car, the detection algorithm first has to ignore measurements beyond 5 m. That is generated in Figure 40, where we could clearly distinguish parked vehicles from open spaces.

Moreover, we notice from Figure 38 that some noise affects the readings, and causes the value of the distance measured by the sensor to dip to 0. These anomalies should be disregarded since they do not represent accurate data.

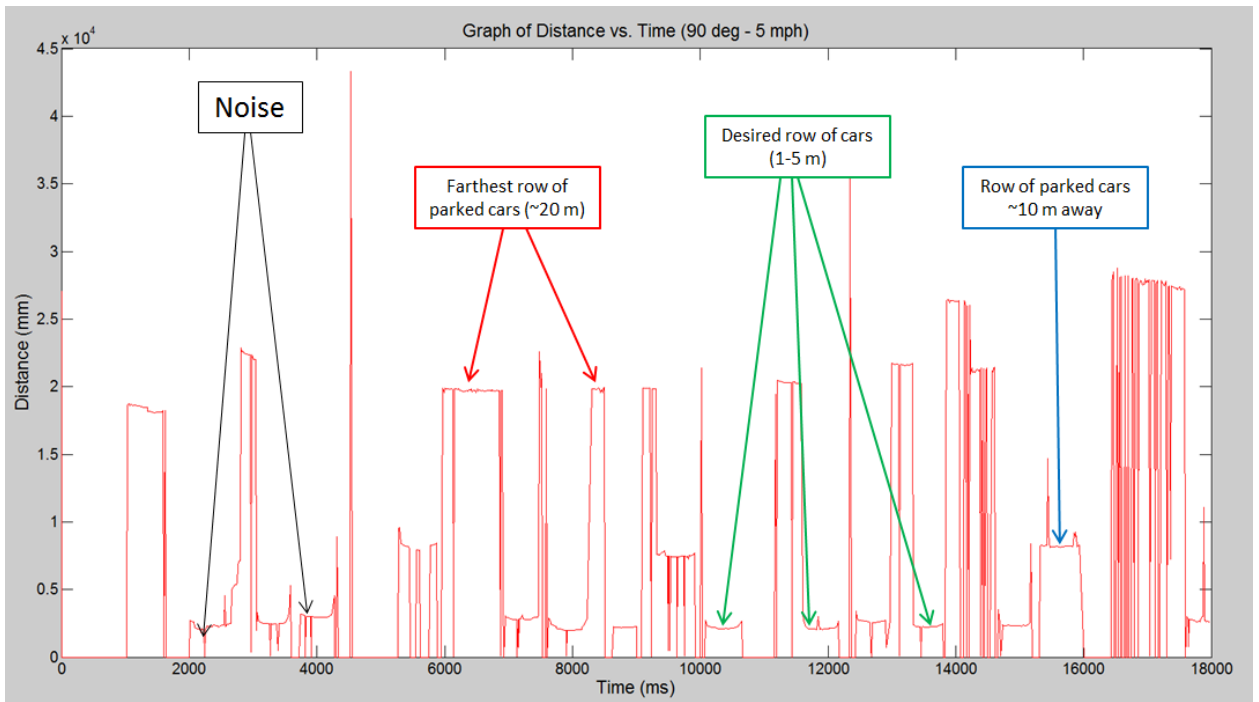


**Figure 38: Raw Data. Driving at 5 mph, scanning 90° parking spots**



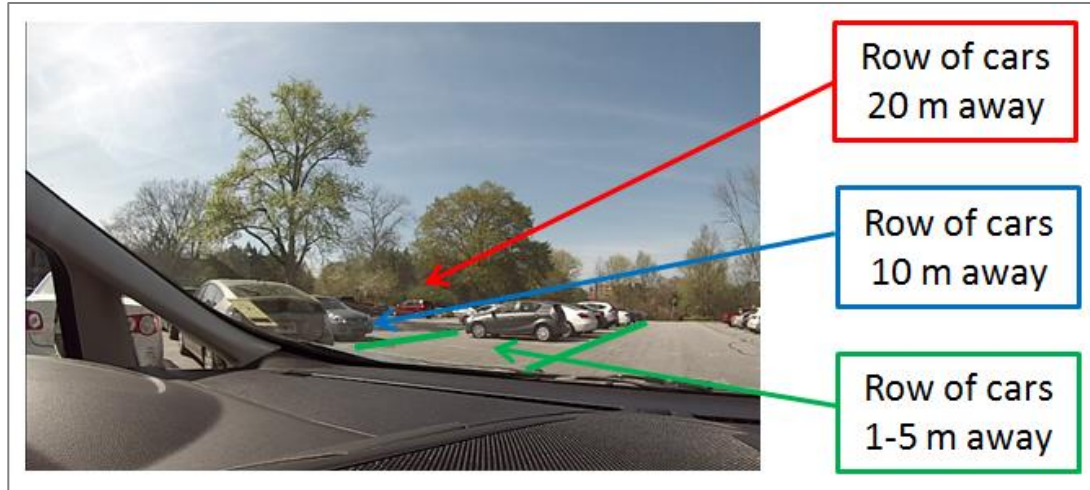


Figure 39: Ground Truth Data from Onboard Camera

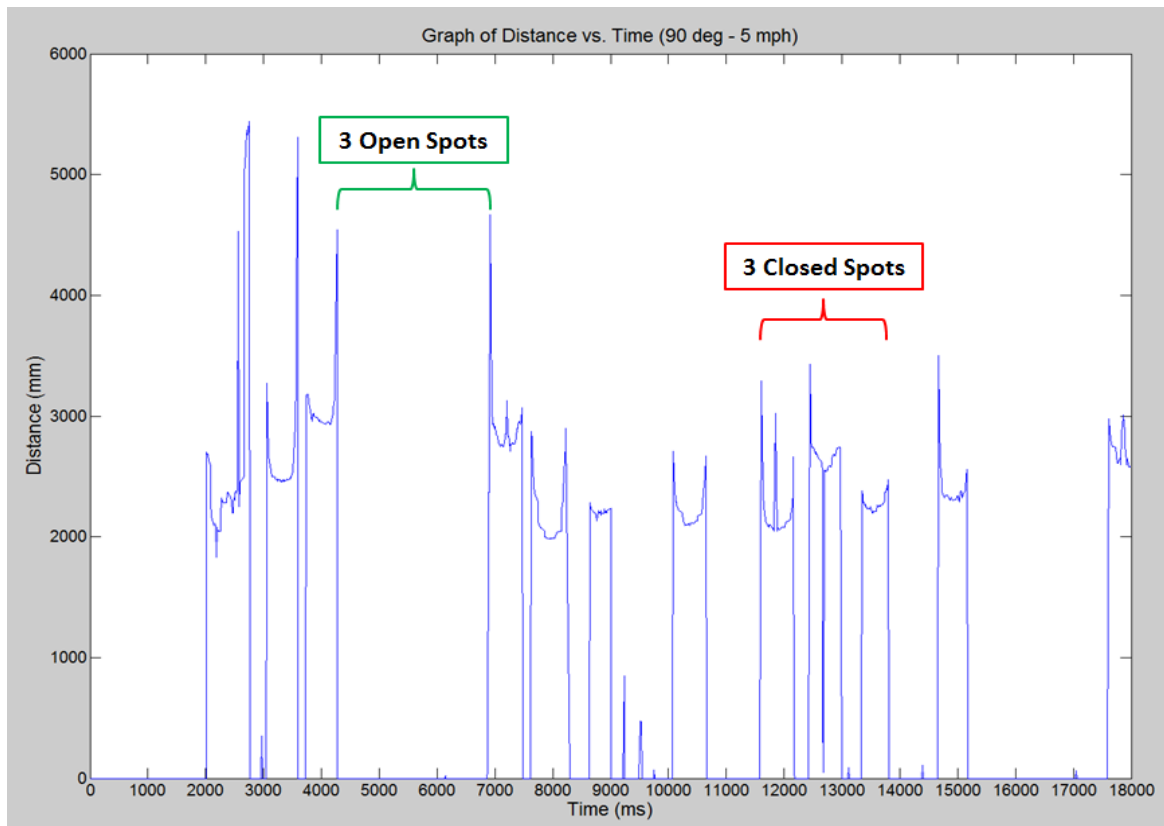
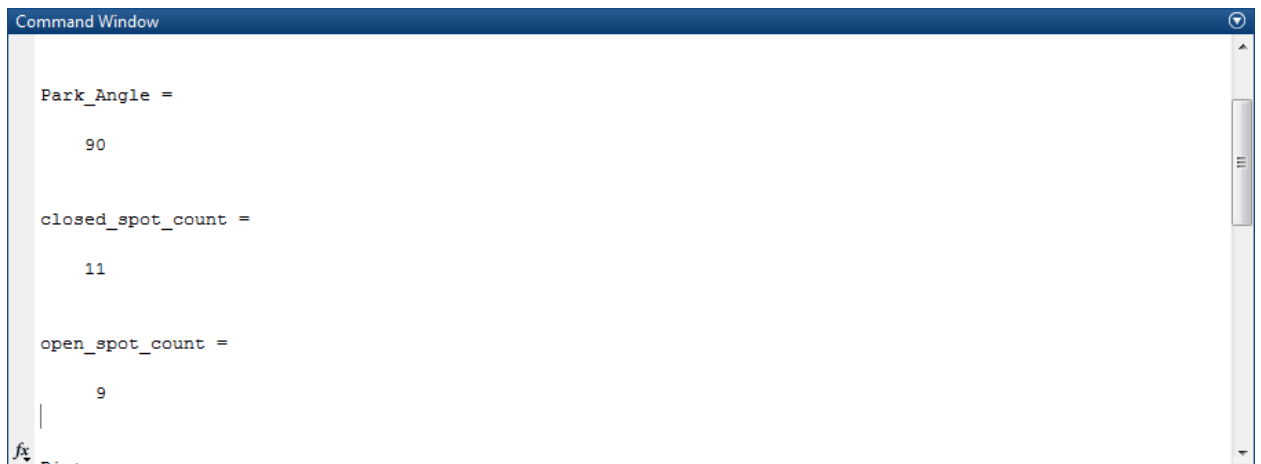


Figure 40: Data after ignoring the secondary and tertiary row of cars

Depending on the number of “dips” and “rises”, the algorithm can generate an accurate number representing closed spots and open spots. In the example shown in Figure 40, ground truth data from the GoPro camera showed that the strip of parking lot contained 20 spots, of which 11 were occupied and 9 were open.

Running the Matlab algorithm for this example, we find:



```
Command Window

Park_Angle =
    90

closed_spot_count =
    11

open_spot_count =
    9
```

**Figure 41: Solution of Matlab algorithm counting the number of closed/open spots for 90 degree parking, at 5 mph**

This shows that at this point, the detection algorithm and laser range sensor are 100 % accurate, compared to ground truth data from the onboard GoPro camera. However, many runs have been performed to calculate the repeatability and accuracy of the setup. The results of these experiments will be shown in Chapter 5.1.

### **3.4 System Description Summary**

Literature has shown that an affordable and adaptable laser sensor would be the ideal instrument to evaluate parking spot availability based on accurate and fast distance measurements. A “LIDAR-Lite” laser range sensor from “PulsedLight” was attached to off-the-shelf hardware and mounted onto a probe vehicle. Experiments were then conducted for different parking configurations, at different driving speeds and under inclement weather conditions. Finally, detection algorithms were run to count the number of open and closed parking spots.

# CHAPTER 4

## EXPERIMENTS CONDUCTED

### 4.1 Experimental Set Up and Hypothesis

The experiments are run on 90°, 60°, 45° and parallel (0°) parking for speeds of 5, 10 and 15 mph (Table 4). The probe car was driven at 15 mph when it was deemed safe. Although the speed limit of a parking lot is usually 10 to 15 mph, testing the system at the speed limit would allow us to evaluate using the sensor for other purposes such as vehicle peripheral sensing, video sensor assist (Makris, Perrollaz, & Laugier, 2013), and possible collision detection/prevention.

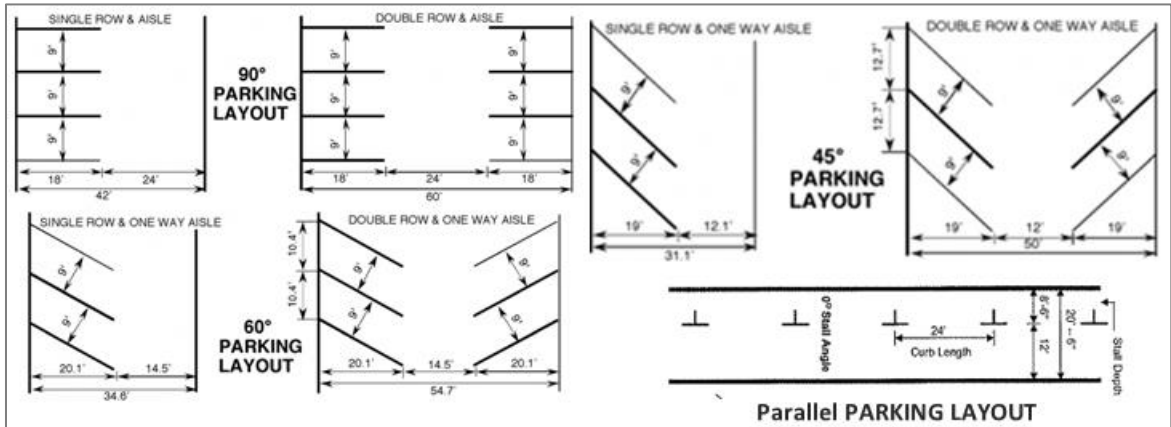


Figure 42: Parking lot layouts

**Table 4: Experimental runs**

<b>Parking Angles</b>	<b>0°</b>		<b>45°</b>		<b>60°</b>		<b>90°</b>		
<b>Speeds (mph)</b>	5	10	5	10	5	10	5	10	15
<b>Number of Runs</b>	15	15	20	20	21	20	13	15	13

For each parking angle, raw laser range sensor data is analyzed by the detection algorithm. All findings are then compared to ground truth data obtained by a GoPro camera installed on the probe car. Statistical analyses will then be performed in order to estimate the accuracy of the sensor, the performance of the detection algorithm, and the number of laps around a parking lot needed to gain different confidence levels.

The experiments were conducted around the Georgia Institute of Technology campus in Atlanta, Georgia. Some of these experiments were carried out in the Department of Mechanical Engineering's parking lot (90° and parallel parking), while others were performed in neighboring parking lots (60° and 45° parking).

The 90° and parallel parking tests were conducted following the routes highlighted in Figure 43 and Figure 44.



Figure 43: Routes followed for 90° parking



Figure 44: Routes followed for parallel parking

## 4.2 Additional Experiments

### 4.2.1 2D Image Generation

The ultimate goal is to generate a 3D map of the parking lot. The motor and sensor setup shown in Figure 35 needs to be tested first by successfully obtaining a 2D image. Figure 45 shows the experimental setup used to generate a 2D plot. As the servo motor rotates the LIDAR to an angle  $\theta$  from a horizontal line (where  $\theta = 0^\circ$ ), the X and Y coordinates of the measured distance can be computed by following the formulas below:

$$X_{pos} = \text{Distance Measured} * \cos \theta$$

$$Y_{pos} = \text{Distance Measured} * \sin \theta$$

**Equation 5: From Polar to Cartesian coordinate system**

It should be noted that if the pivoting angle is negative (laser sensor detecting objects below the horizon line), then the Y Cartesian coordinate is negative, and vice-versa. This is done to correctly visualize the height of detected objects.

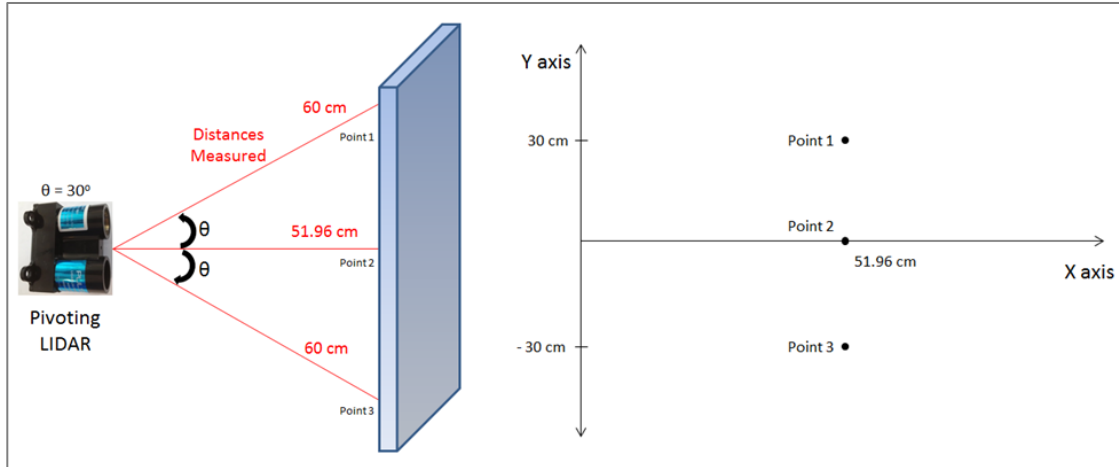


Figure 45: (a) Sample representation of the 2D experiment and (b) desired Cartesian plot output

#### 4.2.2 3D Image Generation

Once 2D plots are successfully generated, 3D images could be obtained by following the steps highlighted for 2D image generation (Figure 45), and adding a 3<sup>rd</sup> dimension: distance travelled by the probe vehicle. In Figure 46, as the probe vehicle is driving by, the laser range sensor is pivoted about its horizontal axis (as explained in Figure 45), generating points in the height vs. depth plane.



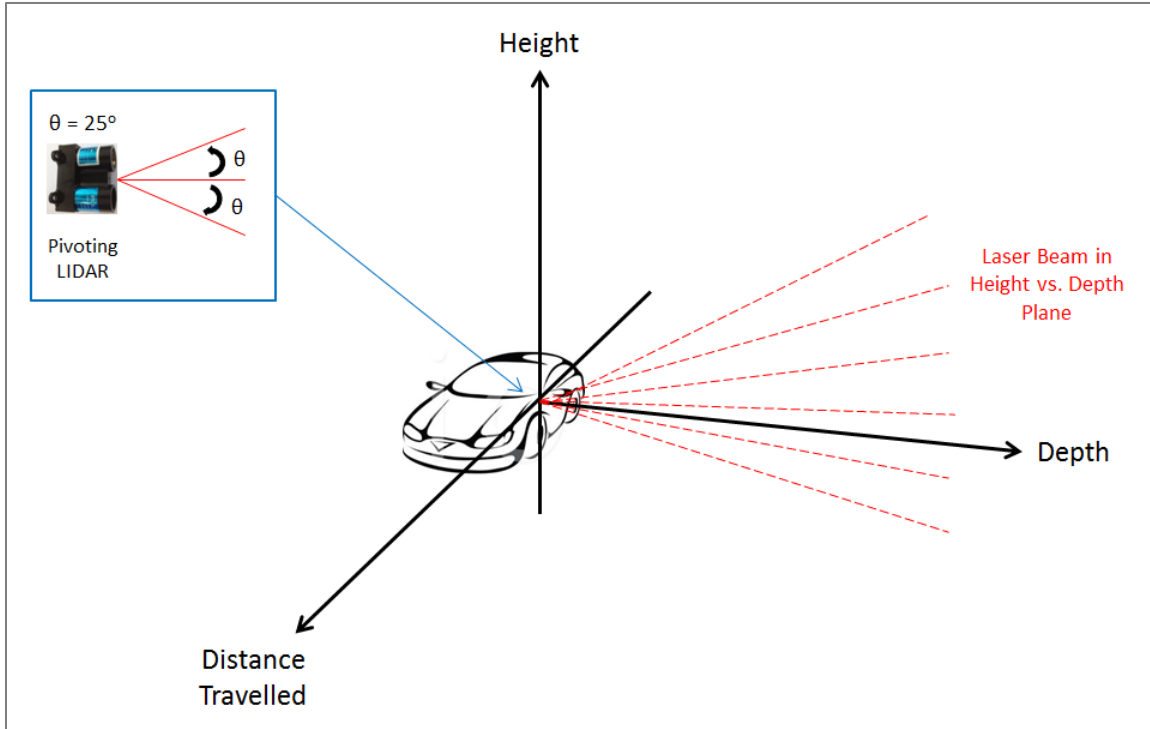


Figure 46: 3D system layout

As the probe car is being driven, distance can be recorded. For the purposes of this experiment the probe vehicle was a golf cart since it is more controllable at lower speeds. To generate distance data, 4 equidistant magnets were attached to the rear right wheel, and a magnetic Hall Effect sensor was installed. The HE sensor counts the number of magnetic pulses generated by the rotating wheel. Distance can be obtained by estimating the arc between each magnet: as the golf cart advances, each magnetic pulse implies that the wheel rotated  $\frac{1}{4}$  of its perimeter. The distance travelled increases by  $\frac{1}{4}$  the perimeter after each magnetic pulse.

Two methods were explored to incorporate this 3<sup>rd</sup> dimension (distance travelled).

#### 4.2.2.1 3D image Generation by Frames

For every vertical sweep of the motor from its highest point (+ 25°) to its lowest point (- 25°), all measured laser sensor readings would have the same golf cart distance driven reported. This method generates a “frame” for every vertical sweep of the motor: in each frame, depth and height information are reported from the sensor. Each frame then has a different location based on the distance driven. A plotting algorithm is then run to combine the frames into a single graph.

This method is used as a proof of concept to visualize the best 3D images that can be generated from pivoting the laser sensor.

#### 4.2.2.2 3D image Generation by Points

For every distance value measured by the pivoting laser range sensor, the actual distance the golf cart traveled is reported. Hence each plotted point on the 3D image would have different depth, height, and distance travelled values. This method is effective for a vehicle driving continuously, and would be the closest representation of the actual capabilities of the rotating laser range sensor system.

### **4.3 Summary of Experimental Setups**

Experiments were conducted for different parking layouts where the probe vehicle was driven at different speeds, in the vicinity of the Georgia Institute of Technology campus. Moreover, to test the limits of this affordable and commercial sensor, 2D and 3D layouts were generated by pivoting the laser range sensor about its horizontal axis.

## **CHAPTER 5**

### **EXPERIMENTAL RESULTS**

#### **5.1 Accuracy of Laser Range Sensor**

Going back to the example mentioned in Chapter 3.3.3.2, where 90 degree parking spots were scanned at 5 mph: 13 runs were undertaken, for a total of 270 spots scanned. Out of all the runs, one closed spot was missed since the measurement began as the sensor was picking up a motorcycle parked parallel to the car. The calculated vehicle width exceeded our limit of 2.2 m, and the algorithm ignored the vehicle. Even at that, for 156 total closed spots, the sensor detected 154 spots, for an accuracy of 98.72%, and 117 out of 117 open spots for 100% accuracy.

These measurements were repeated for the different speeds and parking angles mentioned above, and excel tables were generated summing up the results of each experiment (Appendix A). In the table below, a summary of the experimental results is shown.

**Table 5: Experimental results**

		Experiments								
		0° Parking		45° Parking		60° Parking		90° Parking		
<b>Speed (mph)</b>		5	10	5	10	5	10	5	10	15
<b>Number of Runs</b>		15	15	20	20	21	20	13	15	13
<b>Sensor Data</b>	Open Spots	49	46	63	32	40	44	117	152	133
	Closed Spots	142	130	120	152	80	75	154	160	140
<b>Ground Truth Data</b>	Open Spots	45	45	43	41	20	20	117	150	130
	Closed Spots	142	132	123	158	100	99	156	165	143
<b>Accuracy (%)</b>	Open Spots	91.1	97.8	68.2	78.0	50.0	45.4	100	98.6	97.7
	Closed Spots	100.0	98.4	97.5	96.2	80.0	75.7	98.7	96.9	97.9

Additionally, three different statistical analyses were undertaken to evaluate the sensor’s accuracy.

### 5.1.1 First Statistical Approach

Firstly, a simple statistical analysis can be performed by looking at the final results from the laser range sensor, and compare them to ground truth data retrieved from the onboard GoPro camera.  $O_{Sensor}$  and  $C_{Sensor}$  are the number of open and closed spots, respectively, based on sensor readings. On the other hand,  $O_{GT}$  and  $C_{GT}$  are the number of open and closed spots based on Ground Truth data.

The accuracy of each run can be simulated as follows:

$$P_{Open} = P_O[g(x)] = O_{Sensor}/O_{GT} \text{ where } I\{g(x)\} = \begin{cases} 1 & \text{if } g(x) \text{ is true} \\ 0 & \text{if } g(x) \text{ is false} \end{cases}$$

$$P_{Closed} = P_C[g(x)] = C_{Sensor}/C_{GT} \text{ where } I\{g(x)\} = \begin{cases} 1 & \text{if } g(x) \text{ is true} \\ 0 & \text{if } g(x) \text{ is false} \end{cases}$$

**Equation 6: Probability calculations for open and closed spots.  
Case where ground truth numbers greater than experimental values**

$I\{g(x)\}$  is an indicator function.  $P_{Open}$  is the probability that an open spot is correctly detected, and  $P_{Closed}$  represents the probability that a closed spot is correctly detected. Ideally, both these numbers should approach 1, meaning that the sensor readings match ground truth data readings. This also entails that the number of open or closed spots detected by the sensor should be inferior to the ground truth numbers. Whenever the system overshoots these ground truth numbers, the accuracy is calculated by:

$$P_{Open} = 1 - \frac{O_{Sensor} - O_{GT}}{O_{Sensor}} = \frac{O_{GT}}{O_{Sensor}} \text{ and } P_{Closed} = \frac{C_{GT}}{C_{Sensor}}$$

**Equation 7: Probability calculations for open and closed spots.  
Case where ground truth numbers smaller than experimental values**

This occurrence is highlighted in Table 6 (numbers in bold), and it was observed that open spots uniquely exhibit this behavior. That is in line with our reasoning: as parked cars are not detected, the algorithm assumes that it is an open spot, therefore resulting in a higher number of sensed open spots compared to ground truth data.

Additionally, confidence intervals are calculated to estimate the intervals that will contain the mean of the number of open (or closed) spots 95% or 99% of the time. In

Table 6, confidence intervals are calculated for 1, 2, and 5 runs for accurate detection 95% and 99% of the time.

**Table 6: Probability Calculation - Method 1**

		0° Parking		45° Parking		60° Parking		90° Parking		
Speed (mph)		5	10	5	10	5	10	5	10	15
<b>P<sub>open</sub> (%)</b>		<b>91.84</b>	<b>97.83</b>	<b>68.25</b>	78.05	<b>50</b>	<b>45.45</b>	100	<b>98.68</b>	<b>97.74</b>
<b>Mean Open</b>		3.27	3.07	3.15	1.60	2.00	2.20	9.00	10.13	10.23
<b>P<sub>closed</sub> (%)</b>		100	98.48	97.56%	96.20	80	75.75	98.72	96.97	97.90
<b>Mean Closed</b>		9.47	8.67	6.00	7.60	4.00	3.75	11.85	10.67	10.77
<b>95%</b> <b>1 run</b>	Open	±0.87	±1.82	±2.86	±1.30	N/A	±0.78	N/A	±0.98	±1.13
	Closed	±1.21	±1.98	±2.48	±1.80	N/A	±0.85	±0.71	±1.17	±1.13
<b>95%</b> <b>2 runs</b>	Open	±0.61	±1.29	±2.02	±0.92	N/A	±0.55	N/A	±0.69	±0.80
	Closed	±0.86	±1.40	±1.75	±1.27	N/A	±0.60	±0.50	±0.83	±0.80
<b>95%</b> <b>5 runs</b>	Open	±0.39	±0.81	±1.28	±0.58	N/A	±0.35	N/A	±0.44	±0.50
	Closed	±0.54	±0.89	±1.11	±0.80	N/A	±0.38	±0.32	±0.52	±0.50
<b>99%</b> <b>1 run</b>	Open	±1.14	±2.39	±3.76	±1.71	N/A	±1.03	N/A	±1.29	±1.48
	Closed	±1.59	±2.60	±3.26	±2.36	N/A	±1.12	±0.93	±1.54	±1.48
<b>99%</b> <b>2 runs</b>	Open	±0.81	±1.69	±2.66	±1.21	N/A	±0.73	N/A	±0.91	±1.05
	Closed	±1.13	±1.84	±2.30	±1.67	N/A	±0.79	±0.66	±1.09	±1.05
<b>99%</b> <b>5 runs</b>	Open	±0.51	±1.07	±1.68	±0.76	N/A	±0.46	N/A	±0.57	±0.66
	Closed	±0.71	±1.16	±1.46	±1.06	N/A	±0.50	±0.42	±0.69	±0.66

### 5.1.2 Discussion of First Statistical Approach

The probabilistic results for this first method show that the accuracy of the laser range sensor is highest for closed spots, but also for parallel and 90° parking. In fact, taking the average sensor accuracy for these parking layouts yields a value of 97.82%. This includes averaging the results of 71 experimental runs, for a total of 1223 spots evaluated. This is due to the fact that at these angles, the sensor usually detects the small gaps between parked vehicles, rendering the parked vehicle counting process

significantly easier. For instance, if these gaps were not visible, the sensor might detect two parked cars in a row; the algorithm would then assume a very wide car (SUV or truck) is parked at that location. We therefore see in Table 6 that the accuracy of the sensor/algorithm is usually above 95% for parallel and 90° parking, a very promising result for future market integration.

The lower efficiencies observed for 45 and 60 degree parking are due to the reasons mentioned above, but also because of a low sample size: very few lots have 45 or 60 parking spots in the Georgia Institute of Technology vicinity. Therefore only a single row of a couple of cars can be scanned. As shown in Chapter 6.3, a single black parked car is not successfully detected by the sensor for 60° parking. Table 16 then shows that for the entire 5 cars parked, only 4 are successfully detected (hence the 80% accuracy for closed spots). As seen in Chapter 5.3 however, pivoting the sensor about its horizontal axis improves black vehicle detection.

The confidence intervals calculated show that as the number of runs increases, the size of the interval decreases. This suggest that more runs around a parking lot improve the accuracy of the system, since the interval in question is closer to the mean of the actual number of closed and open spots. To illustrate this concept, we can evaluate the calculated interval upper and lower limits of occupied spots for experiments around parallel (0°) parking at 5 mph. In that case, the upper/lower limits decrease from 10.68/8.26 ( $\pm 1.21$ ) to 10.33/8.61 ( $\pm 0.86$ ) and finally to 10.01/8.93 ( $\pm 0.54$ ), as seen in Table 6. Accurate detection 95% of the time can also be compared to 99% of the time: going from 95% to 99% increases the size of the interval. Using the same example seen before, the upper/lower limits increase from 10.68/8.26 ( $\pm 1.21$ ) to 11.06/7.88 ( $\pm 1.59$ ).



### 5.1.3 Second Statistical Approach

The second statistical approach is performed to correctly estimate the probability of false positives and false negatives occurring. A false positive refers to the probability that the detection algorithm detects a parked car while ground truth video data shows that the parking spot is unoccupied. Conversely, false negatives refer to the fact that a vehicle is parked but the sensor does not correctly detect it (Mathur, et al., 2010).

Equation 8 below explains how to calculate the false positive and false negative probabilities, using the same variables encountered in Equation 6:

$$P_{FP\text{Positive}} = \frac{(O_{\text{Sensor}} - O_{\text{GT}})}{O_{\text{GT}}} \text{ and } P_{FN\text{Negative}} = \frac{(C_{\text{Sensor}} - C_{\text{GT}})}{C_{\text{GT}}}$$

**Equation 8: False Positive and False Negative Probability Calculations**

The results of the second statistical approach are shown in Table 7 below.

**Table 7: False Positive and False Negative Probability Calculations - Method 2**

Speed (mph)	0° Parking		45° Parking		60° Parking		90° Parking		
	5	10	5	10	5	10	5	10	15
<b>P<sub>FP</sub>Positive</b>	8.89%	2.22%	46.51%	<b>-21.9%</b>	50%	54.54%	0%	1.33%	0.00%
<b>P<sub>FN</sub>Negative</b>	0%	<b>-1.52%</b>	2.44%	<b>-3.8%</b>	<b>-25%</b>	<b>-24.2%</b>	<b>-1.3%</b>	<b>-3.03%</b>	2.31%

### 5.1.4 Discussion of Second Statistical Approach

As expected, the probability of false positives and false negatives occurring is low for 90° and parallel parking. This is due to the fact that the laser range sensor detects closed and unoccupied spots with high accuracy for these parking scenarios.

Table 7 also shows that false positive and false negative probabilities increase for the other scenarios (45 and 60 parking angles). For instance, evaluating the probabilities of experiments run at 10 mph for 60° parking, we notice that the probability of false positives increases to 54.54 %. Referring back to the experimental setup, this high number is due to a black vehicle poorly detected: for 20 runs of a 60° parking lot with 1 empty spot (ground truth), a black vehicle is always “missed”, causing the algorithm to assume it is an open spot. This leads to a false positive error almost half the time ( $\approx 50\%$ ).

Moreover, it is seen in Table 7 that some calculated probabilities are negative (in bold). This is noticeable for the experiment evaluating 45° parking at 10 mph, where the probability of false positive is -21.95%. This negative probability signifies that the counted number of open spots by the sensor and algorithm is less than the ground truth data for the total number of open spots. Similarly, for the experiment evaluating 60° parking at 5 mph, the probability of false negative is -25%. Again, this implies that the counted number of closed spots by the sensor is less than the ground truth data for the number of closed spots. These negative probabilities could be ignored (by taking the absolute values in Equation 8), as is done in literature, but should not since they imply that the sensor is underestimating the actual number of open and occupied spots. For actual market implementation, miscalculating the number of closed spots would lead

customers to gain false confidence in a parking lot. That would encourage them to drive to that misrepresented parking lot in search for a parking spot there.

### 5.1.5 Third Statistical Approach

Finally, we could simulate how many runs around a parking lot are needed to correctly locate open and closed spots with a confidence level of 90 and 95%. In our study, we will assume that each run through a parking strip represents an event, which is independent from the next. This assumption is reasonable since the probability of one random event occurring does not affect another event.

After calculating a general and conservative value for the accuracy, the following formulas can be used to estimate the confidence level after N many runs.

Assuming the accuracy of the laser range sensor is 80 %:  $P_{\text{Car}} = 0.8$  and  $P_{\text{No Car}} = 0.2$

In one pass, probability of spotting a car  $\epsilon_1 = P_{\text{Car}} = 0.8 = 1 - P_{\text{No Car}}$

In 2 passes,  $\epsilon_2 = 1 - (P_{\text{No Car}}^2) = 0.96$

In 10 passes,  $\epsilon_{10} = 1 - (P_{\text{No Car}}^{10}) = 0.999999$

Therefore for N runs:

$$\epsilon_N = 1 - (P_{\text{No Car}}^N) \text{ so } N = \frac{\ln(1 - \epsilon_N)}{\ln(P_{\text{No Car}})}$$

**Equation 9: Confidence calculation**

Where  $\epsilon_N$  is the target accuracy achieved after N runs.

The results of the final statistical approach are shown in Table 8 below.

**Table 8: Probability of correctly mapping a parking lot after a number of runs – Method 3**

		Accuracy								
		90 %	80 %	70 %	60 %	50 %	40 %	30 %	20 %	10 %
<b># of Runs</b>	1	90.0	80.000	70.000	60.000	50.000	40.000	30.000	20.000	10.000
	2	99.0	96.000	91.000	84.000	75.000	64.000	51.000	36.000	19.000
	3	99.90	99.200	97.300	93.600	87.500	78.400	65.700	48.800	27.100
	4	99.990	99.840	99.190	97.440	93.750	87.040	75.990	59.040	34.390
	5	99.999	99.968	99.757	98.976	96.875	92.224	83.193	67.232	40.951
	6	99.999	99.994	99.927	99.590	98.438	95.334	88.235	73.786	46.856
	7	100.0	99.998	99.978	99.836	99.219	97.201	91.765	79.029	52.170
	8	100.0	99.999	99.993	99.935	99.609	98.320	94.235	83.223	56.953
	9	100.0	99.999	99.998	99.974	99.805	98.992	95.965	86.578	61.258
	10	100.0	100.000	99.999	99.989	99.902	99.395	97.175	89.263	65.132

### 5.1.6 Discussion of Third Statistical Approach

As explained previously, the sensor accuracy can be generated for detecting open or closed spots. Hence two different confidence level tables can be created, based on which probability value is used. As an ideal case, we can consider the accuracy of experiments for 90° and parallel parking; but for a worst case scenario, we may look into the accuracy of experiments for 60° parking where a black car (out of 5 total cars) was never scanned.

- 90° and parallel parking scenario:

Out of a total of 497 scanned open spots, 487 were actually proven to be unoccupied by ground truth data. This brings the accuracy to 97.988 %. Additionally, out of 726 scanned closed spots 738 were actually closed, generating an accuracy of 98.37 %. Therefore using Equation 9, the following table can be generated:

**Table 9: Confidence for 90° and parallel parking (best case scenario)**

Number of Runs	Confidence	
	Open spots	Closed Spots
1	97.988	98.374
2	99.960	99.974
3	99.999	100.000
4	100.000	100.000
5	100.000	100.000

The table above shows that about 2 runs are required to achieve 99 % confidence, while 3 runs would be needed to map a parking lot with 100 % confidence.

- 60° parking scenario:

Out of a total of 84 scanned open spots, 40 were actually proven to be unoccupied by ground truth data. This brings the accuracy to 47.619 %. Additionally, out of 155 scanned closed spots 199 were actually closed, generating an accuracy of 77.889 %. Again using Equation 9, Table 10 can be generated:

**Table 10: Confidence for 60° parking (worst case scenario)**

<b>Number of Runs</b>	<b>Confidence</b>	
	Open spots	Closed Spots
<b>1</b>	47.619	77.889
<b>2</b>	72.562	95.111
<b>3</b>	85.628	98.919
<b>4</b>	92.472	99.761
<b>5</b>	96.057	99.947
<b>6</b>	97.934	99.988
<b>7</b>	98.918	99.997
<b>8</b>	99.433	99.999
<b>9</b>	99.703	100.000
<b>10</b>	99.844	100.000

The table above shows that about 2 runs are required to achieve 95 % confidence for closed spots, while 5 runs would be needed to map a parking lot with 95 % confidence for open spots. If probe vehicles are fitted with the laser range sensor used for these experiments, this entails that 5 vehicles (worst case scenario) would have to drive through a 60° parking lot to correctly map it with 95 % confidence.

## **5.2 Experiments under Inclement Weather**

In prior art, we have seen researchers explore the possibility of installing ultrasonic, infrared, video and magnetic sensors with different amount of success (Ono, Kagesawa, & Ikeuchi, 2002), (Park, Kim, Seo, Kim , & Lee, 2008), (Abdel-Hafez, Al Nabulsi, Jafari, Al Zaabi, Sleiman, & AbuHatab, 2011), (Thornton, Redmill, & Coifman, 2014), (Son, Kim, & Sohn, 2015), (Makris, Perrollaz, & Laugier, 2013), (Zhang, Tao, &

Yuan, 2014), (Gu, Zhang, Yu, & Liu, 2012), (Chinrungrueng, Sunantachaikul, & Triamlumlerd, 2007), (Tong, Cheng, Li, Wang, & Du, 2014). These authors have not however explored testing their sensors and algorithms under inclement weather such as rain. Some authors, such as Ono et al. and Tong et al. have even installed expensive laser sensors onto their probe vehicles, without studying their efficiency under heavy rain, and whether the data collected would be affected. Moreover, water damage to these systems would be far more expensive (some sensors cost upwards of \$10,000) than any damage to a \$90 easily replaceable sensor.

After experimenting with the laser range sensor, it was determined that it could detect objects through clear and thin material. It was therefore decided to devise a cost effective and simple solution to waterproof the entire system: clear freezer bags were tightly tied around the mount, wires and laser sensor; and rubber bands were used to ensure a tight and waterproof fit (Figure 35.b).

As can be noted in Figure 47.a, the simple waterproofing mechanism worked flawlessly. Moreover, the laser range sensor was not affected by heavy rain, and correctly mapped the strip of the parking lot: compared to ground truth data from the GoPro video (Figure 47.b) the sensor's accuracy matched previous experiments (around 98%).



**Figure 47: (a) Results of testing under adverse weather conditions, and (b) ground truth data**

This step was undertaken to study the efficiency of the entire system under adverse weather conditions, specifically monitoring the behavior of the laser range sensor under heavy rain. For actual implementation in the automotive market, manufacturers would need to devise a more robust and aesthetic waterproofing solution. At this point however, it was proven that the laser range sensor detects parked vehicles through clear material, and is not affected by heavy rain.

### **5.3 Experiments with Pivoting Laser Range Sensor**

Before trying to generate a 3D map of the parking lot, the sensor was pivoted about its horizontal line (Figure 45) to evaluate whether that has any effect on data collection. This information was then compared to “dry runs”, where the sensor is stationary and behaves as explained in Chapter 3.3.3. For the sake of comparison, the properties and conditions were not varied between both runs.



Figure 48 shows a sample run with the pivoting sensor. The experiment is shown in its entirety to prove that the pivoting still efficiently maps a parking lot, differentiating occupied from empty spots.

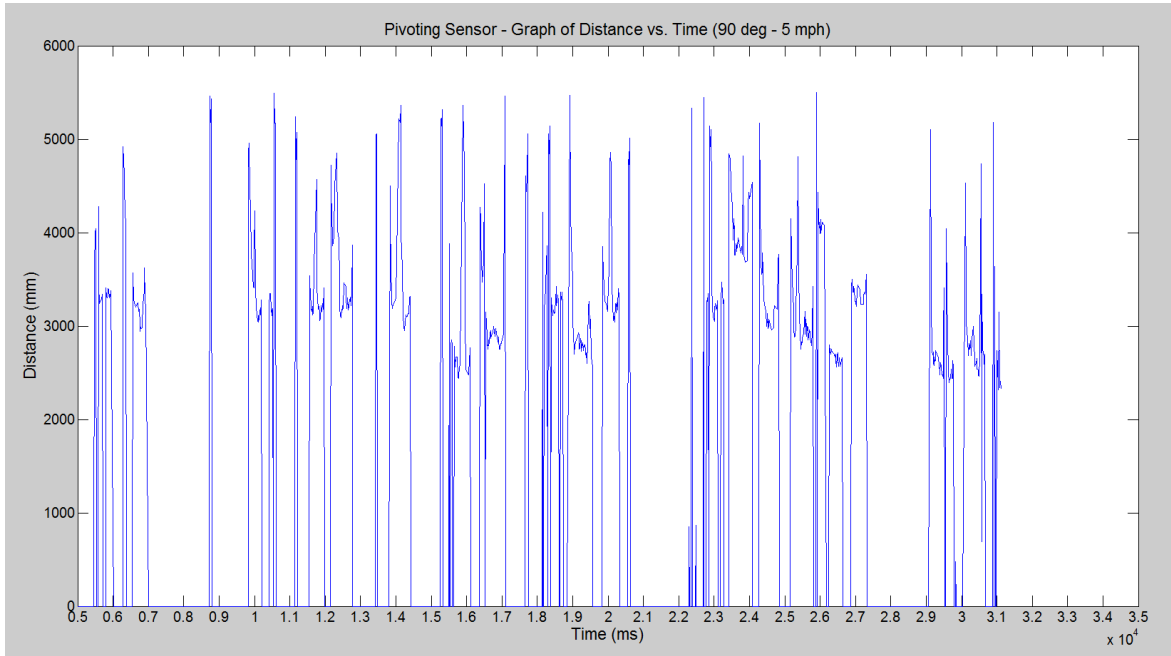


**Figure 48: Sample run with pivoting sensor**

What is notable about these specific experiments is a black parked at the beginning of the parking lot, shown in Figure 49 below. As mentioned previously, laser sensors might not detect some black surfaces; therefore it would be interesting to study the effect of pivoting the sensor on black surface detection.



**Figure 49: Black car parked at the start of the parking lot**

Since the black car is located at the beginning of the experiment, we can focus on the sensor readings between 0 and 8 seconds for the stationary and pivoting sensors. In Figure 50, the data for the black vehicle is circled in red: we notice that in Figure 50.a, multiple successive points are registered, whereas only a limited number of points are registered in Figure 50.b. When the detection algorithm is run for these experiments, the successive points in Figure 50.a are correctly estimated to be a closed spot; however the scarce points in Figure 50.b do not describe the profile of a car, and are therefore ignored.

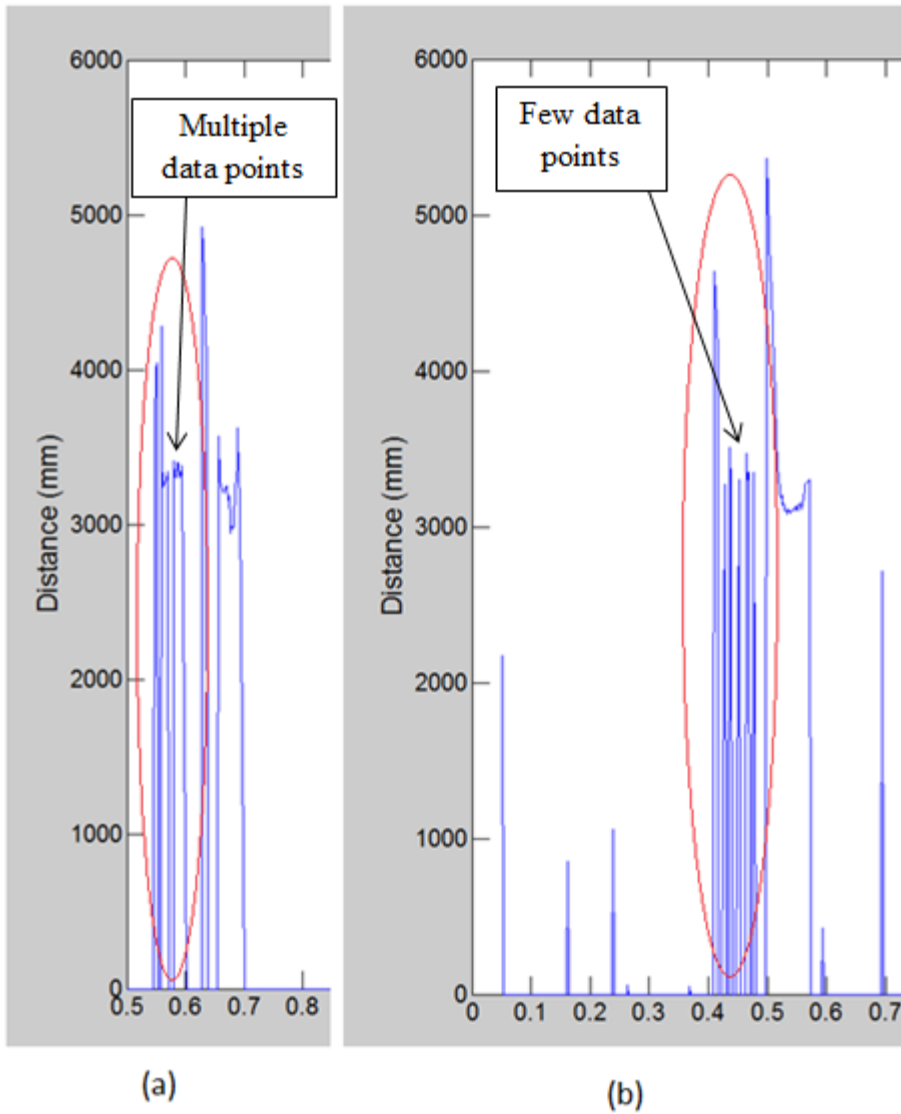
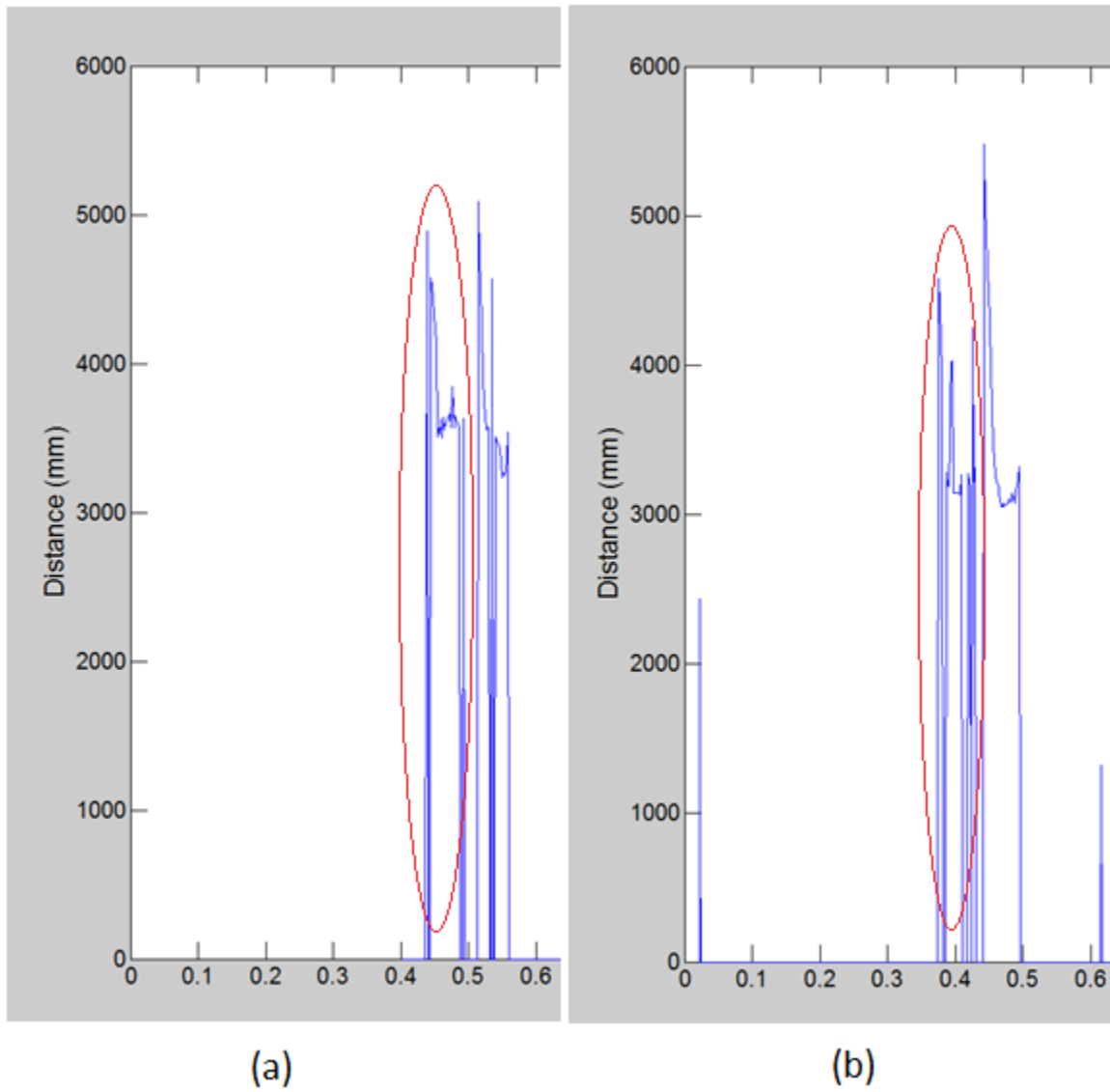


Figure 50: Scanning a black vehicle at 5 mph, (a) with the pivoting sensor and (b) with a stationary sensor

This experiment is repeated for a probe car velocity of 10 mph. The initial sensor data points are shown in Figure 51. In this case, the black car is mapped perfectly while the sensor is pivoting (Figure 51.a); whereas some interruptions can be seen in the stationary sensor points (Figure 51.b).



**Figure 51: Scanning a black vehicle at 10 mph, (a) with the pivoting sensor and (b) with a stationary sensor**

Pivoting the laser range sensor ameliorates data collection, and provides more accurate information when the stationary sensor fails to detect vehicles. Although the algorithm detects the vehicle in question, what if data is affected by noise and therefore not usable for the simulation? That is where a LIDAR generated 3D plot would be very

useful. By looking at the map of parking lot, an algorithm would be able to detect a parked vehicle that was missed by the laser range sensor.

## 5.4 Generating a 2D Image

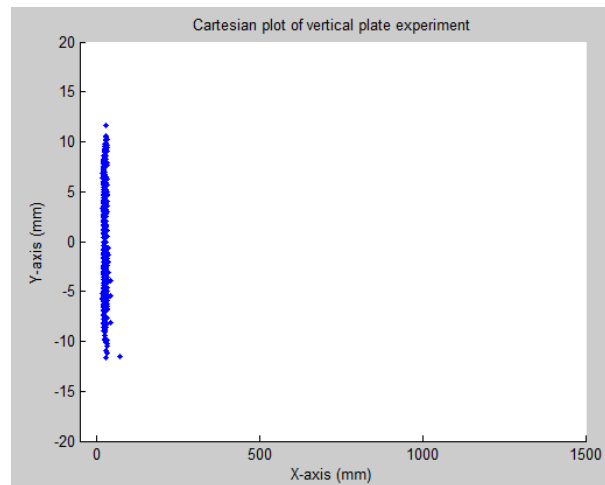


**Figure 52: Experimental result of scanning a vertical plate**

As explained previously, to generate a 3D map, one should ensure the success of obtaining a 2D image first. As seen in Figure 52, converting from polar to cartesian coordinates was effective, and a vertical plate was scanned successfully. However, to verify the sensitivity of the system, a more extensive experiment was conducted: it involved cutting a hole through a vertical plate, and setting a second plate behind it. The pivoting sensor should detect this “hole” on the experimental cartesian plot. As seen in Figure 53.b, it does so successfully. Moreover, the accuracy of the laser range sensor can be observed. The multiple points detecting the plates are less than 15 mm apart,

suggesting a high level of accuracy (Figure 53).

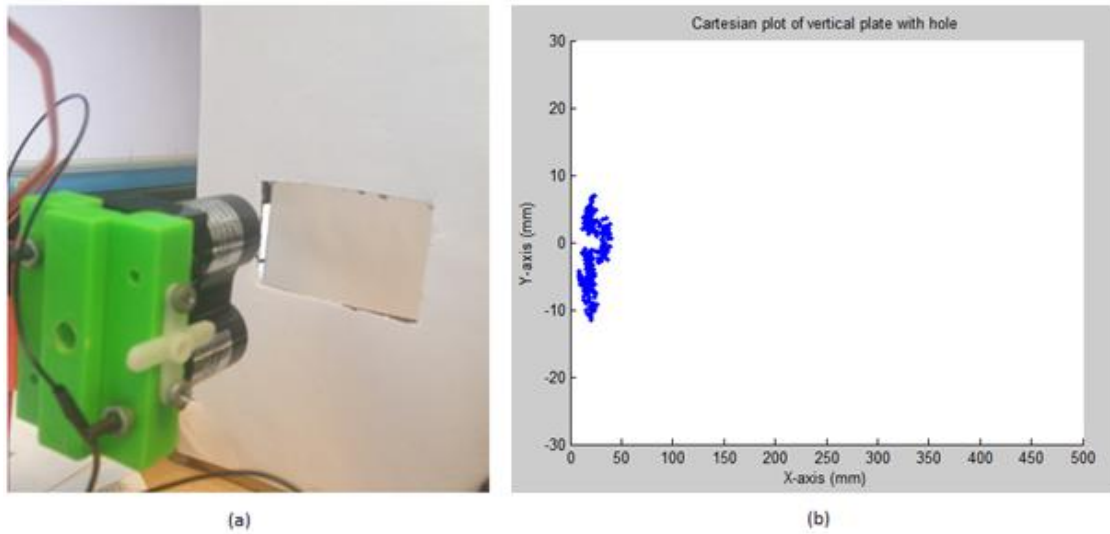


**Figure 53: (a) Setup and (b) experimental result of scanning a vertical plate with a hole**

## **5.5 Generating a 3D Image**

Since pivoting the sensor yielded a favorable outcome, the next step would be to generate a 3D image by combining rotating sensor information with vehicle velocity or distance travelled.

### **5.5.1 Results of 3D imaging by Frames**

This method was used to 3D map the car shown in Figure 54. The result is depicted in Figure 55, where the side of the Jeep can clearly be seen at around 500 mm depth. The background behind the car and pavement in front are also clearly mapped.



Figure 54: Picture of 3D scanned vehicle

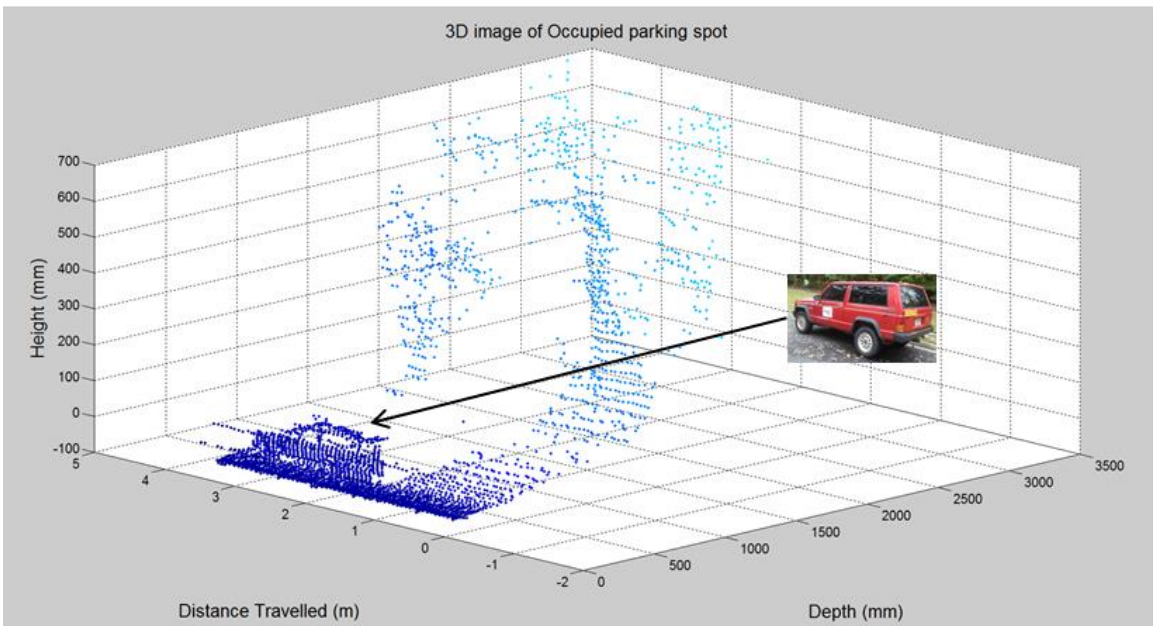


Figure 55: Laser range sensor 3D scanning vehicle by the “Frame Method”

These results are an ideal representation of the capabilities of the pivoting laser range sensor: since the probe vehicle was driven at low speeds, and stopped while generating each frame, it does not accurately represent how the sensor would perform if installed on an actual car.

### **5.5.2 Results of 3D imaging by Points**

Figure 56 depicts the result of using the actual driven distance to 3D scan the vehicle shown in Figure 54. As can be observed in Figure 56, the vehicle seems to be tilted to the right. This is because each distance measured by the laser range sensor is allocated a unique distance driven. Hence as the probe vehicle is driven, no two sensor measurements will have the same driven distance index.

This representation more closely resembles the real-world results obtained by pivoting the sensor: the shape and outline of the scanned vehicle is clearly visible, and video sensing systems would be greatly enhanced by including these 3D maps. Some adjustments need to be performed however, mainly fine-tuning the distance travelled by the vehicle, thus eliminating the “tilt” observed in Figure 56.



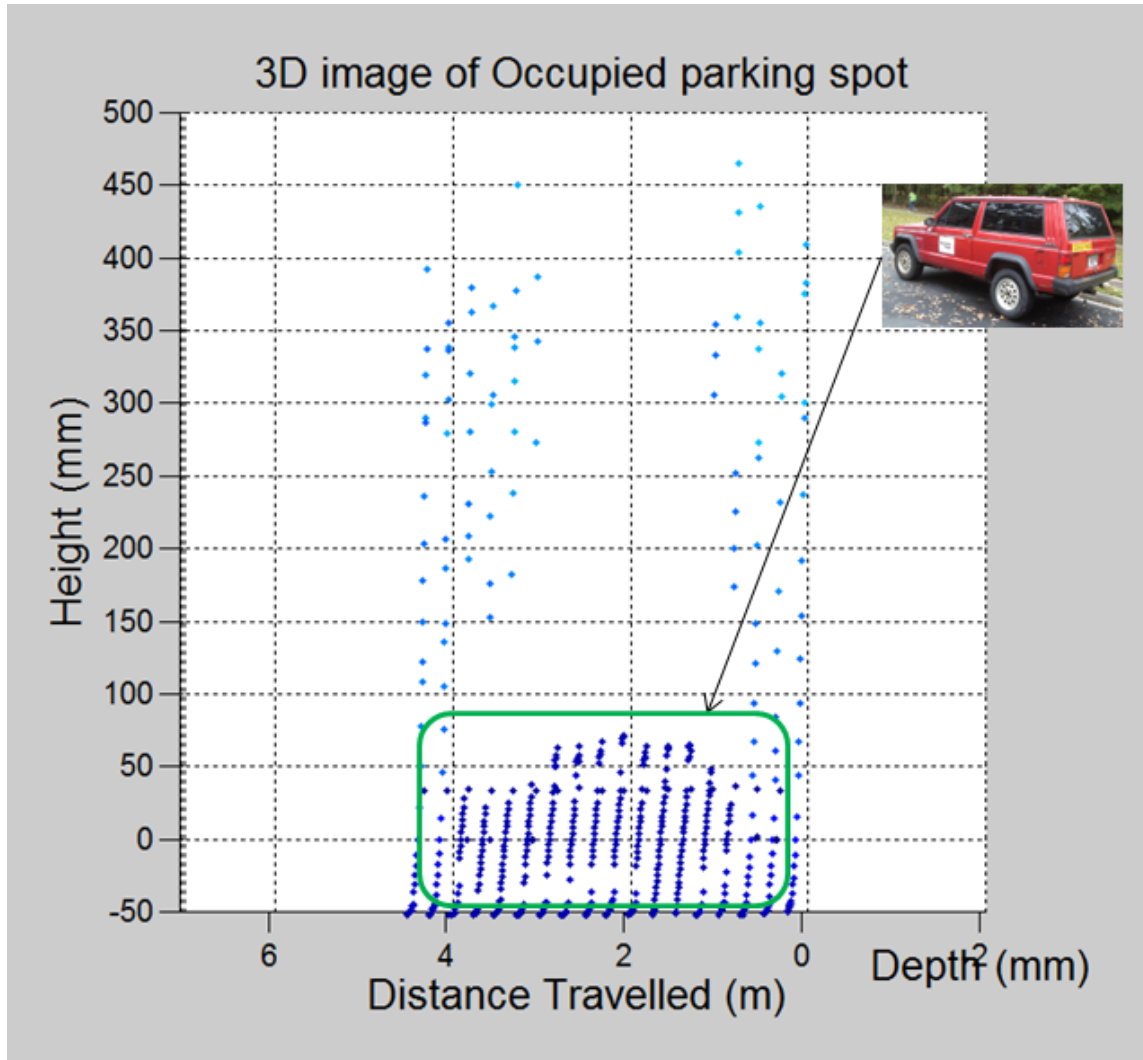


**Figure 56: Laser range sensor 3D scanning vehicle by the “Points Method”**

These efforts were conducted to explore the limits of the installed laser range sensor and compare its performance to more expensive 2D LIDARs used in literature (Thornton, Redmill, & Coifman, 2014).

## 5.6 Enhancement of Parking Angle Detection

One of the ongoing efforts is to have the algorithm differentiate between parking configurations, and possibly inform the user about which parking angle is observable. In Figure 57 for example, a pattern is clearly seen where the right rear edges of parked vehicles are very well mapped.

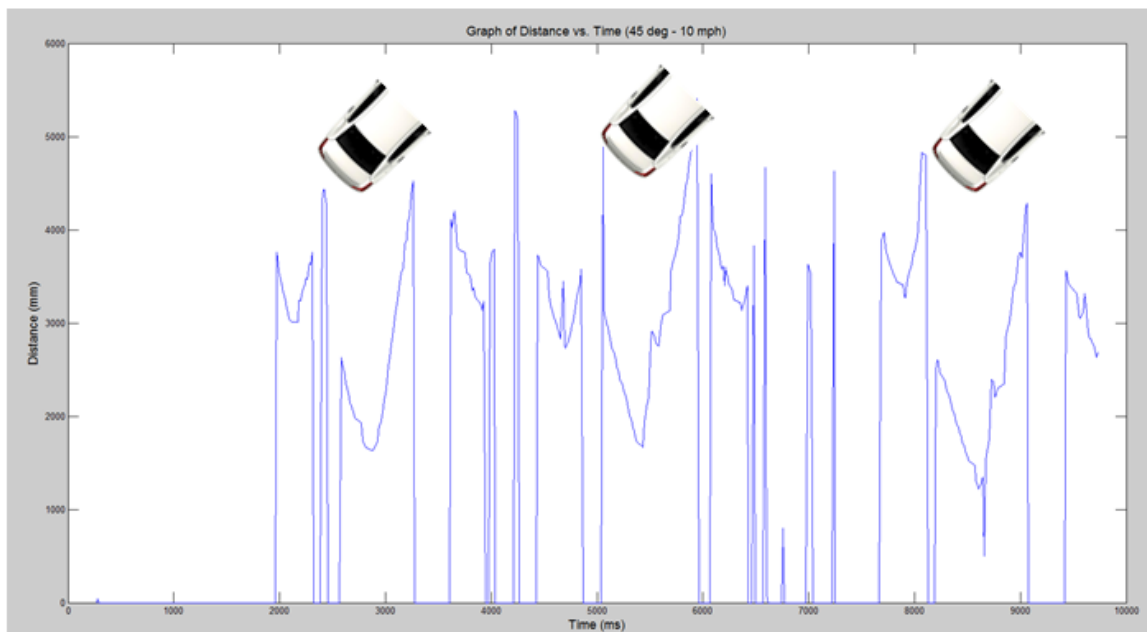


**Figure 57: Possible parking angle detection**

So far, the algorithm can successfully differentiate between parallel and 90° parking. The issue with distinguishing between 45, 60, and 90 degree parking layouts is the assumption that all drivers abide by the white limiting lines when parking. However, since this is not the case, 45° parking might look very similar to 60° parking, thus

providing inaccurate data for the algorithm. This leads to erroneous results, and poor parking angle detection.

## **5.7 Summary and Recommendations**

Experiments were performed to evaluate the accuracy and adaptability of the laser range sensor system. The probe vehicle fitted with the laser range sensor was driven at different speeds around several parking lots, with 45, 60, 90, and 0 degree (parallel) parking angles. Statistical analyses showed that 90° and 0° parking lots were most accurately mapped, with an average accuracy of about 95%. These high efficiencies meant that a parking lot could be mapped with 99% confidence after only 2 runs.

Subsequently, different methods were assessed to explore the enhancement of parking detection. The system was waterproofed in an efficient and affordable manner (freezer bags), and tested under inclement weather. It was found that the sensor detects parked vehicles with high accuracy, unaffected by the weather. The sensor was additionally pivoted about its horizontal axis, enhancing the detection of black vehicles which were initially undetected by a stationary sensor. Finally, 2D and 3D images were generated using that laser range sensor, proving that the technology could be used for several different applications, and could compete with more expensive 2D LIDAR systems explored in literature.

Because of the positive results achieved from these experiments, car manufacturers should implement this affordable laser range sensor technology to enhance

parking spot detection, and possibly replace outdated ultrasonic technology currently found on vehicles.

## CHAPTER 6

### APPLICABILITY TO PRODUCTION VEHICLES AND SUMMARY

#### 6.1 Cost of Installation

Based on the recommendations from Chapter 5.7, the applicability of the system to current production vehicles was evaluated based on cost, installation requirements, and its use in parking applications.

Table 11 shows the total cost of the laser detection system. If the laptop used is disregarded, the total cost would amount to \$144.89. For a complete system with a motor installed, car charger, and a Bluetooth shield to send data to a server (explored in Chapter 6.2.1), the system would cost \$185.45. As mentioned in Chapter 2.1.1, this cost would be minimal compared to fitting each parking spot with ultrasonic sensors (around \$838 per spot).

Table 11: Total cost the suction cup and window mount systems

Item	Quantity	Suction Cup	Mount + motor + Bluetooth Shield
		Unit price	Unit price
Mount	1	26.99	27
Car charger	1	0	4.99
Arduino USB	1	3.95	3.95
Arduino Uno	1	24.95	24.95
Lidar Lite	1	89	89
Stepper motor	1	0	15.56
Bluetooth Shield	1	0	19.99
<b>Total</b>		\$144.89	\$185.45

## 6.2 Applicability to Commercial Vehicles and Enhancements Produced

After determining the high accuracy of the laser range sensor and detection algorithm in detecting parked vehicles and unoccupied spots, the applicability of the system to commercial cars needs to be evaluated. Moreover, the enhancements generated by installing such a system will be listed and explained.

### 6.2.1 Installation on Commercial Vehicles

To eliminate the use of a laptop for data collection, a method for sending laser range sensor data via Bluetooth was evaluated: data was successfully sent from the Arduino microcontroller to an Android device using a Bluetooth shield (Figure 58). The shield enables Bluetooth sending and receiving applications on the microcontroller with the help of simple Bluetooth coding libraries.

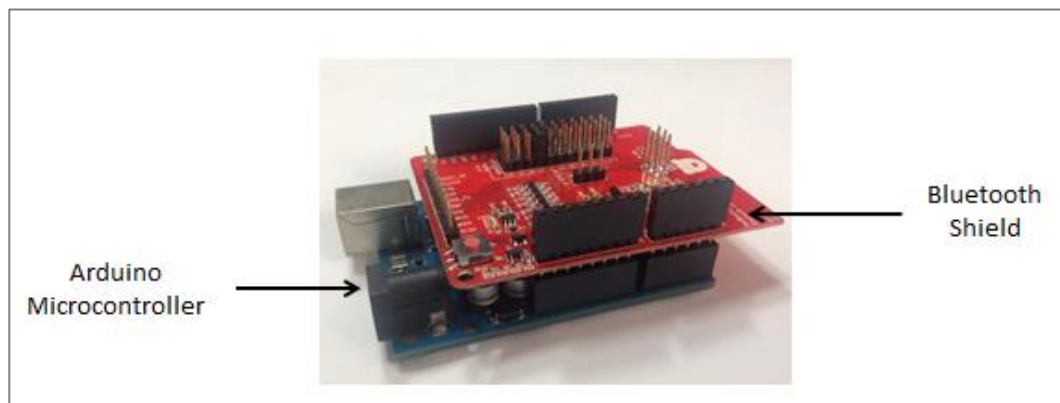
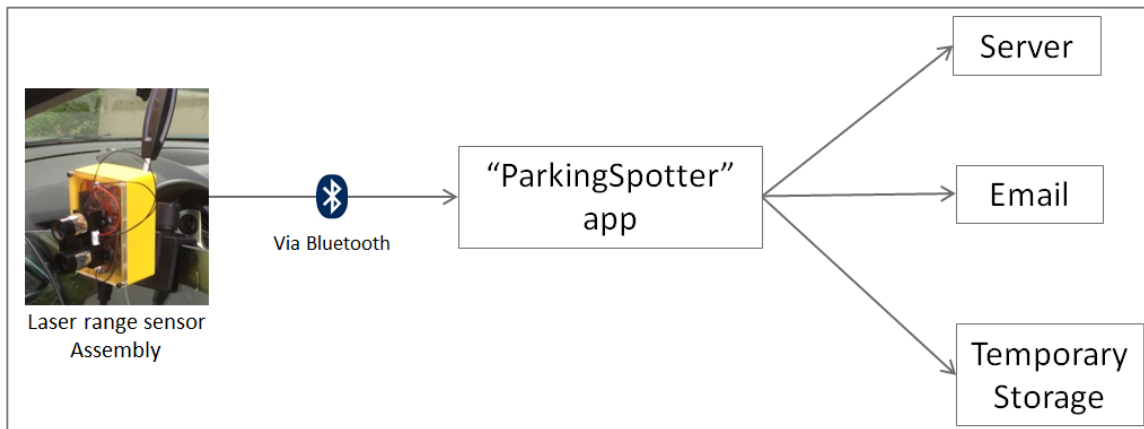


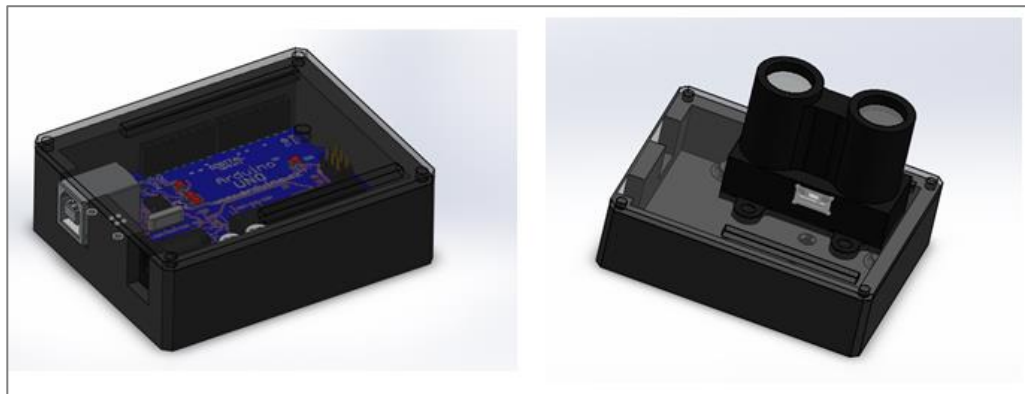
Figure 58: Bluetooth shield installed on Arduino microcontroller

Figure 59 below shows an overview of the system operation. After powering the microcontroller with a USB cord connected to the car's lighter socket, the "ParkingSpotter" app searches for the Bluetooth shield address, and recognizes the microcontroller setup. Laser range sensor data can then be logged, and wirelessly sent to a server or an email, or saved to a temporary storage.



**Figure 59: Diagram of Bluetooth integration**

A 3D representation of the Bluetooth system using SolidWorks is shown in Figure 60. The final product is also displayed in Figure 61.



**Figure 60: 3D drawing of Bluetooth system**



**Figure 61: Final system mounted on a car window**

The process above demonstrated that this sensor could eventually be implemented into production vehicles, thus eliminating the use of more traditional ultrasonic sensors. The Arduino and Bluetooth shield can also be excluded by directly sending sensor information to the vehicle's control box or tablet. Since today's cars are fitted with ultrasonic sensors for parking assistance, replacing these sensors with much more accurate laser range sensors should be feasible. For example, the ultrasonic sensors used in (Fleming, 2008) have a low range of 2-4 m, with a frequency limited to 50 Hz. However, the laser range sensor used in this thesis can reach frequencies of up to 90 Hz (the newer version reaching 200 Hz) with a range of 35-40 m. Replacing the outdated ultrasonic sensors in production vehicles would therefore enhance parking spot detection, and might aid in other driving applications requiring long range distance measurements.



As explained in Chapter 5.2, a simple method for waterproofing was used by wrapping the sensor setup with clear freezer bags. This solution was very effective; but for actual implementation in the automotive market, manufacturers would need to design a more aesthetic and robust waterproofing solution.

### **6.2.2 Enhancement of Parking Spot Detection**

To enhance customers' parking experience, car manufacturers would implement the affordable range sensor to detect parking spot availability. Next, that information could be relayed to dedicated servers. Since today's car manufacturers are installing modems into their vehicles, that internet connection could be used to transmit sensor information to servers devoted for parking data analysis.

Table 9 shows that about 2 runs are required to achieve 95 % confidence for closed spots, while 5 runs would be needed to map a parking lot with 95 % confidence for open spots. If probe vehicles are fitted with the laser range sensor used for these experiments, this entails that 5 vehicles (worst case scenario) would have to drive through a 60° parking lot to correctly map it with 95 % confidence.

Considering a parking lot with significant activity, car manufacturers could combine information retrieved from each vehicle (driving past a parking lane) with GPS data as done in (Mathur, et al., 2010) and (Thornton, Redmill, & Coifman, 2014) to automatically update a parking lot map with available and occupied parking spot. Moreover, for consumers using a GPS application to reach their destination, parking data

can be embedded into the application to help with the final leg of the journey: securing a parking spot. By examining sensor data, the application can rate different parking lots based on open parking space detected, distance from final destination, and cost of parking. The user might then have to compromise and choose which feature he prefers: a guaranteed parking spot, close proximity to destination, or low cost.

### 6.3 Reflectivity Issues

It should be noted that the experiments are conducted with an infrared laser beam, for which darker objects may be tougher to detect (Kikuta, Iwata, & Nagata, 1986). For the tests performed with the probe car, we have noticed that most black cars are successfully detected by the laser sensor and algorithm. However in some instances, a specific car might be coated in a color that is not efficiently detected by the sensor. Taking the case shown in Figure 62.a for instance, we notice that a set of 3 cars are parked in a 60° parking lot, with car 1 having a white coat color while cars 2 and 3 both have a black coat color. Figure 62.b shows the sensor readings obtained after the run is completed. It was observed that for car 2, the sensor only returned a limited number of points, whereas it registered a complete set of points for cars 1 and 3. After running the data through the detection algorithm, cars 1 and 3 were successfully identified as closed spots, whereas car 2 was mislabeled as an open spot. It should be noted that even though car 3 also had a black coat of paint, it was successfully detected by the sensor and algorithm. This leads us to believe that a certain matte color of dark car paint negatively affects the sensor readings.



**Figure 62: Example of black car that is not accurately detected by the sensor: (a) Ground truth from video and (b) sensor readings**

This is an isolated example which seldom occurred in the tests completed; however a solution has been devised where cars with this color are better detected: as seen in a Chapter 5.3, pivoting the sensor about its horizontal axis improved readings and enhanced closed parking spot detection.

## 6.4 Point vs Plane Mapping

As noted in Chapter 5.3, pivoting the sensor about its horizontal axis enhances the detection of black vehicles. These vehicles might not be more efficiently (or hardly) detected with a stationary sensor (point detection). Moreover, Chapters 5.4 and 5.5 explored the effect of pivoting the laser range sensor to generate 2D and 3D images of the probe vehicle's surroundings. As Figure 53 and Figure 55 prove, these experiments were successful and produced accurate 2D and 3D images. Compared to the results from commercial 2D LIDARs, the setup used in this thesis generates comparable 2D and 3D

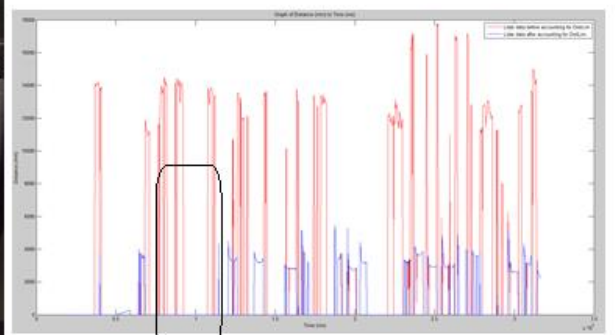
images (with shorter range), but using substantially less expensive equipment: \$10,000 for Thornton et al.'s set up compared to \$185.45 for this thesis's entire setup and mounting system.

## 6.5 Environmental Issues, Limits, and Properties to Consider

In these sets of experiments, a flaw of the stationary sensor was noted: as seen in Figure 63.a, if special care is not given to correctly mount the sensor and ensure the laser beam passes over parked cars, it might overshoot the vehicles and not detect them. Figure 63.b shows how some vehicles are not detected compared to Figure 40. This is where pivoting the laser range sensor is essential: even if it is initially poorly angled, the fact that it will eventually rotate means that it will successfully detect parked vehicles.



(a)



The sensor should have detected 2 vehicles

(b)

**Figure 63: (a) Video and (b) data of sensor overshooting vehicles**

Moreover, during the initial tests, a motorcycle was parked in at the start of the parking strip (Figure 64.a). As seen in Figure 64.b, the sensor successfully detects the motorcycle. However, compared to the following cars parked at a 90° angle, the motorcycle appears to be a parallel parked car on the sensor log. This suggests that the algorithm might not count it as a vehicle, and actually infer that it is an open space. This issue was fixed by modifying the range of acceptable car width in the final algorithm. Some of these special cases need to be considered before installing the laser range sensors in production vehicles. With testing under different conditions, a more robust system can be implemented.

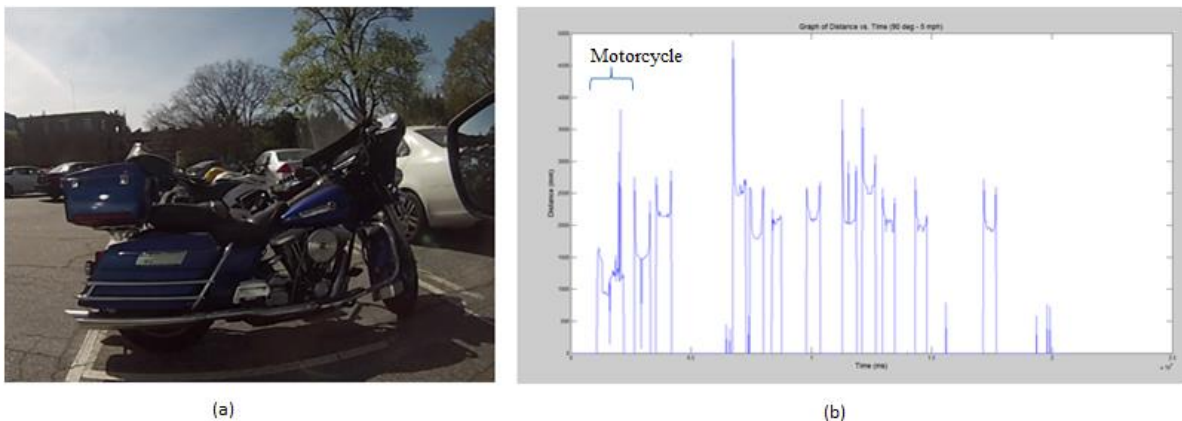


**Figure 64: (a) Motorcycle parked, and (b) picked up by sensor**

Finally, although the system was tested during heavy rainfall, some more severe weather conditions still need to be considered such as snow and fog. For instance, the sensors could be installed on vehicles in northern states. The laser range sensor then

needs to be tested under such extreme conditions, to ensure the robustness of the system but also the validity of the data.

## 6.6 Conclusions

This thesis explored available sensor technologies used for parking spot detection such as ultrasonic sensors, vision sensors, Anisotropic Magnetoresistive sensors, and Wireless Sensor Networks. It was shown from literature that each of these sensors exhibited some drawbacks, rendering their installation on probe vehicles for parking spot detection inefficient.

Because of that, laser technology was investigated. Again, available implementations were looked into, showing promising results for the amelioration of parking spot detection. Alas, some disadvantages such as extremely high cost (\$10,000 to \$60,000 for some systems) and difficult implementation were emphasized.

A solution to those problems would be to use an affordable laser range sensor which would be easily installable onto probe vehicles. An off-the-shelf “LIDAR-Lite” \$90 sensor by “PulsedLight” was therefore utilized. Experiments were performed to evaluate the accuracy and adaptability of that laser range sensor. A probe vehicle was fitted with the laser range sensor system, and was driven at different speeds around several parking lots, with 45, 60, 90, and 0 degree (parallel) parking angles. Statistical analyses were then performed, calculating efficiencies as high as 100%.

Subsequently, different methods were assessed to explore the enhancement of parking detection using a “LIDAR-Lite” sensor. The system was waterproofed in an efficient and affordable manner, and it was found that the sensor detects parked vehicles with high accuracy, unaffected by inclement weather conditions such as heavy rain. The sensor was additionally pivoted about its horizontal axis, enhancing the detection of black vehicles which were unnoticed by a stationary sensor. Finally, 2D and 3D images were generated using that laser range sensor, proving that the technology could be used for several different applications such as parking lot mapping, enhancing GPS data, and assisting in video sensing technologies.

## APPENDIX A

### TABLES OF EXPERIMENTAL RESULTS

After running the experiments, the detection algorithms were used to obtain the number of open and closed spots for different parking lots, at different speeds. Table 12 through Table 20 show the results of these experiments.

**Table 12: Tests performed for parallel parking, at 5 mph**

<b>0 Degrees - 5 mph</b>				
<b>Run Number</b>	<b>Open Spots</b>	<b>Closed Spots</b>	<b>Ground Truth Open Spots</b>	<b>Ground Truth Closed Spots</b>
1	3	10	3	10
2	3	9	3	9
3	4	8	3	9
4	3	10	3	10
5	3	10	3	10
6	3	10	3	10
7	3	9	3	9
8	3	10	3	10
9	3	9	3	9
10	4	9	3	9
11	4	9	3	9
12	4	9	3	9
13	3	10	3	9
14	3	10	3	10
15	3	10	3	10
<b>Summary</b>	49	142	45	142

**Table 13: Tests performed for parallel parking, at 10 mph**

<b>0 Degrees - 10 mph</b>				
<b>Run Number</b>	<b>Open Spots</b>	<b>Closed Spots</b>	<b>Ground Truth Open Spots</b>	<b>Ground Truth Closed Spots</b>
1	3	8	3	8
2	3	9	3	9



3	3	8	3	8
4	3	8	3	8
5	3	9	3	9
6	3	8	3	8
7	1	6	3	9
8	3	10	3	9
9	6	9	3	10
10	3	10	3	10
11	3	9	3	9
12	3	8	3	8
13	3	10	3	9
14	3	9	3	9
15	3	9	3	9
<b>Summary</b>				
	46	130	45	132

Table 14: Tests performed for 45° parking, at 5 mph

<b>45 Degrees - 5 mph</b>				
<b>Run Number</b>	<b>Open Spots</b>	<b>Closed Spots</b>	<b>Ground Truth Open Spots</b>	<b>Ground Truth Closed Spots</b>
1	6	4	5	4
2	6	3	5	4
3	6	4	5	5
4	4	6	3	7
5	4	6	3	7
6	2	5	1	6
7	2	5	1	6
8	2	5	1	5
9	4	6	3	7
10	4	6	3	7
11	1	6	2	8
12	2	8	1	9
13	3	7	2	8
14	2	7	1	8
15	3	7	2	7
16	2	7	1	5
17	2	7	1	5
18	3	7	1	5
19	2	7	1	5
20	3	7	1	5
<b>Summary</b>				
	63	120	43	123

**Table 15: Tests performed for 45° parking, at 10 mph**

<b>45 Degrees - 10 mph</b>				
<b>Run Number</b>	<b>Open Spots</b>	<b>Closed Spots</b>	<b>Ground Truth Open Spots</b>	<b>Ground Truth Closed Spots</b>
1	3	8	3	8
2	1	8	2	8
3	2	9	2	9
4	2	8	2	8
5	2	8	2	8
6	2	8	2	8
7	2	7	2	8
8	1	9	2	9
9	1	8	2	8
10	1	8	2	8
11	3	5	2	6
12	1	7	2	8
13	2	6	2	7
14	1	8	2	8
15	1	8	2	8
16	1	7	2	7
17	2	8	2	8
18	2	8	2	8
19	1	7	2	8
20	1	7	2	8
<b>Summary</b>	32	152	41	158

**Table 16: Tests performed for 60° parking, at 5 mph**

<b>60 Degrees - 5 mph</b>				
<b>Run Number</b>	<b>Open Spots</b>	<b>Closed Spots</b>	<b>Ground Truth Open Spots</b>	<b>Ground Truth Closed Spots</b>
1	2	4	1	5
2	2	4	1	5
3	2	4	1	5
4	2	4	1	5
5	2	4	1	5
6	2	4	1	5
7	2	4	1	5
8	2	4	1	5
9	2	4	1	5
10	2	4	1	5
11	2	4	1	5

<b>12</b>	2	4	1	5
<b>13</b>	2	4	1	5
<b>14</b>	2	4	1	5
<b>15</b>	2	4	1	5
<b>16</b>	2	4	1	5
<b>17</b>	2	4	1	5
<b>18</b>	2	4	1	5
<b>19</b>	2	4	1	5
<b>20</b>	2	4	1	5
<b>Summary</b>	40	80	20	100

**Table 17: Tests performed for 60° parking, at 10 mph**

<b>60 Degrees - 10 mph</b>				
<b>Run Number</b>	<b>Open Spots</b>	<b>Closed Spots</b>	<b>Ground Truth Open Spots</b>	<b>Ground Truth Closed Spots</b>
<b>1</b>	2	4	1	5
<b>2</b>	2	4	1	5
<b>3</b>	3	3	1	5
<b>4</b>	2	3	1	5
<b>5</b>	2	4	1	5
<b>6</b>	3	3	1	5
<b>7</b>	2	4	1	5
<b>8</b>	3	4	1	5
<b>9</b>	2	4	1	5
<b>10</b>	2	4	1	5
<b>11</b>	2	4	1	5
<b>12</b>	2	4	1	5
<b>13</b>	3	3	1	5
<b>14</b>	2	4	1	5
<b>15</b>	2	4	1	5
<b>16</b>	2	4	1	5
<b>17</b>	2	4	1	5
<b>18</b>	2	4	1	5
<b>19</b>	2	4	1	5
<b>20</b>	2	3	1	4
<b>Summary</b>	44	75	20	99

**Table 18: Tests performed for 90° parking, at 5 mph**

<b>90 Degrees - 5 mph</b>				
<b>Run Number</b>	<b>Open Spots</b>	<b>Closed Spots</b>	<b>Ground Truth Open Spots</b>	<b>Ground Truth Closed Spots</b>
1	9	12	9	12
2	9	12	9	12
3	9	12	9	12
4	9	11	9	12
5	9	12	9	12
6	9	12	9	12
7	9	12	9	12
8	9	12	9	12
9	9	12	9	12
10	9	12	9	12
11	9	12	9	12
12	9	12	9	12
13	9	11	9	12
<b>Summary</b>	117	154	117	156

**Table 19: Tests performed for 90° parking, at 10 mph**

<b>90 Degrees - 10 mph</b>				
<b>Run Number</b>	<b>Open Spots</b>	<b>Closed Spots</b>	<b>Ground Truth Open Spots</b>	<b>Ground Truth Closed Spots</b>
1	10	11	10	11
2	10	11	10	11
3	10	11	10	11
4	10	11	10	11
5	10	10	10	11
6	10	11	10	11
7	10	11	10	11
8	10	11	10	11
9	10	10	10	11
10	10	11	10	11
11	10	11	10	11
12	10	11	10	11
13	10	10	10	11
14	10	11	10	11
15	12	9	10	11

<b>Summary</b>	152	160	150	165
----------------	-----	-----	-----	-----

**Table 20: Tests performed for 90° parking, at 15 mph**

<b>90 Degrees - 15 mph</b>				
<b>Run Number</b>	<b>Open Spots</b>	<b>Closed Spots</b>	<b>Ground Truth Open Spots</b>	<b>Ground Truth Closed Spots</b>
<b>1</b>	10	11	10	11
<b>2</b>	10	11	10	11
<b>3</b>	10	11	10	11
<b>4</b>	10	11	10	11
<b>5</b>	10	11	10	11
<b>6</b>	10	11	10	11
<b>7</b>	10	11	10	11
<b>8</b>	10	11	10	11
<b>9</b>	12	9	10	11
<b>10</b>	10	11	10	11
<b>11</b>	10	11	10	11
<b>12</b>	10	11	10	11
<b>13</b>	11	10	10	11
<b>Summary</b>	133	140	130	143

## APPENDIX B

### SYSTEM SPEC LIST

Table 21 System spec List

<b>Item</b>	<b>Details</b>
<b>Sensor</b>	LIDAR-Lite Laser Range Sensor (PulsedLight) - 40 m measuring range - < 0.02 sec acquisition time
<b>Controller</b>	Arduino Uno - R3 Microcontroller
<b>Laptop</b>	Lenovo ThinkPad T510 notebook
<b>Motor</b>	Servo - Generic High Torque (Standard Size) - 6 volts - 83.47 oz-in. of maximum torque at 0.16 sec/60°
<b>USB Connection</b>	USB Cable - Standard A-B - 3 ft/1m
<b>Mount</b>	Panavise 809 Camera Window Suction-Cup Mount
<b>Wiring</b>	Hook-Up Wire - Assortment (Solid Core, 22 AWG)

# APPENDIX C

## LIDAR-LITE DATA SHEET

### Introduction

PulsedLight has targeted the need for high performance, very compact optical distance measurement sensors for cost sensitive markets such as UAV's, robotics and automotive. These applications benefit from substantially improved measurement range, high accuracy and reduced size over competing technology. Our single chip processing solution in combination with minimal supporting hardware enables a new class of optical distance measurement sensors that exceed the performance of current solutions at a substantially lower cost. PulsedLight's signal processing technology can be applied to applications ranging from single beam distance measurement to multi-pixel applications such as line scanning or complex 3-D imaging.

Our single board implementation of less than one square inch allows the use of a variety of optical sources such as LED's, VCSEL's (Vertical-Cavity Surface-Emitting Lasers) or edge emitting lasers. Our standard detector is based on a Si PIN diode but optionally; a Si APD can be used to provide greater sensitivity and range.

### LIDAR-Lite Specifications

General	Technical Specifications
Power	4.75-5.5V DC Nominal, Maximum 6V DC
Weight	PCB 4.5 grams, Module 22 grams with optics and housing
Size	PCB 44.5 X 16.5mm (1.75" by .65") Housing 20 X 48 X 40mm (.8" X 1.9" X 1.6")
Current Consumption	<2ma @ 1Hz (shutdown between measurements), <100ma (continuous operation)
Max Operating Temp.	70° C
External Trigger	3.3V logic, high-low edge triggered
PWM Range Output	PWM signal proportional to range, 1msec/meter, 10µsec step size
I2C Machine Interface	100Kb – Fixed, 0xC4 slave address. Internal register access & control.
Supported I2C Commands	Single distance measurement, velocity, signal strength
Mode Control	Busy status using I2C, External Trigger input / PWM outputs

### Laser Sensor PCB Technical Specifications – PIN detector without optics

General	Technical Specifications
NEP (PIN detector)	12nW rms, 1.5pF detector capacitance, 1mm virtual detector size
Min Detectable signal	1nW – 256 integrated bursts (maximum integration time)
Transmit Power (laser)	1.5Watts peak 14mm @ 3amps drive, 75µm single stripe laser junction
Transmit Power (LED)	200mW within +/- 3 degree beam @ 1amp

## LIDAR-Lite Specifications (Continued)

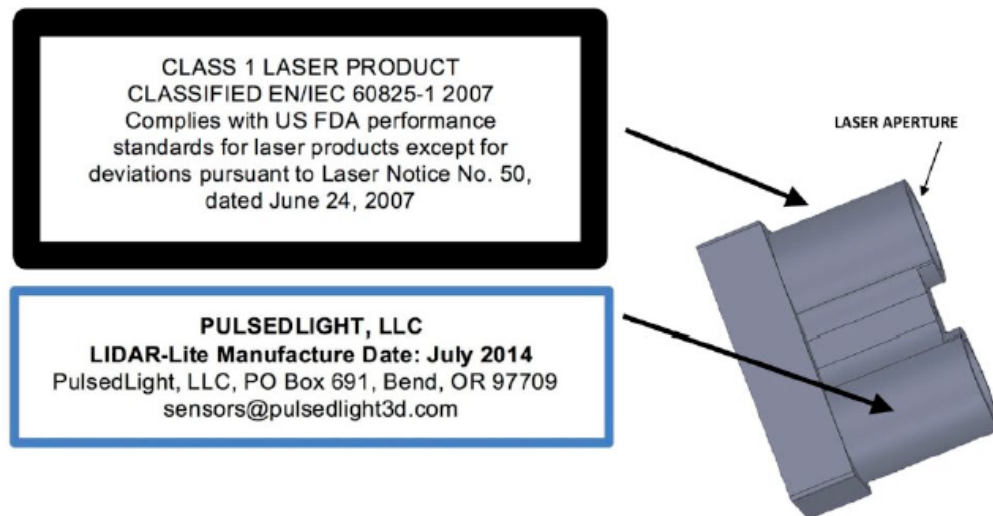
System Parameters	LED/Pin	LED/Pin with Optics <sup>1</sup>	Laser/Pin with Optics <sup>2</sup>
TX Emitter	5mm Plastic LED, 6° divergence	5mm Plastic LED, 6° divergence	75um, 1 watt, 4mrad, 14mm optic
RX Detector	5mm Plastic Si PIN, 30° FOV	12mm diameter 8mm effective aperture, 10° FOV	14mm diameter aperture, 3° FOV
Detector Gain	1x	1x	1x
TX /RX Focal Length	n/a	n/a	25mm/25mm
Max Range @ 1Hz 30% target	3 meters	10 meters	30 meters
Max Range @ 1Hz 90% target	5 meters	20 meters	60 meters
Accuracy	+/- 0.025 meter	+/- 0.025 meter	+/- 0.025 meter
Acquisition Time	<0.02 sec	<0.02 sec	<0.02 sec
Max Rep Rate	100 Hz	100 Hz	100 Hz, 10Hz Class 1

**1) Uses standard surface mount PIN detector instead of T 1 ¾ lamp style detector.**

**2) Uses custom laser housing & optics with surface mount PIN detector instead of T 1 ¾ lamp style detector.**



## Laser-Safety



LIDAR-Lite is a laser rangefinder that emits laser radiation. This Laser Product is designated Class 1 during all procedures of operation. This means that the laser is safe to look at with the unaided eye. However, it is *very* advisable to avoid looking into the beam and power the module off when not in use.

No regular maintenance is required for LIDAR-Lite. In the event that the unit becomes damaged or is inoperable, repair or service of LIDAR-Lite is only to be handled by authorized, factory-trained technicians. No service of LIDAR-Lite by the user is allowed. Attempting to repair or service the unit on your own can result in direct exposure to laser radiation and the risk of permanent eye damage. For repair or service please contact PulsedLight directly for a return authorization.

No user should modify LIDAR-Lite or operate it without its housing or optics. The Operation of LIDAR-Lite without a housing and optics or modification of the housing or optics that exposes the laser source may result in direct exposure to laser radiation and the risk of permanent eye damage. Removal or modification of the diffuser in front of the laser optic may result in the risk of permanent eye damage.

**Caution** – Use of controls or adjustments or performance of procedures other than those specified herein may result in hazardous radiation exposure. PulsedLight is not responsible for injuries caused through the improper use or operation of this product.

## REFERENCES

- Tang, V. W., Zheng, Y., & Cao, J. (2006). An Intelligent Car Park Management System based on Wireless Sensor Networks. *1st International Symposium on Pervasive Computing and Applications*, 1(1), 65-70.
- Abdel-Hafez, M. F., Al Nabulsi, A., Jafari, A. H., Al Zaabi, F., Sleiman, M., & AbuHatab, A. (2011). A Sequential Approach for Fault Detection and Identification of Vehicles' Ultrasonic Parking Sensors. *Modeling, Simulation and Applied Optimization (ICMSAO), 2011 4th International Conference on Modeling, Simulation and Applied Optimization*. Kuala Lumpur.
- Chinrungrueng, J., Sunantachaikul, U., & Triamlumlerd, S. (2007). Smart Parking: An Application of Optical Wireless Sensor Network. *Applications and the Internet Workshops, 2007. SAINT Workshops 2007. International Symposium*. Hiroshima.
- Decavalles-Hughes, G., & Ching, F. (2011). *City Council Report: Purchase and Installation of New Parking Meters*. Santa Monica.
- Federal Highway Administration. (2015, 02 20). *United States Department of Transportation - Federal Highway Administration*. Retrieved 09 10, 2015, from <https://www.fhwa.dot.gov/ohim/onh00/bar8.htm>
- Fleming, W. J. (2008). New Automotive Sensors—A Review. *Sensor Journal, IEEE*, 8(11), 1900 - 1921.
- Gu, J., Zhang, Z., Yu, F., & Liu, Q. (2012). Design and implementation of a street parking system using wireless sensor networks. *Industrial Informatics (INDIN), 2012 10th IEEE International Conference*, 1212-1217.
- IHI Corporation. (2010). *IHI 3D Laser Radar*. Retrieved 2015, from IHI: [http://www.ihi.co.jp/3DLaserRadar/en/product\\_01.html](http://www.ihi.co.jp/3DLaserRadar/en/product_01.html)
- Kikuta, H., Iwata, K., & Nagata, R. (1986). Distance measurement by the wavelength shift of laser diode light. *Applied Optics*, 25(17), 2976-2980.
- Klappenecker, A., Lee, H., & Welch, J. L. (2014). Finding available parking spaces made easy. *Ad Hoc Networks*, 12, 243–249.
- Kohler, P., Connette, C., & Verl, A. (2013). Vehicle Tracking using Ultrasonic Sensors & Joined Particle Weighting. *IEEE International Conference Robotics and Automation (ICRA)* (pp. 2900-2905). Karlsruhe: IEEE.

- Makris, A., Perrollaz, M., & Laugier, C. (2013). Probabilistic Integration of Intensity and Depth Information for Part-Based Vehicle Detection. *IEEE TRANSACTIONS ON INTELLIGENT TRANSPORTATION SYSTEMS*, 14(4), 1896-1906.
- Mathur, S., Jin, T., Kasturirangan, N., Chandrashekharan, J., Xue, W., Gruteser, M., et al. (2010). ParkNet: drive-by sensing of road-side parking statistics. *MobiSys '10 Proceedings of the 8th international conference on Mobile systems, applications, and services*. New York.
- Ono, S., Kagesawa, M., & Ikeuchi, K. (2002). A Probe Car For Parking-Vehicle Detection by Using Laser Range Sensor. *Intelligent Vehicle Symposium*, 2, 322-327.
- Park, W.-J., Kim, B.-S., Seo, D.-E., Kim, D.-S., & Lee, K.-H. (2008). Parking Space Detection Using Ultrasonic Sensor in Parking Assistance System. *Intelligent Vehicles Symposium, IEEE*, (pp. 1039-1044). Eindhoven.
- Pulsed Light. (2015). *lidarlite*. Retrieved 2015, from pulsedlite3d: <http://lidarlite.com/docs/v2/pdf/LIDAR-Lite-v1-docs.pdf>
- Schrank, D., Eisele, B., & Lomax, T. (2012). *TTI's 2012 URBAN MOBILITY REPORT*. College Station: Texas A&M Transportation Institute .
- Shoup, D. (2006). Cruising for parking. *Elsevier*(13), 479-486.
- Son, J., Kim, S., & Sohn, K. (2015). A multi-vision sensor-based fast localization system with image matching for challenging outdoor environments. *Expert Systems with Applications*, 42(22), 8830-8839.
- Srikanth, S., Pramod, P., Dileep, K., Tapas, S., Patil, M., & Sarat, N. (2009). Design and Implementation of a prototype Smart PARKing (SPARK) System using Wireless Sensor Networks. *2009 International Conference on Advanced Information Networking and Applications Workshops*. Bradford.
- Thornton, D. A., Redmill, K., & Coifman, B. (2014). Automated parking surveys from a LIDAR equipped vehicle. *Transportation Research Part C*, 39, 23-35.
- Tong, L., Cheng, L., Li, M., Wang, J., & Du, P. (2014). Integration of LiDAR Data and Orthophoto for Automatic Extraction of Parking Lot Structure. *APPLIED EARTH OBSERVATIONS AND REMOTE SENSING*, 7(2), 503-514.
- Yang, J., Portilla, J., & Riesgo, T. (2012). Smart parking service based on Wireless Sensor Networks. *IECON 2012 - 38th Annual Conference on IEEE Industrial Electronics Society*. Montreal.

Zhang, Z., Tao, M., & Yuan, H. (2014). A Parking Occupancy Detection Algorithm Based on AMR sensor. *Sensors Journal, IEEE2*, 15(2), 1261-1269.